Advances in Condensed Matter Physics

Coherent States in Double Quantum Well Systems

Guest Editors: Yogesh Joglekar, Melinda Kellogg, Milica Milovanovic, and Emanuel Tutuc

Coherent States in Double Quantum Well Systems

Advances in Condensed Matter Physics

Coherent States in Double Quantum Well Systems

Guest Editors: Yogesh Joglekar, Melinda Kellogg, Milica Milovanovic, and Emanuel Tutuc

Editorial Board

Contents

Hindawi Publishing Corporation
Advances in Condensed Matter Physics
Volume 2011, Article ID 970349, 1 page
doi:10.1155/2011/970349

Editorial

Coherent States in Double Quantum Well Systems

Yogesh Joglekar,[1] Melinda Kellogg,[2] Milica Milovanovic,[3] and Emanuel Tutuc[4]

[1] *Indiana University-Purdue University Indianapolis, Indianapolis, IN 46202, USA*
[2] *The University of Virginia's College at Wise, Wise, VA 24293, USA*
[3] *Institute of Physics Belgrade, 11080 Belgrade, Serbia*
[4] *University of Texas at Austin, Austin, TX 78712, USA*

Correspondence should be addressed to Yogesh Joglekar, yojoglek@iupui.edu

Received 21 September 2011; Accepted 21 September 2011

Coherent states, where a macroscopic system of many quantum particles exhibits properties of a single quantum particle, have been a topic of intense investigations in physics. The formation of such states is usually accompanied by and experimentally indicated by dissipationless transport of mass, charge, or spin.

Excitonic condensation occurs when an electron-hole system develops spontaneous coherence between the electron and hole bands. This effect, predicting the coherent state of electron-hole pairs, has led to a deeper theoretical understanding of condensates with metastable particles. Over the past two decades, this field has seen tremendous experimental developments, starting with the development of spatially separated electron and hole quantum wells, which increased the exciton lifetime by orders of magnitude. The increased exciton lifetime, in turn, has led to a detailed exploration of electrical transport, drag, and photoluminescence properties in such double quantum well systems. These systems have been traditionally fabricated using semiconductor heterojunctions; however, recently, graphene and topological insulators have emerged as promising new candidates as well.

The goal of this special issue is to review the recent theoretical and experimental developments on coherent states in such systems. With the rapid progress in fabrication techniques, it is possible to study coherent states with multiple broken symmetries. Thus, this issue starts with the state of experimental efforts on excitonic condensation in semiconductor quantum wells that are doped or optically pumped. It is followed by theoretical analyses of excitonic condensation in bilayer quantum Hall systems. The last paper extends the discussion on coherent states in graphene double layers.

Acknowledgment

This issue would not have been possible without generous contributions to this new journal from our colleagues. With articles by leading experts in the field of excitonic condensation, we hope that this special issue will form a timely, open-access resource for experts and novice alike.

Yogesh Joglekar
Melinda Kellogg
Milica Milovanovic
Emanuel Tutuc

Hindawi Publishing Corporation
Advances in Condensed Matter Physics
Volume 2011, Article ID 938609, 7 pages
doi:10.1155/2011/938609

Review Article

Coherence and Optical Emission from Bilayer Exciton Condensates

D. W. Snoke

Department of Physics and Astronomy, University of Pittsburgh, Pittsburgh, PA 15260, USA

Correspondence should be addressed to D. W. Snoke, snoke@pitt.edu

Received 15 June 2010; Accepted 13 October 2010

Academic Editor: Emanuel Tutuc

Experiments aimed at demonstrating Bose-Einstein condensation of excitons in two types of experiments with bilayer structures (coupled quantum wells) are reviewed, with an emphasis on the basic effects. Bose-Einstein condensation implies the existence of a macroscopic coherence, also known as off-diagonal long-range order, and proposed tests and past claims for coherence in these excitonic systems are discussed.

1. Introduction: Two Types of Bilayer Excitons

Condensates of electron pairs have long been known as the basis of superconductivity [1]. In superconductors, two spin-1/2 electrons bind into a Cooper pair, which is a boson. These bosons then undergo a type of Bose-Einstein condensation, in which a macroscopic number of the Cooper pairs enter a single wave function (see, e.g., [2, Section 11.2.3]). In principle, the same thing should be possible with pair states made of electrons and holes instead of two electrons. In this case, the attraction between the fermions is not a phonon-mediated effect, but the Coulomb attraction between particles with positive and negative charge.

In the past two decades, a number of experiments have focused on demonstrating Bose condensation in this type of system [3–5]. One version is the well-known polariton condensates [6], which have several dramatic effects of the condensation. The polaritons have very short lifetime, however. Although this makes them quite interesting for experiments with optical coupling, it also means that the polariton condensates are never in complete equilibrium. Another set of experiments, which we will review here, has focused on creating excitons that are either stable or metastable. These experiments are based on semiconductor structures with two coupled, parallel quantum wells.

There are two versions of this system, with important similarities and differences. In the first system [7, 8], which we will call Type A, two quantum wells are created parallel to each other with a thin barrier in between. Doping is used to create a permanent population of free electrons shared by the two wells. A DC magnetic field is then generated perpendicular to the wells, to create Landau levels. When the magnetic field and free electron density are tuned to the right values, the lowest Landau level in each quantum well will be half filled. One can visualize each of these levels as half full of electrons and half full of holes. Because the wells are near enough to each other for the Coulomb force to be significant, the electrons and holes in different wells will be correlated at low-temperature. The state of the system can be described as excitons, as shown in Figure 1(a). In this case, the excitons are not generated optically by taking an electron from the valence band to the conduction band; instead, the excitons in this system are generated by imagining that we start with one well with a full Landau level and the other with a completely empty Landau level, then an electron from the full Landau level tunnels through the barrier to the empty Landau level in the other well. Since the state in which each well has a half-filled Landau level is the ground state of the system, the excitons created this way are stable.

The second type of system, which we will call Type B, also uses two parallel quantum wells. In this case there is not normally a magnetic field (though one can be added); instead there is an electric field perpendicular to the wells. Free electrons and holes are generated optically and then move

into adjacent wells under the influence of the electric field, as shown in Figure 1(b). These excitons are known as "spatially indirect" excitons, or simply "indirect" excitons. In general, all excitons created by optical excitation are metastable and can decay, but if the applied electric field is high enough, the spatially indirect excitons created this way can have very long lifetime, since the lifetime increases exponentially with increasing electric field [9]. In recent experiments, exciton lifetimes up to 40 μs have been measured [10, 11], but much longer lifetime is possible; the main reason for not making the lifetime infinite is to use the optical emission to measure properties of the exciton gas. It is also possible [12, 13] to generate indirect excitons by injecting holes from a p-doped region on one side of the structure and electrons from an n-doped region on the opposite side. An analogous system has also been proposed for graphene bilayers [14–16].

There are several important differences between these two types of exciton systems.

1.1. Exciton Density and Disorder. The excitons in the Type B system can be generated with densities ranging from very low to very high, where high-density is defined as $na^2 > 1$, with n the area density and a the radius of the exciton, that is, the electron-hole correlation length. The exciton density in this case is directly controlled by the intensity of the pump laser which generates the free electron and holes, or the amount of current, if p-n current generation is used.

In the low-density limit, the excitons can act as a dilute Bose gas, with the critical temperature for Bose-Einstein condensation increasing with increasing density. In the high-density regime, a condensate of excitons will be in the BCS limit, with critical temperature for condensation decreasing with increasing density. (For a review see [17]; see also [3, Section 10.3]). This limit was studied theoretically already in the 1970s under the name of the "excitonic insulator." It is still proper to talk about bosonic electron-hole pairs and a condensate in this limit, because there is still a weak binding between the electrons and holes.

The excitons in the Type A system are always in this high-density regime. In principle, one could make a dilute exciton gas in this system by having one well keep most of the electrons and the other well have a nearly empty Landau level. The fraction of electrons in each well can be controlled by an electric field perpendicular to the wells. However, the experiments show that when the imbalance is more than a small fraction, the pairing of the carriers is destroyed. In the BCS-like state with nearly equal numbers of electrons and holes in each well, the binding energy of the excitons in the high-density limit is very weak due to the screening of the Coulomb interaction, which implies very low critical temperature; typical temperatures for these experiments are in the milliKelvin range.

When disorder in the wells is taken into account, there is an advantage to working in this high-density, low-temperature regime. Typical disorder fluctuations in the GaAs samples used for these experiments are a fraction of a meV. One meV corresponds to 10 K. If the excitons are at low density and low-temperature, they will simply fall into local minima in the disorder potential, below the so-called "mobility edge." In this case they will no longer act as a gas; instead they will act as an ensemble of pinned particles. This limit has been seen in experiments in which the diffusion constant of the excitons in a Type B structure was measured optically; at low density the diffusion constant became nearly zero [18].

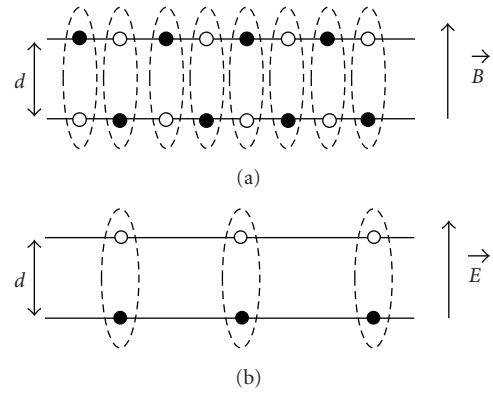

Figure 1: (a) Schematic representaion of the electrons and holes in a Type A bilayer system. (b) Schematic representaion of the electrons and holes in a Type B bilayer system.

A high-density, the electrons and holes will each form a Fermi level that can be larger than the disorder fluctuations. In this case the effect of the disorder potential will be washed out and the electron and hole states will be extended states. Because the disorder fluctuations are a nonnegligible fraction of the exciton Rydberg energy (typical intrinsic exciton-binding energies are 4 meV or so in these structures), there is not much room to increase the density above this point before hitting the high-density regime where $na^2 \sim 1$. As discussed in Section 2.5.4 of [2], the condition $na^2 \sim 1$ is equivalent to the condition $E_F \gg \mathrm{Ry}_{ex}$, where $\mathrm{Ry}_{ex} = e^2/4\pi\epsilon a$ is the intrinsic two-dimensional exciton-binding energy and $a \simeq 4\pi\hbar^2\epsilon/e^2\mu$ is the intrinsic excitonic Bohr radius, with ϵ the dielectric permittivity of the medium and μ the reduced mass of the electron and hole. As noted above, being in the high-density regime does not prevent condensation, but it reduces the critical temperature, as the condensate looks more and more like a BCS state with pair binding energy small compared to the Fermi energy.

The effect of the disorder is substantially reduced in wider quantum wells [10], but if the wells are too wide, the intrinsic binding energy of the excitons will be reduced too much, because the binding energy depends on the distance between the electrons and holes [9]. The optimum well width for GaAs-based structures appears to be around 15 nm.

1.2. Tunneling Current and Recombination. Another significant difference between the Type A and Type B systems is the role of tunneling current. In the Type A system, there is normally no bias normal to the plane of the wells to drive current from one to the other; in-plane electrical bias is used, however, to drive an in-plane current within each well. In the Type B system, a large electric field normal to

the plane of the wells is used to enforce the separation of the electrons and holes into different wells. This will always lead to some current through the barriers. Tunneling from one well to the other is responsible for the creation of the spatially indirect excitons, but stops once the excitons are formed. The electric field normal to the wells also creates tunneling current into the wells from outside, however, from carriers from the doped substrate and the doped capping layer of the structure. This can be suppressed by various methods, but can still play a large role in the temperature of the excitons, since carriers tunneling in from the substrate and capping layer will be very hot compared to the lattice, up to hundreds of degrees [18].

A perpendicular magnetic field acts to suppress this tunneling current, since the Landau orbits of the free carriers inhibit them from finding weak spots in the outer barriers to tunnel through [19]. In general, when there is not a magnetic field, the tunneling current through barriers in semiconductor heterostructures is not uniform; since the current is exponentially sensitive to the barrier thickness and alloy content, tiny regions with slightly thinner barrier or lower barrier height will attract most of the current, in "filaments" which have been seen dramatically in several experiments [20]. A magnetic field suppresses these filaments by forcing the carriers into large Landau orbits which average over the disorder.

2. Coherence in Exciton Condensates

Figure 2 gives the general structure of the phase diagram for a system with equal number of electrons and holes (or any system with equal numbers of equal-mass, opposite-sign fermions), when disorder is negligible. Since there is actually much confusion about both the terminology and the physics, it is worthwhile to take some time to discuss this phase diagram.

The solid line is the phase boundary for BEC in the dilute limit. This is nominally given by the condition that the thermal deBroglie wavelength λ of the particles be comparable to the average distance between them, r_s, which goes as $n^{-1/2}$ in two dimensions. Since $\lambda \propto \sqrt{\hbar^2/mk_BT}$, the condition $\lambda \sim r_s$ implies that the critical temperature for the transition is proportional to n. (Strong interactions and correlations of the excitons can substantially affect this estimate [21].)

A separate transition is the exciton-plasma phase transition, indicated by the thin solid line in Figure 2. This is sometimes called the "Mott" transition, but it is not the same as the condition $na^2 \sim 1$. The exciton-plasma phase transition, or ionization transition, actually has a quite complicated structure that depends on the details of the exciton-exciton and exciton-free carrier collisions and on the screening of the Coulomb interaction by free carriers [22–25]. ("Ionization" here refers to dissociation of the electron and hole from each other, not ionization of the underlying atoms.) There is still much debate about the form of this phase boundary. In general terms, we can say that in the high-density regime, we expect a critical temperature

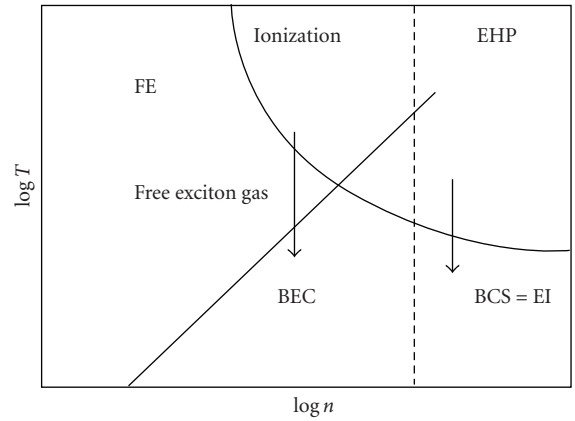

Figure 2: General structure of the phase diagram of an electron-hole system. FE: free excitons; EHP: electron-hole plasma; BEC: Bose-Einstein condensate of excitons; EI: exciton insulator state, which is a BCS-like state with a Fermi level for the electrons and for the holes. The transition from BEC to BCS may be gradual. At high pair density n, decreasing the temperature gives one critical T_c in which both pairing and condensation occur, in the EI (BCS-like) state. At lower density, there can be two critical temperatures: one for pairing and a second for condensation.

for ionization, equal to some fraction of the exciton-binding energy, while at high temperature, we expect a critical density above which the exciton gas will become disassociated by collisions. At low density and low temperature the gas should be purely free excitons.

The condition $na^2 = 1$, indicated by the dashed line in Figure 2, corresponds to the point at which the Fermi statistics of the electrons and holes become important; that is, the Fermi level becomes larger than the exciton-binding energy. At low enough temperature, the $na^2 > 1$ state corresponds to a BCS condensate, as discussed above.

One crucial fact to gain from this phase diagram is that *pairing and condensation are not the same*. The BCS pair state assumes condensation and coherence (see, e.g., [2, Section 11.2.3]), but it is not the only possible paired state to write down. In a standard superconductor, condensation and pairing occur at the same critical temperature, and for this reason the two different transitions are equated in many people's minds. Looking at the right-hand, high-density side of the phase diagram in Figure 2, if the carrier density is high, and the temperature is increased from zero, the pairs will unbind at temperatures well below the point at which $\lambda \sim r_s$. This is what happens in a standard BCS superconductor and in the excitonic insulator (EI) phase discussed above: because the binding energy of the pairs is small, pair breaking controls T_c. However, in an excitonic system with strong pairing, it is easily possible to have a situation in which the pairs are strongly bound but $\lambda \ll r_s$, as on the left side of the phase diagram of Figure 2. All exciton gases are comprised of pairs, but these are incoherent pairs, uncorrelated with each other, until they undergo BEC at low temperature.

At intermediate particle densities, it is possible to have a situation in which there is a plasma-exciton transition

to bound pairs (excitons) which are uncorrelated with each other, and then a second transition to a BEC at lower temperature. The transition from electron-hole plasma to excitons may be sharp or may correspond to a gradual increase of the number of exciton pairs as the temperature is decreased, according to the Saha equation [25].

In the Coulomb drag experiments [7, 8, 13], there is ample evidence that electron-hole pairs form which move together as excitons do. The evidence for condensation in those experiments, however, is much more indirect. A condensate is a coherent state, and therefore evidence of condensation is most directly seen in evidence of coherence, especially interference. This is seen, for example, in the Josephson effect in superconductors, including SQUIDs [2], in the interference of two condensates in cold atom gases [26], in measurements of first- and second-order coherence in polariton condensates [27–29], and in superradiant Brillouin scattering in magnon condensates [30]. It is also evidenced in observation of quantized vortices in liquid helium and in superconductors.

It is important to understand what we mean by coherence in this context. One type of coherence refers to the phase coherence in the wave function of a single electron and hole in a pair. This is seen, for example, in enhanced tunneling between the two layers [31]. Another type of coherence, the kind which is crucial to the notion of a condensate, is macroscopic coherence of many bosons in the same quantum state. This type of coherence is evidenced by in-plane correlation. For a true condensate, this type of coherence, known as off-diagonal long-range order, will lead to infinite in-plane coherence length. In a translationally invariant two-dimensional system, this cannot occur, and instead a Berezhinskii-Kosterlitz-Thouless transition can occur to a quasicondensate state with coherence correlation falling with a power-law dependence [32]. In a finite, trapped two-dimensional system, for example, the indirect excitons trapped in harmonic potentials using inhomogenous strain [33], the coherence length can be comparable to the size of the trap.

If all the carriers are in excitonic pair states, then there will be enhanced tunneling between the two layers simply due to the pairing, even if the excitons are not correlated with each other in the plane. This effect, which occurs in the Type A bilayer systems [31], is equivalent to the well-known enhancement of the oscillator strength for optical recombination in a Type B bilayer system when electrons and electrons and holes form excitons.

It is common to interpret many of the results of Coulomb drag and tunneling experiments in Type A systems in terms of a BCS wave function [31, 34, 35]. A BCS wave function is equivalent to a coherent state of bosons (see [2, Section 11.2.3]). However, the fact that a BCS wave function can be used to describe some experimental results is not the same as showing coherence; it must also be shown that the results can *not* be described by an ensemble of independent pairs. As discussed above, enhanced tunneling and interlayer drag can be explained by electron-hole pairing, without invoking coherence among the pairs.

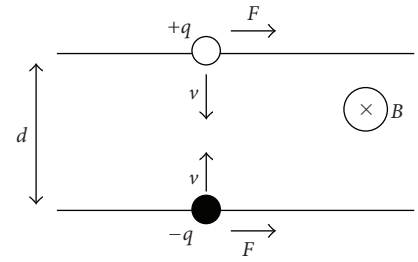

Figure 3: Schematic representaion of the effect of a DC in-plane magnetic field on electrons and holes in a bilayer system with tunneling.

It has been argued [36] that experiments with a weak in-plane magnetic field in addition to the large perpendicular magnetic field give evidence of long-range in-plane correlation. In these experiments, when an in-plane magnetic field is applied, the tunneling current is suppressed. A natural in-plane length scale λ is defined by setting the flux quantum $\Phi = h/q$ equal to $BA = B(d\lambda)$, where d is the interlayer separation, which implies $\lambda = h/qBd$. Experimentally, the measured in-plane B field which suppresses the tunneling implies $\lambda \sim 2\,\mu$m. This natural length scale can in turn be expressed as an in-plane momentum $\hbar k = h/\lambda = qBd$.

Figure 3 shows how this momentum comes about. If a carrier tunnels through the barrier with thickness d in a time τ, it will have an effective velocity of $v = d/\tau$. This leads to an in-plane force of magnitude $F = qvB = qdB/\tau$. This force leads to a momentum since $F = \Delta p/\Delta t$. Since $\Delta t = \tau$ here, we obtain $\Delta p = qdB$. The forces for the negative-charge electrons and positively-charged holes are both in the same direction.

The in-plane B-field therefore introduces a finite momentum to the tunneling carriers, and the suppression of the tunneling current can be viewed as a measurement of a critical velocity of the excitons. One explanation for this may be related to the Landau critical velocity for superfluids (e.g., [2, Section 11.1.4]). Other effects may lead to a critical velocity, such as ionization of the weakly-bound excitons due to collisions with defects in the lattice. The fact that no critical temperature has been measured for the bilayer resonant tunneling effect in Type A structures makes it difficult to assess whether it is related to condensation.

3. Optical Signatures of Exciton Coherence

In the case of Type B excitons, the observation of coherence is expected to be much easier, but experimental results so far have not provided definitive evidence.

Since the excitons in this type of system couple directly to photons that leave the system, the coherence of the excitons should map directly to optical coherence of the emitted photons, and the in-plane coherence length can be measured by first-order interference. This has been done with polariton condensates [27–29], but with indirect excitons in Type B structures, the evidence is not as clear. Butov and coworkers [37] have reported interference of light emitted from indirect

excitons in a Type B structure at low-temperature. The spectral width of this emission was around 2 meV, which by the W-K theorem (see, e.g., [2, Section 9.6]) implies a coherence time of about 300 femtoseconds, much less than the lifetime of the excitons, and not too different from what would be expected for incoherent light from a small source, although there was clearly an enhancement of the coherence in these experiments as the temperature decreased.

Coherent light emission alone is not a sufficient test for exciton condensation, because lasers also emit coherent light, and laser light comes from unpaired, incoherent electrons and holes. To show that the electrons and holes make up a coherent excitonic condensate, it is also necessary to show (a) that there is long-range in-plane correlation of the coherent emission, and (b) that the excitons are still good quantum states and are not strongly dephased. Both of these have been shown in the polariton systems, in which two transitions, one for condensation and a second, at higher pair density, for lasing have been demonstrated [38, 39].

Balatsky et al. [40] proposed an interesting test for the presence of a condensate of indirect excitons in a Type B structure. Similar to the experiment represented in Figure 4, an in-plane magnetic field is used, but this time an AC, time-varying field. By Maxwell's equation $\nabla \times \vec{E} = -\partial \vec{B}/\partial t$, this implies a time-varying difference of the in-plane component of the electric field between the two spatially separated planes. (Perpendicular electric field can be eliminated by symmetry if the in-plane magnetic field is spatially homogeneous.) Since the electron and hole have opposite charge, this leads to a net in-plane force on the excitons.

If the excitons are incoherent, then their motion under this force should follow an Ohm's law-type drift behavior in which their velocity is proportional to the force qE. On the other hand, if the excitons are superfluid, then they should have an acceleration proportional to the force. If the magnetic field oscillates sinusoidally, then the superfluid component should oscillate in phase with the magnetic field while the normal component oscillates out of phase. This could, in principle, be measured by optical imaging of the exciton motion.

The magnitude of the oscillation is estimated by the following calculation. The electric field magnitude is $E_0 = \omega B_0 d$, and the maximum acceleration of the exciton is related to the maximum amplitude of the spatial motion, x_0, by $a_0 = \omega^2 x_0 = qE_0/m$. This implies

$$x_0 = \frac{q}{m}\frac{B_0 d}{\omega}. \tag{1}$$

If we want x_0 to be around $10\,\mu$m, to be resolvable by standard far-field optical imaging, then for AC oscillation frequency of 100 kHz (to match the typical exciton lifetime), $d \sim 10$ nm, and mass of the order of typical effective masses of carriers, about 1/10 of a vacuum electron mass, this implies $B_0 \sim 1T$. It is probably experimentally too difficult to have a magnetic field of this magnitude oscillate at 100 kHz, but if the spatial resolution of the imaging can be reduced, the required magnitude of the magnetic field can also be reduced. Alternatively, the frequency of the oscillation can be reduced by making the exciton lifetime longer, which will decrease the optical emission signal used to detect the motion.

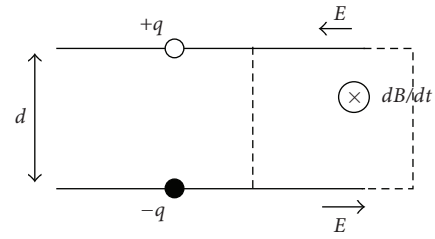

Figure 4: Schematic representaion of the effect of an AC in-plane magnetic field on electrons and holes in a bilayer system with no tunneling.

This proposal was greeted with some controversy in the transport community because of questions about the current [41]. If there is zero tunneling between the two layers, then a circuit cannot be completed and no net current can flow. In the context of the indirect excitons, this means that if the exciton density is constant, then excitons will pile up at one end of the structure and repel other excitons from moving. However, in typical experiments with Type B structures, the exciton density is not constant, and the region over which the excitons are created and the amplitude of the spatial oscillation due to the time-varying field are both small compared to the size of the whole structure. There will therefore be no back EMF produced by the lack of completion of the circuit, and the excitons will move essentially the same as if they were single excitons in an empty, infinite two-dimensional space.

Of course, the motion of the excitons is measured by looking at the photons emitted by them when they recombine, which involves tunneling through the barrier. But this lifetime can be made arbitrarily long, as discussed above, so that this current is negligible. In optical experiments, the photon emission functions as a probe in which only a tiny fraction of the excitons are destroyed at any time. We can therefore ignore the current due to exciton recombination leading to photon emission in these experiments.

4. Conclusions

There is still much work to be done to demonstrate condensation in bilayer systems. There is no question that there is pairing in both Type A and Type B systems, which leads to enhanced tunneling through the barrier between the wells. But off-diagonal long-range order in the plane of the wells has not yet been clearly demonstrated in either system with a direct test.

Probably the best bet for doing a direct test of coherence in the Type A bilayer systems would be a transport experiment analogous to a Josephson junction. Two regions with bilayer condensate could be separated by a tunneling junction, and the tunneling current through this in-plane barrier could be measured.

For the indirect excitons in Type B structures, the proposal of Littlewood and coworkers to use a time-varying, in-plane magnetic field to see undamped superfluid exciton motion is reasonable, but requires high magnetic fields or very tiny spatial resolution which may be unobtainable. First-order coherence in the optical emission is also a test of coherence of the exciton condensate, but requires additional tests to distinguish it from standard lasing and to distinguish it from interference from an incoherent source analogous to stellar interferometry.

Acknowledgments

This work has been supported by the Department of Energy through Project no. DOE-DE-FG02-99ER45780. The author thanks J. P. Eisenstein and P. B. Littlewood for helpful discussions.

References

[1] A. J. Leggett, *Quantum Liquids*, Oxford University Press, New York, NY, USA, 2006.

[2] D. W. Snoke, *Solid State Physics: Essential Concepts*, Pearson/Addison-Wesley, Reading, Mass, USA, 2009.

[3] S. A. Moskalenko and D. W. Snoke, *Bose-Einstein Condensation of Excitons and Biexcitons and Coherent Nonlinear Optics with Excitons*, Cambridge University Press, Cambridge, UK, 2000.

[4] D. Snoke, "Spontaneous Bose coherence of excitons and polaritons," *Science*, vol. 298, no. 5597, pp. 1368–1372, 2002.

[5] D. Snoke, "Condensed-matter physics: coherent questions," *Nature*, vol. 443, no. 7110, pp. 403–404, 2006.

[6] D. Snoke and P. Littlewood, "Polariton condensates," *Physics Today*, vol. 63, no. 8, pp. 42–47, 2010.

[7] A. D. K. Finck, J. P. Eisenstein, L. N. Pfeiffer, and K. W. West, "Quantum hall exciton condensation at full spin polarization," *Physical Review Letters*, vol. 104, no. 1, Article ID 016801, 2010.

[8] E. Tutuc, R. Pillarisetty, and M. Shayegan, "Giant frictional drag in strongly interacting bilayers near filling factor one," *Physical Review B*, vol. 79, no. 4, Article ID 041303, 2009.

[9] M. H. Szymanska and P. B. Littlewood, "Excitonic binding in coupled quantum wells," *Physical Review B*, vol. 67, no. 19, Article ID 193305, pp. 1–4, 2003.

[10] Z. Vörös, R. Balili, D. W. Snoke, L. Pfeiffer, and K. West, "Long-distance diffusion of excitons in double quantum well structures," *Physical Review Letters*, vol. 94, no. 22, Article ID 226401, pp. 1–4, 2005.

[11] N. Sinclair, J. Wuenschel, D. Snoke, L. Pfeiffer, and K. West, "Indicate lifetimes of indirect excitons at least as long as 40 μs".

[12] Y. N. Joglekar, A. V. Balatsky, and M. P. Lilly, "Excitonic condensate and quasiparticle transport in electron-hole bilayer systems," *Physical Review B*, vol. 72, no. 20, Article ID 205313, pp. 1–6, 2005.

[13] J. A. Seamons, C. P. Morath, J. L. Reno, and M. P. Lilly, "Coulomb drag in the exciton regime in electron-hole bilayers," *Physical Review Letters*, vol. 102, no. 2, Article ID 026804, 2009.

[14] O. L. Berman, Y. E. Lozovik, and G. Gumbs, "Bose-Einstein condensation and superfluidity of magnetoexcitons in bilayer graphene," *Physical Review B*, vol. 77, no. 15, Article ID 155433, 2008.

[15] C.-H. Zhang and Y. N. Joglekar, "Excitonic condensation of massless fermions in graphene bilayers," *Physical Review B*, vol. 77, no. 23, Article ID 233405, 2008.

[16] Y. Barlas, R. Côté, J. Lambert, and A. H. MacDonald, "Anomalous exciton condensation in graphene bilayers," *Physical Review Letters*, vol. 104, no. 9, Article ID 096802, 2010.

[17] B. I. Halperin and T. M. Rice, *Solid State Physics: Advances in Research and Applications*, vol. 21, Academic Press, New York, NY, USA, 1968.

[18] Z. Vörös and D. W. Snoke, "Quantum well excitons at low density," *Modern Physics Letters B*, vol. 22, no. 10, pp. 701–725, 2008.

[19] S. Denev, V. Negoita, D. W. Snoke, B. Laikhtman, K. Eberl, and L. Pfeiffer, "Optical detection of magnetic fields using giant magnetoresistance in undoped coupled quantum wells," *Physical Review B*, vol. 66, no. 20, Article ID 205304, pp. 1–6, 2002.

[20] L. V. Butov, "Condensation and pattern formation in cold exciton gases in coupled quantum wells," *Journal of Physics Condensed Matter*, vol. 16, no. 50, pp. R1577–R1613, 2004.

[21] B. Laikhtman and R. Rapaport, "Exciton correlations in coupled quantum wells and their luminescence blue shift," *Physical Review B*, vol. 80, no. 19, Article ID 195313, 2009.

[22] T. M. Rice, *Solid State Physics: Advances in Research and Applications*, vol. 32, Academic Press, New York, NY, USA, 1977.

[23] D. Semkat, F. Richter, D. Kremp, G. Manzke, W.-D. Kraeft, and K. Henneberger, "Ionization equilibrium in an excited semiconductor: Mott transition versus Bose-Einstein condensation," *Physical Review B*, vol. 80, no. 15, Article ID 155201, 2009.

[24] D. W. Snoke and J. D. Crawford, "Hysteresis in the Mott transition between plasma and insulating gas," *Physical Review E*, vol. 52, no. 6, pp. 5796–5799, 1995.

[25] D. Snoke, "Predicting the ionization threshold for carriers in excited semiconductors," *Solid State Communications*, vol. 146, no. 1-2, pp. 73–77, 2008.

[26] M. R. Andrews, C. G. Townsend, H.-J. Miesner, D. S. Durfee, D. M. Kurn, and W. Ketterle, "Observation of interference between two bose condensates," *Science*, vol. 275, no. 5300, pp. 637–641, 1997.

[27] J. Kasprzak, M. Richard, S. Kundermann et al., "Bose-Einstein condensation of exciton polaritons," *Nature*, vol. 443, no. 7110, pp. 409–414, 2006.

[28] A. Baas, K. G. Lagoudakis, M. Richard, R. André, L. S. Dang, and B. Deveaud-Plédran, "Synchronized and desynchronized phases of exciton-polariton condensates in the presence of disorder," *Physical Review Letters*, vol. 100, no. 17, Article ID 170401, 2008.

[29] R. Balili, V. Hartwell, D. Snoke, L. Pfeiffer, and K. West, "Bose-Einstein condensation of microcavity polaritons in a trap," *Science*, vol. 316, no. 5827, pp. 1007–1010, 2007.

[30] V. E. Demidov, O. Dzyapko, S. O. Demokritov, G. A. Melkov, and A. N. Slavin, "Observation of spontaneous coherence in Bose-Einstein condensate of magnons," *Physical Review Letters*, vol. 100, no. 4, Article ID 047205, 2008.

[31] J. P. Eisenstein, "Evidence for spontaneous interlayer phase coherence in a bilayer quantum Hall exciton condensate," *Solid State Communications*, vol. 127, no. 2, pp. 123–130, 2003.

[32] O. L. Berman, Y. E. Lozovik, and D. W. Snoke, "Theory of Bose-Einstein condensation and superfluidity of two-dimensional polaritons in an in-plane harmonic potential," *Physical Review B*, vol. 77, no. 15, Article ID 155317, 2008.

[33] Z. Vörös, D. W. Snoke, L. Pfeiffer, and K. West, "Trapping excitons in a two-dimensional in-plane harmonic potential: experimental evidence for equilibration of indirect excitons," *Physical Review Letters*, vol. 97, no. 1, Article ID 016803, 2006.

[34] A. A. Burkov, Y. N. Joglekar, E. Rossi, and A. H. MacDonald, "Collective transport in bilayer quantum Hall systems," *Physica E*, vol. 22, no. 1–3, pp. 19–24, 2004.

[35] K. Park and S. Das Sarma, "Coherent tunneling in exciton condensates of bilayer quantum Hall systems," *Physical Review B*, vol. 74, no. 3, Article ID 035338, 2006.

[36] J. P. Eisenstein, private communication.

[37] S. Yang, A. T. Hammack, M. M. Fogler, L. V. Butov, and A. C. Gossard, "Coherence length of cold exciton gases in coupled quantum wells," *Physical Review Letters*, vol. 97, no. 18, Article ID 187402, 2006.

[38] R. Balili, B. Nelsen, D. W. Snoke, L. Pfeiffer, and K. West, "Role of the stress trap in the polariton quasiequilibrium condensation in GaAs microcavities," *Physical Review B*, vol. 79, no. 7, Article ID 075319, 2009.

[39] B. Nelsen, R. Balili, D. W. Snoke, L. Pfeiffer, and K. West, "Lasing and polariton condensation: two distinct transitions in GaAs microcavities with stress traps," *Journal of Applied Physics*, vol. 105, no. 12, Article ID 122414, 2009.

[40] A. V. Balatsky, Y. N. Joglekar, and P. B. Littlewood, "Dipolar superfluidity in electron-hole bilayer systems," *Physical Review Letters*, vol. 93, no. 26, Article ID 266801, 2004.

[41] A. MacDonald and J. Ye, private communication.

Hindawi Publishing Corporation
Advances in Condensed Matter Physics
Volume 2011, Article ID 727958, 22 pages
doi:10.1155/2011/727958

Review Article

Experimental Progress towards Probing the Ground State of an Electron-Hole Bilayer by Low-Temperature Transport

K. Das Gupta,[1] A. F. Croxall,[1] J. Waldie,[1] C. A. Nicoll,[1] H. E. Beere,[1] I. Farrer,[1] D. A. Ritchie,[1] and M. Pepper[1,2]

[1] *Cavendish Laboratory, University of Cambridge, J.J. Thomson Avenue, Cambridge CB3 0HE, UK*
[2] *Department of Electronic and Electrical Engineering, University College, London WC1E7JE, UK*

Correspondence should be addressed to K. Das Gupta, kd241@cam.ac.uk

Received 27 May 2010; Accepted 27 October 2010

Academic Editor: Milica Milovanovic

Recently, it has been possible to design independently contacted electron-hole bilayers (EHBLs) with carrier densities $< 5\times10^{10}$ cm^2 in each layer and a separation of 10–20 nm in a GaAs/AlGaAs system. In these EHBLs, the interlayer interaction can be stronger than the intralayer interactions. Theoretical works have indicated the possibility of a very rich phase diagram in EHBLs consisting of excitonic superfluid phases, charge density waves, and Wigner crystals. Experiments have revealed that the Coulomb drag on the hole layer shows strong nonmonotonic deviations from a $\sim T^2$ behaviour expected for Fermi-liquids at low temperatures. Simultaneously, an unexpected insulating behaviour in the single-layer resistances (at a highly "metallic" regime with $k_F l > 500$) also appears in both layers despite electron mobilities of above $\sim 10^6$cm^{2}V^{-1}s^{-1} and hole mobilities over $\sim 10^5$cm^{2}V^{-1}s^{-1}. Experimental data also indicates that the point of equal densities ($n = p$) is not special.

1. Introduction

Bringing two layers of 2-dimensional electron gases (2DEG) or a 2-dimensional hole gases (2DHG) in close proximity opens up possibilities that do not exist when the layers are very far apart. We give a simple example to show why interaction-driven phases can arise more readily in bilayers. Let us recall that the ratio of the kinetic energy of a system of electrons and their potential energies due to mutual Coulomb interaction is measured by the parameter $r_s = E_{ee}/E_f$ (where $E_{ee} = e^2\sqrt{(\pi N)}/4\pi\epsilon_0\epsilon_r$ and $E_f = \pi\hbar^2 N/m^*$ in 2-dimensions, with N electrons per unit area). The ratio is not material independent; it depends on parameters like the relative dielectric constant ϵ_r and the band effective mass m^* of the material. Confining a large number of particles in a small area makes the interparticle spacing small and hence the Coulomb repulsion large, but the kinetic energy of the particles increases even faster—making r_s smaller. This somewhat counterintuitive fact is a straightforward consequence of Fermi statistics and is true in all dimensions. Consider now two parallel layers of electrons or holes with 10^{11} cm^{-2} electrons in each—which is a typical density in many experiments based on GaAs-AlGaAs heterostructures. If they are now brought closer to each other, the particles in one layer not only interact with others in the same layer but also with those in the other layer. The interparticle spacing in the same layer stays fixed and is about 30 nm. It is now possible to make the distance between the two layers about 10 nm with negligible tunneling taking place. 10 nm is approximately the excitonic Bohr radius in gallium arsenide (GaAs) and is an important length scale. We thus get an electron to "see" another electron (or hole) only 10 nm away, without paying the kinetic (Fermi) energy cost, because the two layers continue to be two separate Fermi systems. To get the same average interparticle separation (i.e., 10 nm) within a layer, a 9-fold increase in density (and hence Fermi energy) would have been necessary. As a consequence interaction-driven phases may be expected to occur more readily in bilayers. The case of the electron-hole bilayer may have some remarkable possibilities—particularly if we can make the interlayer attractive interaction stronger than the intralayer repulsive interactions. This will require a bilayer system

where the particles have low enough densities, such that the intralayer separation between the particles is larger (or of the same order) than the interlayer distance. In practice, this implies that if the layer densities are about 10^{11} cm^{-2}, then the interlayer distance would have to be about 10–20 nm.

First, because of the attractive interaction between the electrons and holes, bound pairs may form. Indeed, bound pairs of electrons and holes (excitons) are well known in bulk semiconductors. However, there is a crucial difference here. In bulk, the lifetime of the excitons can rarely exceed a few nanoseconds, because of radiative decay. The idea that spatially separating electrons and holes could be a fruitful way of obtaining large exciton lifetimes and possible "bosonic" phases was first proposed in 1975 [1, 2]. Although this is a very exciting possibility, there can be many legitimate questions about how stable such a condensate would be, whether in 2-dimensions one can get a long-range coherence at all, and so forth. It is not known how to measure the momentum distribution (characteristic of a condensate) of a bunch of particles by transport—but there is another class of transport-based experiments [3–5] that can turn out to be very useful; these are measurements of the transresistivity of the bilayer, which can be directly related to the interlayer scattering rate and may also provide indications of a condensate phase [6–8]. Passing current in both layers in an opposite sense (counterflow) is predicted to couple to the excitons and is expected to be dissipationless for a superfluid [9]. A large increase in the drag resistivity is also expected [6, 10]. Noise measurements, response to parallel magnetic field, and Josephson junction-like behaviour across a weak link are also anticipated [9, 10].

The first proposals [1, 2] relied on n-semiconductor-insulator-p-semiconductor structures to achieve this. However, only with the rapid improvements in GaAs/AlGaAs, heterostructure technology in the 1980s and subsequent development of closely spaced double quantum-well structures in the 1990s led to the first realistic possibilities of making such a system. In 2D, the relationship between the critical density and the superfluid transition temperature (T_{KT}) is expected to be given by the Kosterlitz-Thouless condition

$$n_{\mathrm{ex}} \sim \frac{1}{\hbar^2} m^*_{\mathrm{ex}} k_B T_{\mathrm{KT}}, \tag{1}$$

where n_{ex} is the exciton density and m^*_{ex} is the effective mass of the exciton [2]. In semiconductors, the small effective mass of an exciton ($\sim 0.2m_e$) means that the transition temperature is anticipated to be much higher than that required for atomic BEC. The possibility of excitonic BEC in EHBLs has been reviewed by Littlewood and Zhu [11].

The second possibility is somewhat less intuitive. It involves the densities of the two layers developing a spontaneous periodic modulation. Loosely speaking, it would remind one of a homogeneous liquid freezing to a solid which has a crystal structure. Such spontaneous ordering may be characterized by the divergence of the relevant susceptibility function at a particular wavevector. Simple theories describing the susceptibility of a 2DEG (Lindhard response function) would predict that the susceptibility remains nearly constant till $q = 2k_F$ (where k_F is the Fermi wavevector) and drops rapidly to zero after that. This indeed is the correct behaviour at long wavelengths, but it leads to certain unphysical results at short-length scales. A theory of susceptibility also leads to predictions for the two particle probability distribution $g(r)$. This is not hard to see. Susceptibility is the density-density response function of a system, which by the fluctuation-dissipation theorem is directly related to the density-density fluctuation or the structure factor. The structure factor, in turn is the Fourier transform of the two particle probability distribution. Among the well-known attempts [12–14] to get the physically reasonable (nonnegative) values of $g(r)$ at small distances is a self-consistent local-field theory of Singwi et al. This approach connects the charge susceptibility, structure factor, and the local-field corrections for the screened Coulomb potential. With the advent of double quantum well structures in the early 1990s, this was extended successfully to the bilayer [15–17]. A striking prediction of [17, 18] is that the electron-hole bilayer would be more susceptible to a charge density wave (CDW) formation at wavevectors much smaller than k_{F} than the electron-electron bilayer. The density-modulated phases are indicated by the divergence of one of the eigenvalues of the bilayer susceptibility matrix, but this does not require the divergence of the single-layer susceptibilities—which may still occur at much higher r_s. An excitonic state may be indicated by a divergence in the interlayer pair-correlation function $g_{12}(r)$ at $r = 0$; Liu et al. [18] had proposed that such a divergence would be preceded by a CDW.

How close do we want the two layers to be? If we want to make the interlayer interaction stronger than the intralayer interaction, then we need the interlayer distance (d) to be smaller than the intralayer separation (l) of the particles. Thus, for example, for $N = 10^{11}$ cm^{-2} in each layer, we would want $d \approx$ 10–20 nm. It is easy to see that the d/l ratio would be indicative of the relative strength of the interlayer and intralayer interactions. At the same time, it is important to ensure that the electron and mobilities are sufficiently high such that their behaviour is not predominantly dictated by localisation and inhomogeneity.

2. Making Real Bilayers

While remarkable possibilities were predicted for EHBLs, making them experimentally turned out to be difficult and challenging. In this section, we will try to see why the basic requirements for making transport measurements in EHBLs turned out to be difficult. Since the first attempt by Sivan et al. [19], there was a continued interest in these devices marked by the work of Kane et al. (1994) [20], Rubel et al. (1998) [21], Pohlt et al. (2002) [22], Keogh et al. (2005) [23], and Seamons et al. (2007) [24]. There are a few key requirements for working with bilayers:

(i) independent ohmic contacts to each layer,

(ii) gate voltage control of the densities of each layer,

(iii) very low leakage through the barrier separating the two layers.

2.1. Making Independent Ohmic Contacts. Achieving independent ohmic contact to each layer in an EHBL is considerably more difficult than in electron-electron or hole-hole bilayers. Let us first look at the basic idea behind independently contacting a 2x2DEG. Figure 1 shows how the ohmic contact, usually indium or a gold-germanium-nickel alloy, is deposited at selected places using standard photolithographic techniques. The subsequent annealing process causes the metal to diffuse into the semiconductor and pass through both wells. The contacts are not independent at this stage, since they pass through and contact both layers. To achieve independent contact to the bottom layer, the front gate (on the surface side) is biased negatively with respect to the ohmics such that only the upper electron gas is depleted. The gate raises the conduction band, creating a potential hill just below it. So, the left contact (as in Figure 1) contacts only the bottom 2DEG. If we now have a similar gate at the bottom of the sample, then a negative voltage on that gate would locally deplete the lower 2DEG, allowing us to contact only the top 2DEG (as shown on the right). The gates below the 2x2DEG must be aligned to the topside features of the device, correct to a few microns, to ensure that the lower 2DEG is selectively depleted.

There is also another practical point. The topgate is typically only a few hundred nanometers above the upper 2DEG, so a small voltage on that gate will have sufficient effect on the 2DEG. But the substrate (gallium arsenide) is itself about half a millimeter (500 microns) thick. So, a voltage on the backgate (irrespective of whether it is aligned or not), will have 1000 times less effect on the 2DEG. Therefore, the sample needs to be thinned to lower the biases required. It is practical to make the samples about 50 microns in thickness and still handle them. So, the voltages required would come down to about 50–100 volts, which is practical. This was done by Eisenstein et al. in 1990 [25]. Aligning the backgate with topside features is another crucial requirement. This in general requires a double-sided mask aligner. A process to achieve this with a single-side mask aligner and thinned substrates ($\approx 50\,\mu$m) was developed by the authors' group and has been described in detail in [26].

There are two possible ways of bringing the backgate almost as close to the quantum wells as the topgate so that the voltages required are comparable. One of these is based on the Focussed Ion Beam (FIB) technique. The second involves making the sample itself 1-2 microns thick by etching from the back, using an etch stop layer, using a technique named "Epoxy bond and stop etch" (EBASE) described by Weckwerth et al. [27].

If a conducting region could be grown (during MBE) only at places where we want the backgate (as in Figure 1), then this would be a nice way to selectively deplete the bottom 2DEG. Doped GaAs conducts because the dopants (Si) occupy some of the Ga lattice sites and contributes one electron to the conduction band. If certain regions are selectively subjected to a beam of heavy ions, then the regions become nonconducting. Large defect densities may be created which trap the electrons released by the donor atoms or the Si atoms may be displaced—in either

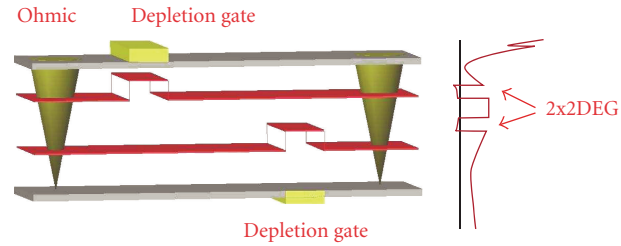

Figure 1: A schematic representation for independent ohmic contacts to a 2x2DEG. A similar method will work for a 2x2DHG as well. Notice that the 2DEG exists due to carriers from ionised dopants before the contacts are made. The sketch on the right hand side shows the rough profile of the bottom of the conduction band.

case, electrons from the donor atoms would not be able to populate the conduction band. Experimentally, this can be done by using a beam of Ga ions at 30 keV or so from a focussed ion gun. Ion doses like 10^{12}–$10^{13}\,\mathrm{cm}^{-2}$ would disrupt the lattice sufficiently and the n^+ layer would be rendered resistive (say $10^{14}\,\Omega$ at 1.5 K). The beam can be directed with high accuracy and write out a desired a pattern. The layers which make up the double quantum well (DQW) structures are grown after this stage. The entire patterning process and subsequent growth is done without removing the sample from the ultra high vacuum (UHV) environment, to prevent contamination. This is the basis of the focussed-ion-beam (FIB) method and has also been successfully used for making transport measurements on independently contacted DQW by Hill et al. [28] and Linfield et al. [29]. Notice that the area on which the active region of the sample will be located is actually not the beam damaged area—this still allows high 2DEG mobilities to be reached. A pertinent question at this stage is how to align the later photolithographic stages with the damaged/undamaged area pattern written out by the beam. Very high ion doses of $10^{17}\,\mathrm{cm}^2$ or so can be used to etch alignment marks away from the central region where the 2DEG forms. This level of beam damage makes the subsequent growth on those areas visibly different due to high concentration of defects. The later stages can thus be aligned with the buried backgates.

3. The Electron-Hole Bilayer

Is it possible to extend a modulation doping-based method of making 2x2DEGs and 2x2DHGs to make an electron-hole bilayer (EHBL)? The answer is that it is possible only if we are satisfied with very large layer separations $d > 100$ nm [21]. At that distance, the interlayer Coulomb interaction would not be dominant. Consider a situation where we try to create two modulation-doped gases, (one 2DEG and one 2DHG) in close proximity, say 10–20 nm. The Fermi level must come above the conduction band for a 2DEG to form; similarly, it must fall slightly below the valence band for a hole gas to form. Now, the top of the valence band and the bottom of the conduction band are separated by 1.5 V, which is the bandgap of GaAs. Thus, if a 2DEG and a 2DHG exist at the same electrochemical potential, then the bands must have a

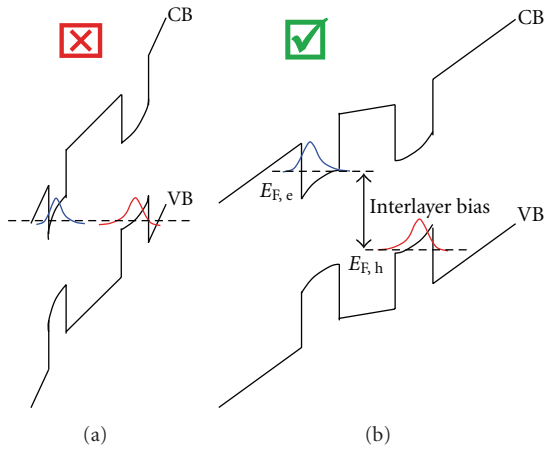

FIGURE 2: The band bending shown on (a) is not possible to achieve in GaAs for a closely spaced EHBL. The electric field in the barrier would be too high to sustain or even obtain self-consistently by modulation doping alone. One has to resort to making the electrochemical potential discontinuous (as shown on (b)). This was already understood in 1992.

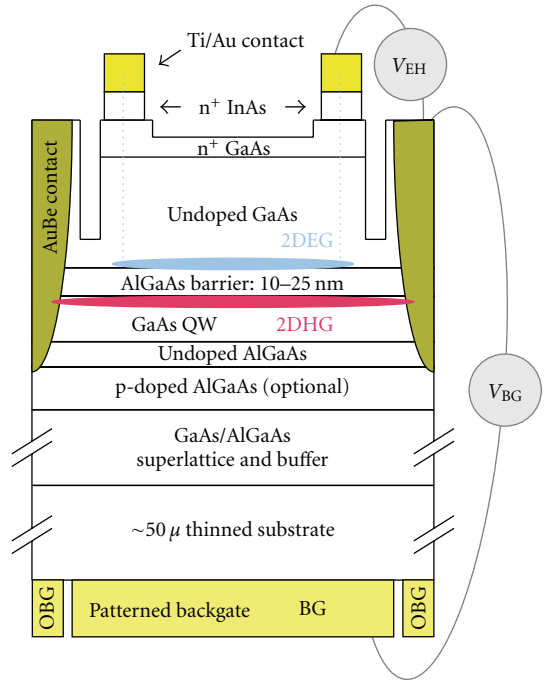

FIGURE 3: The schematic representation of the EHBL developed in the authors' group. Note that two voltage biases are in general needed for operating the device. However, the outer backgate below the ohmic contacts (V_{obg}) to the holes is often biased differently from the backgate in the central region (V_{bg}).

very large slope in the region between the two layers. This implies an electric field of $\sim 10^8$ V/m, which is too high to sustain. The structure would simply collapse. See Figure 2. As an aside, the bandgap of Silicon is about 1.1 V, so the required field would be slightly less. In fact, recently, two groups have succeeded in making EHBLs in Si [29, 30], where the electrons and holes stay at the same chemical potential. If at some point independent contact to bilayer graphene is made, then it would be very interesting from the point of view of an EHBL, because the bandgap of graphene is zero. However, in the GaAs-AlGaAs system, the only way around would be to make the electrochemical potential itself discontinuous. This means that we need to connect a battery from outside between the two layers which would allow the two gases to exist without requiring a huge band slope.

Notice that even before we made independent contacts, it was possible to create a a 2x2DEG. In the case of the EHBL, the contact must exist before the electron and hole gases can be formed. This also calls for the barrier between the two layers to be exceptionally uniform and robust. At the heart of most bilayer devices (particularly EHBLs) is this barrier that separates the two layers. For closely spaced (10 nm) bilayers, a single growth defect in an area $\sim 100\,\mu\text{m} \times 100\,\mu\text{m}$ will cause everything to be dominated by catastrophic leakage and not bilayer physics! This extremely stringent requirement on the uniformity of the barrier layer is equivalent to placing two sheets of cloth over an area of a football field while maintaining a uniform vertical distance of 1 cm between them throughout (if we scale all the lengths by a factor of a million). These issues were quite well appreciated, and the first EHBL device was made in early 1990s by Sivan et al. But this device had limited range of operation as far as the density and temperatures (above 9 K only) were concerned [19]. Only in last 3-4 years, it has been possible to make EHBLs where transport can be measured down to millikelvin temperatures, densities can be tuned over a large range, and the interlayer interaction can be made stronger than the intralayer interaction due to d/l values reaching below 1.

3.1. Recent Designs Of Electron-Hole Bilayers. The discussion in the previous section makes it clear that for an EHBL to exist in a GaAs/AlGaAs structure, the electron and hole layers must be held at different electrochemical potentials, and hence each layer must act as a gate for the other. Thus, a combination of modulation doping and biasing can be used to achieve a stable electron and hole population. Here, we describe the device fabricated by the authors' group [23, 26, 31]. We begin with an inverted hole gas created with a very low level of doping so that it can be backgated. A high level of doping would prevent the backgate from acting on the 2DHG. Exactly what level of doping would stop a gate from working is an interesting and somewhat difficult question [26]. Making contact to this hole layer is not difficult. This is usually done by depositing some gold-beryllium alloy and annealing the metal to make it diffuse into the semiconductor. See Figure 3 for a device schematic representation and Figure 4 for a self-consistent band structure.

Now, using the hole layer as a gate, we can induce an electron layer on the other side of the AlGaAs barrier (see Figure 4). Electrons start accumulating soon after the bias reaches the bandgap, provided there is some n-type ohmic contact to the electron layer, from where carriers can be pulled into the heterointerface. Fabricating such a device

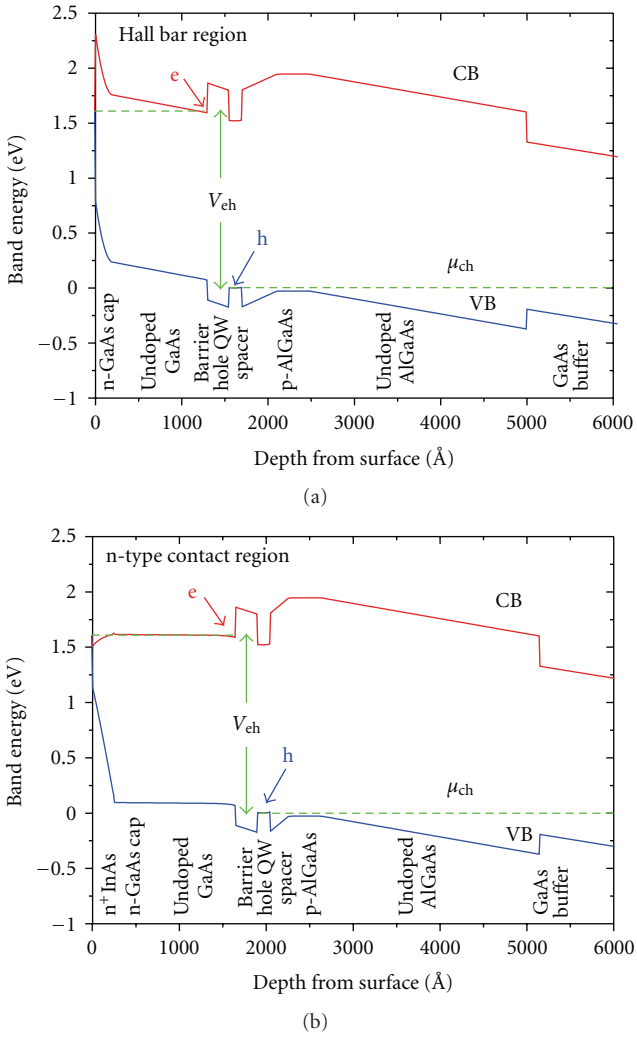

FIGURE 4: Self-consistent band structure calculations (a) of the Hall-bar region and (b) the n-type contact region of the device developed in the authors' group.

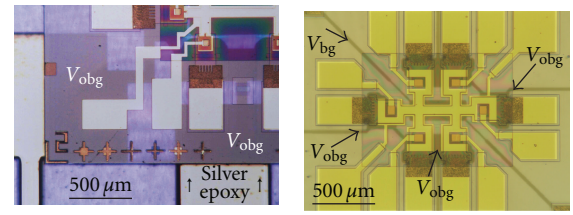

FIGURE 5: Composite IR and visible photographs (a) Backgated sample mounted on host substrate with etched channels indicated to contact backgate with silver epoxy. (b) Thinned sample with outer backgates (V_{obg}) and central backgate (V_{bg}) visible.

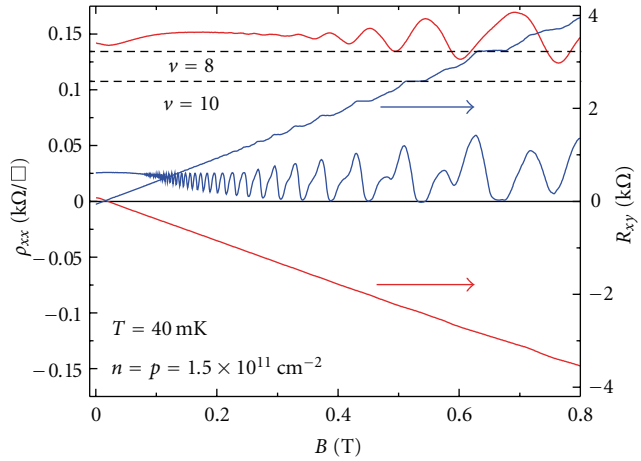

FIGURE 6: 2DEG and 2DHG in an EHBL made by the method described in [23, 26, 31] (Cavendish Laboratory).

requires some new thinking. An usual diffused ohmic would not work, because it would penetrate the barrier and reach the hole layer as well. The method would work only if we can find a "nonspiking" ohmic. Fortunately, there is a way. A heavily doped capping layer of InAs (8×10^{18} cm^{-3} Si) is used to pin the Fermi-level *above* the conduction band at the surface of the wafer. A selective etchant (conc. HCl) is used to remove the InAs from all regions except from where the n-type contacts are to be formed. Any metal which adheres well to this surface (e.g., Ti/Au) can be used to inject electrons into the InAs layer at any infinitesimal bias. A "Schottky barrier", normally observed at a metal semiconductor interface, is not formed in this case. Though calculations indicate a small barrier at the interface of the InAs and n-GaAs, unless the composition is smoothly graded, experimentally, we have not found evidence of such a barrier. A flatband condition (see Figure 4) is maintained in the region below the contacts down to the 2DEG, forming a completely "nonspiking" contact to the electron QW induced above the barrier. However, the 2DEG must not be allowed to extend out to the spiking p-type contacts, else independent contact between the two layers would be lost. A carefully controlled isolation etch is introduced between each pair of n and p contacts. The etch removes sufficient GaAs to depopulate the upper electron QW, but does not interrupt the lower hole QW. Fully independent contacts are thus achieved without the need of any depletion gates, focussed ion beam, ion implantation, or shadow masking during MBE growth. All the necessary processing can be done with standard photolithographic techniques.

A composite IR and visible photo is shown in Figure 5(b) of a finished backgated device. The three independently controllable backgates are shown ($2 \times V_{obg}$ are tied together and V_{bg}). Each backgate is contacted at each end so that its continuity can be verified.

Figure 6 shows that the electron (blue) and hole (red) layers behave as 2-dimensional layers as expected.

The crucial point is that there must be independent contacts existing to both the electron and hole layers so that we can apply a voltage bias between them to get both layers to form. Another way was shown by Seamons et al. [24]. This design relies on two back-to-back field-effect transistors (FETs), one of which is an n-channel device, and the other

is p-channel. Under such circumstances, the gate of the FET needs a small overlap with the ohmic contact to ensure that there is continuous path from the contact to the channel which has the carriers. The device is in reality less than a micron thick and has to be supported on a substrate using a method described by Weckwerth et al. [27].

3.2. The $\nu = 1/2 + 1/2$ QHE Bilayer. In closely spaced 2x2DEGs and 2x2DHGs, excitonic BEC is believed to occur in large magnetic fields in the quantum Hall regime and to be observable with transport. When both layers are in the $\nu = 1/2$ state, the half-filled Landau levels may be considered to be half full of electrons and half full of holes [32]. Striking experiments in bilayer electrons by Kellogg et al. [33], Tiemann et al. [34] and in bilayer holes by Tutuc et al. [35] reveal almost dissipationless counterflow transport and vanishing counterflow Hall resistance. While in some ways these systems emulate exciton superfluidity in an EHBL (for zero magnetic field), there does exist a vacuum of Landau levels and the screening will be very different in magnetic fields. The relation between the physics in the $\nu = 1/2 + 1/2$ and the EHBL would doubtlessly be a very interesting area in near future—however, for the purposes of this paper, we have not addressed this question.

4. The Coulomb Drag Experiment

The ability to make independent contacts to bilayers makes some new transport measurements possible. These go by names like Coulomb drag, counterflow, parallel flow transport, and so forth. and can give us some information that single-layer measurements cannot. The basic importance of the drag measurement lies in the fact that it probes the interlayer scattering rate directly. The measurement involves sending a known current through one layer (I_{drive}) and measuring the open circuit voltage developed in the other layer as a result (V_{drag}). In the linear response regime, we can define a "drag resistance" $\rho_{\text{drag}} = V_{\text{drag}}/I_{\text{drive}}$, in analogy with normal resistance. In general, this has a strong temperature dependence. The electrons in one layer can see the Coulomb potential due to the electrons (or holes) in the other layer. Of course, this potential is not the bare Coulomb potential, but it would be the "screened" potential. The net result of this scattering is that the electrons in the drive layer try to impart a little bit of the momentum they have to the electrons in the other layer. This means that if we closed the circuit in the "drag" layer, a small current would actually flow, which has got nothing to do with leakage. This is very much like viscous drag between layers of a fluid. Usually, we prevent any current from flowing in the "drag" layer. So, a small pile up of charge occurs in one end of the layer which results in a voltage appearing across the "dragged" layer. This is the voltage we measure. The interesting (and useful) point is that the magnitude of this voltage is directly proportional to the scattering rate between the particles in different layers. As in any quantum mechanical calculation, the scattering rate is a product of a "matrix element" and another factor that gives the density of available states or the phase space" factor. The scattering rate between two electron gases was first measured by Gramilla et al. in 1991 [36].

In reality, one almost always uses low-frequency (few Hz) alternating current for these measurements, the measured voltage thus has an in-phase and an out-of-phase component. It can be shown that the out of phase component is proportional to the single-layer resistance and the measuring frequency.

4.1. Boltzmann Transport Analysis of the Drag Measurement. This problem has been quite extensively analysed by several authors in the context of 2x2DEGs (or 2x2DHGs) [5, 37–40] and for EHBLs as well [16, 41], using the linearized Boltzmann transport equation. Linearization is done in the way the Fermi distribution in the drive layer is assumed to change due to the current flow. Here, we quote the final result and point out a few important relevant features. Summing over all momentum exchange (q) between particles in the driven layer (layer 2) and dragged layer (layer 1), one gets [5]

$$\rho_{\text{drag}} = \frac{\hbar^3}{8\pi^2 e^2 kT n_1 n_2} \int d\omega \int \frac{d\mathbf{q}}{(2\pi)^2} W(1,2 \longrightarrow 1',2') \times \frac{q^3}{\sinh^2(\hbar\omega/2kT)} \operatorname{Im}\left(\chi_1^0(\mathbf{q},\omega)\right) \operatorname{Im}\left(\chi_2^0(\mathbf{q},\omega)\right). \tag{2}$$

Here, $W(1,2 \rightarrow 1',2')$ denotes the probability of the elastic scattering in which the momentum of a particle changes by q. χ_1^0 and χ_2^0 denote the noninteracting susceptibilities of the layers. n_1 and n_2 denote the carrier densities. Equation (2) is applicable to 2x2DEGs, 2x2DHGs, and EHBLs. The ratio of drag resistivity to single-layer resistivity is usually a small number, even for high-mobility double quantum well structures, around $T \sim 1K$, $\rho_{\text{drag}}/\rho_{\text{singlelayer}} \sim 10^{-2}$ or so at most.

Note that individual layer mobilities ($\mu = e\tau/m^*$, where τ is the intralayer relaxation time) do not occur in the expression. This is crucial and stems from the fact that while ordinary resistance is a measure of momentum lost to to all possible channels, the drag resistance is actually a direct measure of the momentum transferred to a single channel only.

Second, at small ω, $\operatorname{Im}(\chi(q,\omega)) \propto \omega$. This is useful at low temperatures, because as the frequency increases a little, the sinh factor in the denominator would start becoming large. Thus, it is easy to estimate the low T behaviour. We do not expect $W(1,2 \rightarrow 1',2')$ to have a strong temperature dependence, because the dielectric screening function does not have strong T dependence at small T. Substituting $\hbar\omega/kT = x$, then the dominant T dependence is easy to extract. We make a very robust prediction that measured drag (interlayer scattering rate) will be approximately $\propto T^2$, and go zero as $T \rightarrow 0$, due to the nature of the Fermi distribution function alone, independent of many details. It can be shown that for "weak coupling" (i.e., high density) at $T/T_{\text{F}} \ll 1$, and for a peak-to-peak separation of the two wavefunctions, d, one gets [5]

$$\rho_{\text{drag}} \propto \frac{T^2}{d^4 (n_1 n_2)^{3/2}}. \tag{3}$$

This prediction is well verified for 2x2DEGs and 2x2DHGs.

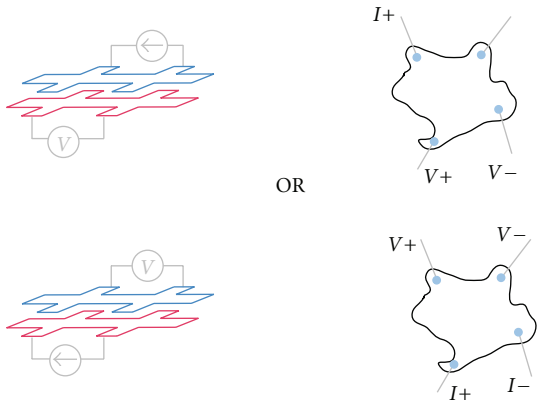

Figure 7: Schematic representation for the Coulomb drag measurement—notice that the measurement can be made in two ways. We may not look into the internal details of the sample and think of it as a "black box". Then, it just corresponds to changing the voltage and current probes, as shown on the right.

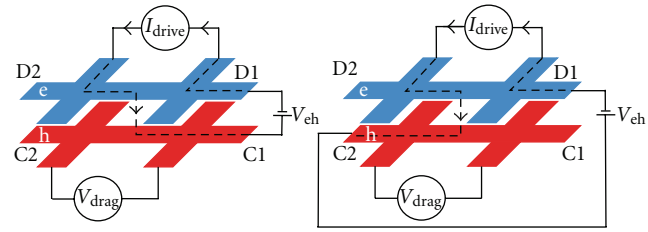

Figure 8: Diagram showing that a sign reversal of any error in drag due to excitation current leaking between layers is expected when biasing points (named C1, C2, D1, and D2) are altered, as direction in drag layer changed. A little bit of the drive current may be leaking into the other layer and flowing through a parallel path that includes part of the second layer. The resistive drop due to this would appear between the voltage probes. But it is possible to decide whether the measured voltage is due to this. If we change the point at which the second layer is grounded, the path of the leakage current would then be reversed causing the measured voltage to change. Thus, by shifting the point at which the "drag layer" is voltage referenced, we can verify if the measured voltage was due to leakage or not.

The coefficient of the T^2 term, however, requires a good model of dynamical screening of the interlayer Coulomb interaction. For the transition probability, we can use the Born approximation

$$W(1,2 \longrightarrow 1',2') = \frac{2\pi}{\hbar} \left| M_{1,2,\,1',2'}(q) \right|^2. \tag{4}$$

Here, M denotes the matrix element for a transition from state $(1,2)$ to a state $(1',2')$ The transitions are caused by the screened Coulomb potential of a particle in layer 1, as seen by another particle in layer 2. Thus, the measured drag gives us a very direct experimental handle on the generic physics of screening in a many body context. Here, we quote some of the relevant important results.

The *unscreened* Fourier component of the interaction potential due to a point charge in layer 1, as seen in the same layer ($\tilde{v}_{11}$), and in the other layer ($\tilde{v}_{12}$) can be written as

$$\begin{pmatrix} \tilde{v}_{11}(q) \\ \tilde{v}_{12}(q) \end{pmatrix} = \frac{e^2}{2\epsilon_0 \epsilon_r q} \begin{pmatrix} F_{11}(q) \\ F_{12}(q) \end{pmatrix}, \tag{5}$$

where the form factors $F_{ij}(q)$ takes into account the averaging of the potential over the subband charge distribution of each 2D gas. We can define $\tilde{v}_{21}$ and $\tilde{v}_{22}$ similarly

$$F_{ij}(q) = \int dz \int dz' \left| \psi_i(z) \right|^2 e^{-q|z-z'|} \left| \psi_j(z) \right|^2. \tag{6}$$

For infinitely narrow wells, the charge distributions approach delta functions. If these are separated by a distance d, then $F_{11}(q) = 1$ and $F_{12}(q) = e^{-qd}$.

The physically important screened components (v_{11},v_{12}) are obtained from the unscreened components ($\tilde{v}_{11}$,$\tilde{v}_{12}$) by summing the contributions of the original charge and the charges induced by the potential of the original charge. The connection is provided by the dielectric screening function $\epsilon(q,\omega)$, which is a 2×2 matrix in this case

$$\begin{pmatrix} v_{11} \\ v_{12} \end{pmatrix} = \epsilon(q,\omega)^{-1} \begin{pmatrix} \tilde{v}_{11} \\ \tilde{v}_{12} \end{pmatrix}. \tag{7}$$

The dielectric function can be written as

$$\epsilon(q,\omega) = \epsilon_r \begin{pmatrix} 1 - \tilde{v}_{11}\chi_1 & -\tilde{v}_{12}\chi_2 \\ -\tilde{v}_{21}\chi_1 & 1 - \tilde{v}_{22}\chi_2 \end{pmatrix}. \tag{8}$$

The individual layer susceptibilities can be determined from the well known expressions given by Stern [42]. From (7), we can determine the screened component v_{12} and hence determine the matrix element $M_{1,2,1',2'}$. It is also clear that the result cannot depend on whether the interaction is attractive (electron-hole) or repulsive (electron-electron and hole-hole). We thus see that within Random Phase Approximation (RPA), the (minor) differences between the EHBL and a 2x2DEG can arise from the difference in their band effective masses and the shape of the subband wavefunction for the holes. As far as the authors understand, the only way to appreciate (theoretically) the crucial difference between attractive and repulsive interaction within Born approximation is to take the next step to RPA by introducing the "local-field corrections".

RPA is known to fail for $r_s > 1$. By the inclusion of a local-field correction $G_{ij}(q)$, the short-range potentials can be improved upon $(v_{ij}(q)(1 - G_{ij}(q)))$. One approach to solving for $G_{ij}(q)$ is the Hubbard approximation [12] that includes the effect of exchange. The potentials can also be calculated self-consistently using Singwi et al. (1968) [13] (STLS) approach. This was done for the electron-electron and electron-hole bilayer by Świerkowski et al. [16, 43], who found that STLS gave a significant drag enhancement over the RPA, due to the effect of short-range correlations.

The drag resistivity in an EHBL was predicted to be larger than the electron-electron bilayer for three reasons, with the

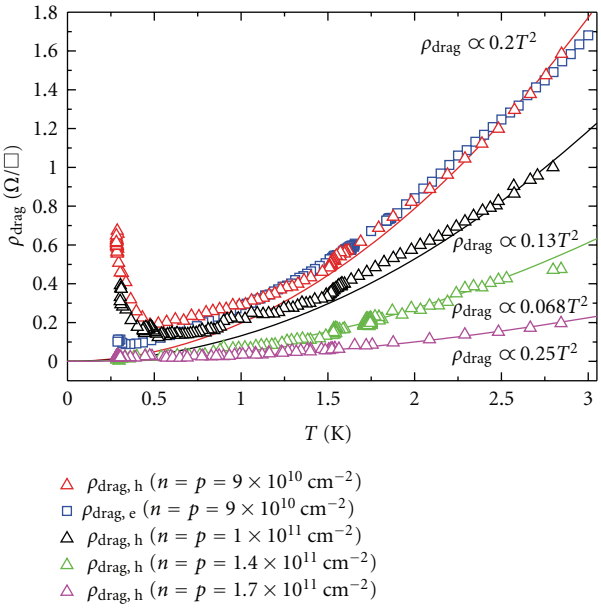

FIGURE 9: Hole drag resistivity versus temperature shown for $n = p = 9, 10, 14, 17 \times 10^{10}$ cm^{-2}, down to 300 mK. Electron drag is only shown for $n = p = 9 \times 10^{10}$ cm^{-2} for clarity. (Device: B138/C4-1-10 nm Barrier). The drag voltage was measured in two ways, by sending current through the electrons and measuring the open-circuit voltage across the holes ($\rho_{drag,h} = V_h/I_e$) or by sending current through the holes and measuring the voltage across the electrons ($\rho_{drag,e} = V_e/I_h$). As long as the current is low enough so that the system is in the linear response regime, thermodynamic arguments [54] predict that $\rho_{drag,e} = \rho_{drag,h}$.

larger hole mass responsible for two. First, the excitations in the EHBL are lower in energy, as T_F is lower for the heavier hole layer. Second, the intralayer correlations are larger in the heavier hole layer (greater r_s), which reduces the interlayer screening. The third contribution arises from the attractive interlayer interaction in the EHBL that enhances the interlayer correlations (larger pair-correlation function $g(r)$ for small r), with the opposite effect in the repulsive electron-electron bilayer. Subsequently, the interlayer local-field correction in the EHBL is negative whereas in the electron-electron case, it is positive. Hence, the modified potential in the EHBL is *larger* leading to an increased drag resistivity.

If the determinant of $\epsilon(q, \omega)$ vanishes then those regions can make large contributions to ρ_{drag}. These are the plasmon modes of the bilayer. The location of the (two) plasmon branches with respect to the single-particle excitation spectrum of the particles in the two layers in the (q, ω) plane, is an important aspect of the physics of the bilayer. These modes were studied (within RPA) by Das Sarma and Madhukar (1981) [44] and Hu and Wilkins (1991)[45]. Later work of Liu et al. (1996) [17] and Hwang and Das Sarma [41] that go beyond RPA has also highlighted how the plasmon contribution can differ in 2x2DEGs and EHBLs. However, it is not possible to get a finite drag at $T = 0$ due to contributions from the plasmon modes.

Yurtsever et al. (2003) [38] compared the 2x2DEG drag data of Kellogg et al. [46], with RPA, STLS, and their own method based on the Hubbard approach. The RPA and TF underestimate the drag whereas the STLS method gives an overestimate of the drag. Good agreement with their Hubbard model was found. Similar work was done by Hwang et al. (2003) [47] looking at data from 2x2DHG of Pillarisetty et al. [48] that had a drag resistivity 2-3 times larger than drag in corresponding electron-electron bilayers [46]. They used the Hubbard approximation and included scattering with $q \sim 2k_F$, appropriate for large r_s, and phonon-mediated drag. A deviation from T^2 was found ($T^{2.4}$) as $T \approx T_F$ for the holes and an enhanced phonon contribution for the hole-hole bilayer compared to the electron-electron system. The intralayer correlations are dependent on r_s which affects the screening at low densities. A comprehensive comparison of the predictions of various local-field theories, and the Fermi hypernetted chain approximation for Coulomb drag has been done by Asgari et al. [39], more recently.

For the RPA, STLS, and Hubbard methods, a stronger dependence on density is predicted, $(n_1 n_2)^{-2}$ [38] (rather than $(n_1 n_2)^{-3/2}$ for the TF model [5]), which has been observed [46]. The T^2 relationship is only exact in 3D. For 2D, there exist corrections from the divergences in phase space for $q \sim 0$ and $2k_F$, corresponding to forward and backward transitions on the Fermi surface. A correction proportional to $T^2 \ln T$ is expected [49], but should be small. This correction is believed to have been observed in low-density electron-electron bilayers [46].

A similar temperature dependence of $-T^2 \ln(T/T_\tau)$ ($T_\tau \equiv \hbar/k_B\tau$) is expected [50], when a large amount of disorder ($l < d$, where l is the mean free path) is included at very low temperatures.

Hwang and Das Sarma [41], calculated the drag resistivity (and single-layer resistances) for EHBLs with parameters fitted to the devices of Seamons et al. [51, 52], with 20 nm and 30 nm barriers. Using local-field corrections and dynamical screening, they were able to show that the coupled bilayer plasmon modes in the EHBL greatly enhance the drag resistivity with respect to the electron-electron and hole-hole bilayers.

5. Coulomb Drag in Electron-Hole Bilayer: Experimental Results

Coulomb drag at $T < 1$ K in EHBLs in a regime where $d/l \sim 1$, has recently been measured by the authors' group and an experimental group in Sandia [51, 53]. Our results show that drag measured in a device with a 10 nm $Al_{0.9}Ga_{0.1}As$ barrier (device B138/C4-1) is shown in figure 9 for matched electron and hole densities ($n = p$). For the two highest densities ($n = p = 1.4, 1.7 \times 10^{11}$ cm^{-2}), the hole drag resistivity is monotonic over this temperature range and appears to go towards zero as the temperature does. However, for the lower-density traces ($n = p = 9, 10 \times 10^{10}$ cm^{-2}), an upturn is seen in the hole drag. The lower-density trace has a larger upturn and the corresponding electron drag trace ($n = p = 9 \times 10^{10}$ cm^{-2}) is also shown. Only a very

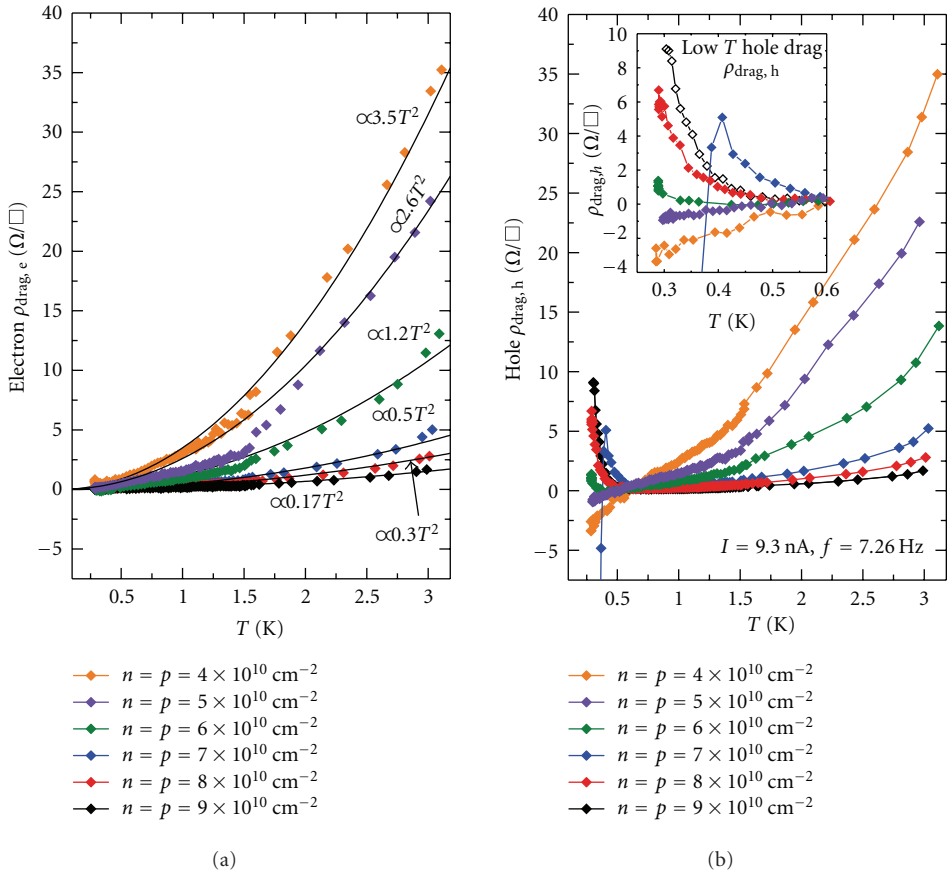

FIGURE 10: Drag resistivity measured on electron (a) and hole layer (b) versus temperature for $n = p = 4, 5, 6, 7, 8, 9 \times 10^{10}$ cm^{-2}, down to 300 mK. (Inset) Expanded low-temperature drag resistivity measured on hole layer. For the lowest density, $k_F d \approx 1.25$, $r_{s,e} = 2.8$, and $r_{s,h} \approx 14.1$. (Device: B138/C4-2-10 nm Barrier).

small upturn (if any) is found in the electron drag, with $\rho_{\text{drag},h} \neq \rho_{\text{drag},e}$ below ~1 K.

In another 10 nm barrier device (B138/C4-2) fabricated from the same wafer (I.D. A4268), lower-matched densities could be reached. Electron and hole drag resistivities are shown in Figure 10 for $n = p$ between 4 and 9×10^{10} cm^{-2}. The high-temperature drag is a good fit to T^2 and $\rho_{\text{drag},h} = \rho_{\text{drag},e}$. For 9×10^{10} cm^{-2}, the T^2 coefficient is similar ($\sim 0.2\,\Omega/\square\text{K}^{-2}$) to the first device B138/C4-1 (see Figure 9). At lower densities (Figure 10), the upturn does not increase (as seen in Figure 9) but becomes smaller, with the lowest two densities ($4, 5 \times 10^{10}$ cm^{-2}) displaying no upturn at all and a *sign-reversal* at the lowest temperatures. For an intermediate density 7×10^{10} cm^{-2}, the upturn is followed by a sharp negative downturn around 300 mK. In contrast, the electron drag resistivity remains monotonic and follows the expected T^2 dependence for two Fermi liquids. It is interesting to note that the departure from the T^2 dependence in the hole drag is relatively insensitive to density and occurs at ~700 mK. Note that at $n = p = 4 \times 10^{10}$ cm^{-2}, $d/l \approx 0.5$ is reached.

Nonreciprocity at low temperatures is an unexpected and puzzling result, since the drag is clearly in the linear regime. The drag resistivity was found to be independent of the excitation current frequency, up to ~100 Hz. Switching the grounding point between the layers can detect whether the measurement circuit is equivalent in the two drag configurations. Shifting the grounding and bias points was found not to affect the anomalous low-temperature data. At higher temperatures, the drag is reciprocal, this too verifies that the measurement circuit is set up correctly. The following section reports drag measured in EHBL devices below 300 mK in a dilution refrigerator.

5.1. Coulomb Drag down to 50 mK. Coulomb drag in sample B138/C4-1 was measured down to 50 mK. In Figure 11, drag is shown for $n = p = 9, 11 \times 10^{10}$ cm^{-2}. For the 9×10^{10} cm^{-2} traces, the high-temperature dependence is similar to that in Figure 9 measured in a different system. An upturn in the hole drag is seen, which appears to be larger for the lower density. Deviation from T^2 appears at a higher temperature for the lower density. However, for this density, below 250 mK the hole drag peaks and starts falling. A smaller upturn is seen in the electron layer, despite the I-V plot (Figure 11(b)), showing that the electron drag is still linear down to lower excitation currents (0.5 nA).

In a 25 nm barrier, undoped device (B135/C3-4) with resulting higher hole mobilities, the drag resistivity measured down to 35 mK is shown in Figure 12 for

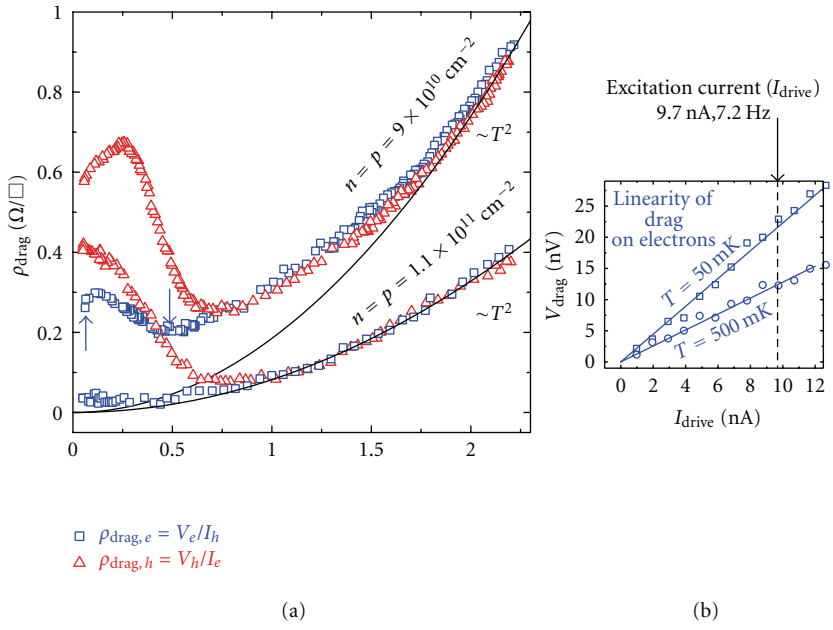

FIGURE 11: (a) Electron and hole drag resistivities versus temperature for $n = p = 9$ and 11×10^{10} cm^{-2} versus temperature, down to 50 mK. T^2 coefficients are 0.08 and 0.19 Ω/□K^{-2}, respectively. (b) I-V trace for drag on electron layer for $n = p = 9 \times 10^{10}$ cm^{-2}, indicated by arrows (a). Electron and hole layer mobilities at $T = 1.5$ K, $\mu_e = 1.5 \times 10^6$ cm^{2}V^{-1}s^{-1} and $\mu_h = 1.1 \times 10^5$ cm^{2}V^{-1}s^{-1}. (Device: B138/C4-1-10 nm Barrier).

$n = p = 7, 11 \times 10^{10}$ cm^{-2}. For the lower-density traces, an upturn is seen in the hole drag, though it peaks, then falls and below 200 mK saturates at a small negative value. As shown in Figure 12(b), even the negative hole drag appears to be linear down to small currents. But the corresponding electron drag trace still appears to follow the T^2 dependence. The features in the low-temperature drag are not hysteretic with temperature. All points were taken as the sample was cooled, except the I-V traces that were taken as the sample was warmed. The resistances corresponding to these traces are shown as black circles in Figure 12 and agree well with the other data. Figure 12(c) shows the in- and out-of-phase component of the hole drag signal for $n = p = 7 \times 10^{10}$ cm^{-2}. This shows no anomalies in the out-of-phase signal coincident with the anomalous behaviour seen in the in-phase signal, ruling out artefacts from capacitive effects or ohmic contact failure. For the higher-density traces ($n = p = 1.1 \times 10^{11}$ cm^{-2}), a small upturn in the electron drag is seen whereas a small negative downturn is seen in the hole drag (see inset, Figure 12).

For an excitonic superfluid phase, an upturn in the drag is predicted that would diverge, approaching the single-layer resistivities [6], which themselves would diverge as the number of unpaired electrons and holes that are able to carry single-layer current fall. But such a strong effect is not seen. Besides in the excitonic phase, there is no reason to expect Nonreciprocity. Electrostatic binding within an exciton may explain the upturn seen in the drag and departure from the behaviour expected for weak particle-particle scattering. However, an excitonic phase is unlikely to have a preference for the lighter or heavier layer and cannot account for the lack of reciprocity seen at low temperatures. An indicator for the presence of excitons would be an enhancement of the drag at $n = p$, particularly for a BCS-like state where nesting of the electron and hole Fermi surfaces is required.

5.1.1. High-Temperature T^2 Dependence. The magnitude of drag in the EHBL is expected to be greater than in electron-electron and hole-hole bilayers, due to the additional plasmon enhancement [41] and due to larger correlations between the layers [55], including the high-temperature ($\sim T^2$) regime. The T^2 coefficient ($\rho_{drag} = AT^2$) for the data in Figure 10 (10 nm barrier) can be compared with that for 10 nm barrier electron-electron and hole-hole bilayers. The electron-electron data of Kellogg [56] for $n_1 = n_2 = 5 \times 10^{10}$ cm^{-2} gives a coefficient of $A = 0.3\,\Omega/\square K^{-2}$, compared to $A \approx 2.6\,\Omega/\square K^{-2}$ in the EHBL. This shows an enhancement by a factor of ~9. In the hole-hole bilayer of Pillarisetty et al. [48], for $p_1 = p_2 = 7 \times 10^{10}$ cm^{-2}, $A \approx 0.7\,\Omega/\square K^{-2}$ compared to $A \approx 0.5\,\Omega/\square K^{-2}$ in the EHBL. These are similar, despite the hole-hole bilayer having a larger r_s in both layers. However, at these densities, for an accurate comparison, the correction to account for the different r_s must be made.

Comparing the data in Figures 10 and 12 for 10 nm and 25 nm barrier devices at $n = p = 7 \times 10^{10}$ cm^{-2}, the dependence on interlayer separation d can be examined. The respective T^2 coefficients are $A = 0.5\,\Omega/\square K^{-2}$ and $A = 0.051\,\Omega/\square K^{-2}$, a ratio of ~10. By measuring the interlayer capacitance, the wavefunction peak to peak d can be estimated. The 10 nm and 25 nm barriers correspond to d of 25 nm and 40 nm, respectively. From (3), one expects $A \propto d^{-4}$. Hence, an expected ratio of

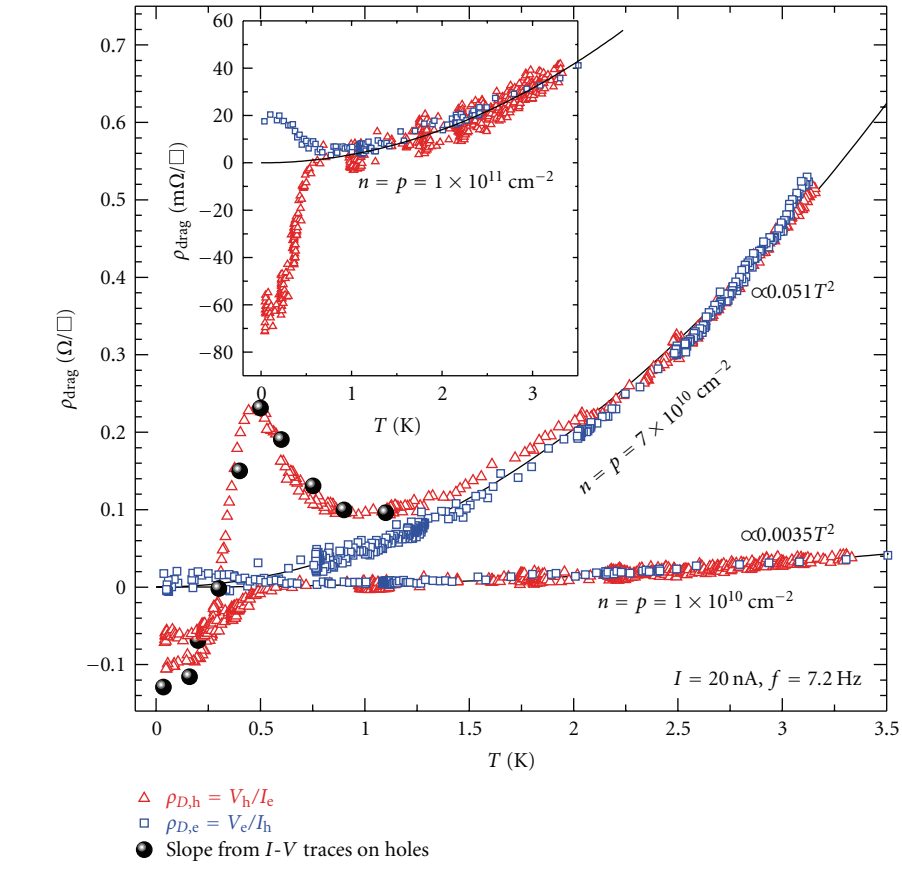

(a)

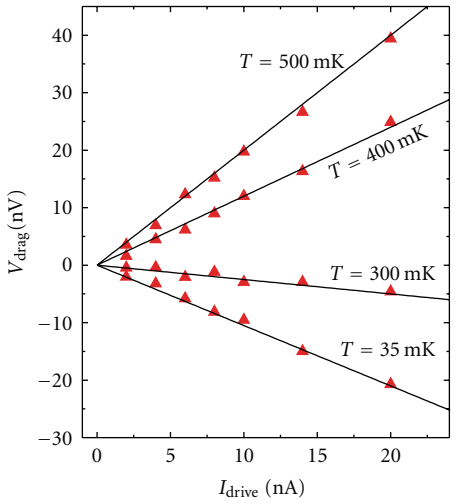

(b)

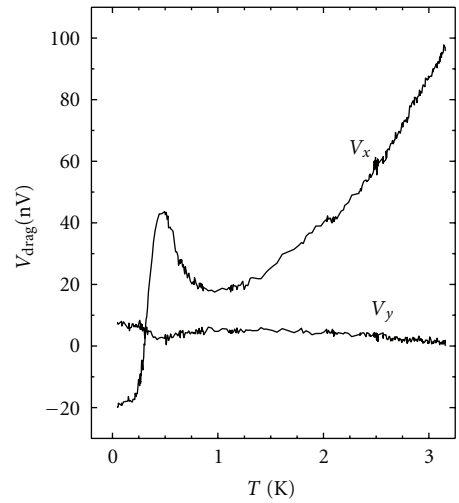

(c)

FIGURE 12: (a) Electron and hole drag resistivity versus temperature for $n = p = 7$ and 11×10^{10} cm^{-2} versus temperature, down to 50 mK. T^2 coefficients are 0.0035 and 0.051 Ω/□K^{-2}, respectively. (b) I-V (a.c. $f = 7.2$ Hz) trace for drag on hole layer for $n = p = 9 \times 10^{10}$ cm^{-2} at temperatures indicated. The resistances found from these slopes are displayed on (a). (c) In- and out-of-phase components of the drag voltage (V_{drag}) for the $n = p = 7 \times 10^{10}$ cm^{-2} trace. Electron and hole layer mobilities for $n = p = 7 \times 10^{10}$ cm^{-2} at $T = 1.5$ K; $\mu_e = 6.8 \times 10^5$ cm^{2}V^{-1}s^{-1} and $\mu_h = 3.3 \times 10^5$ cm^{2}V^{-1}s^{-1}. (Device: B135/C3-4-25 nm Barrier).

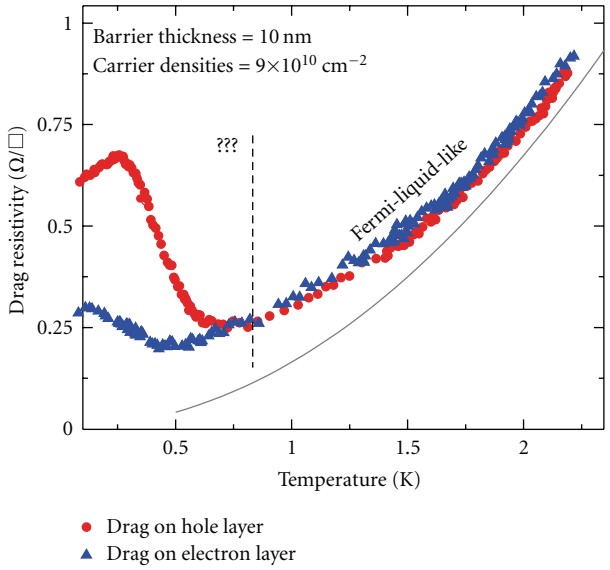

Figure 13: Electron (blue) and hole (red) drag resistivity versus temperature for $n = p = 9 \times 10^{10}\,\mathrm{cm}^{-2}$, down to 50 mK. The data of Figure 11 is reproduced along with the result of the calculation (solid line) described in the text. We considered a cosine wavefunction for the holes and a Fang-Howard type wavefunction for the electrons.

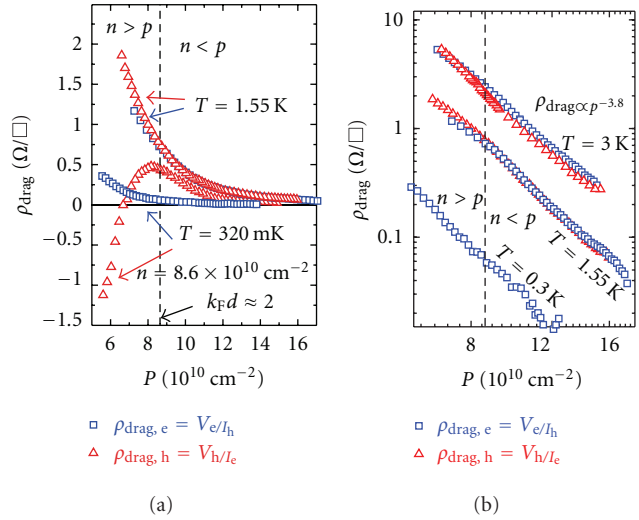

Figure 14: Electron and hole drag resistivities with electron density held constant at $n = 8.6 \times 10^{10}\,\mathrm{cm}^{-2}$ versus hole density at $T = 320$ mK, 1.55 K, and 3 K. (Device: B138/C4-1-10 nm Barrier).

$d^4_{(25\,\mathrm{nm})}/d^4_{(10\,\mathrm{nm})} = 40^4/25^4 = 6.6$, close to the measured 10. An increase in interlayer correlations with reducing separation may explain the enhancement over the expected value. The density dependence of the T^2 coefficient is examined next.

We have been able to describe our high-temperature (above 1 K) drag measurements using the linear Boltzmann formalism as in (2), provided that the average intralayer particle spacing is smaller than the average interlayer particle spacing. We used a simple model with temperature-dependent Lindhard functions and accounted for the finite-thickness of the wavefunctions. Intralayer correlations were taken into account using a Hubbard local-field correction as described by Yurtsever et al. [38], but interlayer correlations were neglected. We also neglected phonon effects. This model works well for 10 nm and 25 nm barrier devices at high enough densities (see Figure 13). For very low densities, the model underestimates the drag, suggesting that interlayer local-field corrections might be large because particles in different layers are closer together than particles in the same layer. We have also noticed that the calculated drag is sensitive to the shape of the wavefunction. However, the low-temperature drag observations cannot be explained by a Boltzmann-type even if local-field corrections are taken into account.

5.2. Drag at Mismatched Densities. Data at constant electron density ($n = 8.6 \times 10^{10}\,\mathrm{cm}^{-2}$) with p varied, is shown for device B138/C4-1 in Figure 14. At higher temperatures ($T = 1.55$ K and 3 K), where the anomalous drag is not seen, agreement is found between the electron and hole drags, and a good fit to a power-law dependence is found ($\rho_{\mathrm{drag}} \propto p^{-3.8}$). At the lowest temperature, the electron drag still has the same power-law dependence on p. However, as p is lowered the hole drag no longer agrees with the electron drag, and exhibits the upturn found in Figure 9 at $n = p = 9 \times 10^{10}\,\mathrm{cm}^{-2}$. A maximum is seen in the hole drag close to $n = p$, but for $n > p$ a sharp downturn that goes *negative* is found. It is unclear from these observations whether $n = p$ or the value of the hole density ($k_F d \approx 2$, transition to large-angle scattering) is important, and more work is required to analyse this point. However, achieving the upturn is not dependent on matching the densities exactly. This point was also investigated by Morath et al. [52]. While a peak is seen in the hole drag close to matched densities (Figure 14), it cannot be concluded that this is excitonic (or phonon/plasmon) in origin.

Considering the data in Figure 10 for $n = p$, the T^2 coefficients are plotted against layer density ($\rho_{\mathrm{drag}} = AT^2$) in Figure 15. A power-law dependence for $A \propto n^a p^b$, with $a + b = -4.0$ is found. This total has been predicted by the RPA, Hubbard-like and STLS calculations performed by Yurtsever et al. [38] for the electron-electron bilayer. These go beyond the (high-density) weak coupling limit (TF) where $(np)^{-3/2}$ is predicted (3). In Figure 14, a dependence of $\rho_{\mathrm{drag}} \propto p^{-3.8}$ is found, which together implies a weaker dependence ($|a| < |b|$) on n rather than p. For drag taken when the hole density is held constant at $p = 1.5 \times 10^{11}\,\mathrm{cm}^{-2}$ and the electron density is varied (data not shown), the T^2 coefficient is plotted in Figure 15 against n, showing $A \propto n^{-0.5}$. Some inaccuracy will occur as the interlayer separation (d) is to some extent a function of the interlayer bias that determines the electron density. This effect was studied by Morath et al. [57]. Similarly, the position of the hole wavefunction will be affected by the backgate bias. Depleting holes will push the wavefunction peak towards the barrier. Nevertheless, it is expected that the drag will be more sensitive to the layer with greater r_s [47, 48]. Earlier work in the EHBL showed the

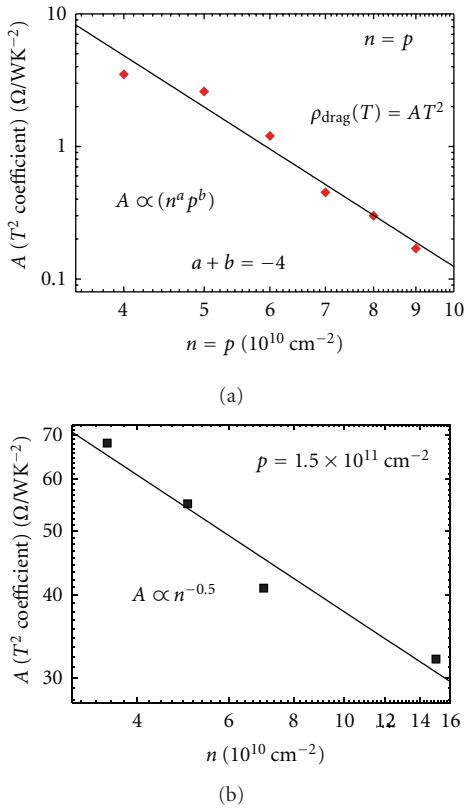

FIGURE 15: Fit for T^2 coefficient A for ρ_{drag} with p constant $p = 1.5 \times 10^{11}$ cm^{-2} and n varied (b) (data not shown). Same for $n = p$ (data shown Figure in 10) (a). (Device: B138/C4-1 (a), B138/C4-2 (b) −10 nm Barrier).

opposite result that the drag was found to be more sensitive to the electron density [19], but this work was performed above $T = 9$ K, where other processes such as phonon-mediated drag will be significant.

5.3. Interlayer Leakage. In all biased structures, finite leakage currents will exist. In the EHBL, the interlayer bias (∼1.5 V across ∼10 nm) acts across a small distance and measurable leakage exists, though it is typically far smaller than the measurement currents used. In the best devices, $I_{leak} \approx 100$ pA, while the measurement currents are typically between 0.5–10 nA. The effect of the leakage current on transport measurements is important, particularly if it can influence the drag measurement or the state of the system. There are several possible mechanisms whereby leakage can influence measurements directly. Firstly, the electrons/holes that leak through the barrier will be much hotter than the 2DHG and 2DEG, which will have reached thermal equilibrium with the lattice. It must be possible for these energetic particles to lose this energy on a shorter timescale (thermalisation time) than the characteristic lifetime of any coherent phase existing in the bilayer, so that the leakage event will be forgotten quickly by the system. Likewise, the leakage events must be infrequent, relative to the phase lifetime (such as the lifetime of an exciton).

As discussed earlier, the leakage is most likely caused by barrier defects and carriers will probably lose energy via transitions through defect states that exist mid-gap. In this respect, backgate leakage is not likely to be as important. While much larger biases are used, a charged particle is unlikely to travel the distance from the backgate to the 2DHG ballistically, and energy will be dissipated to the lattice. It is necessary for the particles to be in local equilibrium for the true ground state to emerge, despite the two layers being at different electrochemical potentials. It is unknown how much leakage will affect this condition. For a superfluid-like state, the lifetime due to leakage between the layers must be larger than $\tau \sim \hbar/\Delta$, where Δ is the energy gap. For the effect of the gap to be observed, we need $T \lesssim \Delta/k_B$, which assuming a lowest measurable temperature of 50 mK, gives a bound of $\tau < 150$ ps. A typical interlayer leakage current in our device is ∼50 pA, over an area ($A_{overlap}$) of 0.14 mm^2 (including any leakage due to radiative recombination). The characteristic timescale between leakage events (how long the particle remains in one layer) is $\tau_{leak} = enA_{overlap}/I_{leak}$. Hence, an approximate leakage lifetime (for $n = p = 1 \times 10^{11}$ cm^{-2}) is $\tau_{leak} \sim 0.4$ s, which is much longer than any typical transport lifetime ($\tau_{drag} \sim 10$ ns, $\tau_{xx} \sim 10$ ps) in these devices and any lifetime corresponding to a gapped phase that could exist within the measured temperatures.

The drag resistivity at low temperatures is typically smaller than 1 Ω/□, and stray currents can adversely affect the measurement due to the larger single-layer resistivities. All measurements were conducted with a.c. phase sensitive detection. Incoherent d.c. leakage cannot contribute directly to an error in the measurement. However, a weak point in the barrier may allow a path for the a.c. excitation current to cross into the other layer and return via the interlayer bias supply (battery) (Figure 16), which appears to the a.c. as a low resistance path. As shown in Figure 16(a), by changing the interlayer biasing points, the effect can be reversed. For device B138/C4-2 at $n = p = 8 \times 10^{10}$ cm^{-2}, changing the bias has little effect on the Nonreciprocity or the upturn in the hole drag. The electron drag is also unaffected.

6. Discussion

Features are seen in the drag resistivity at low temperatures that cannot be explained within the framework of Fermi-liquid theory [41]. For two Fermi gases, the phase space allowed for interlayer particle-particle scattering must go to zero as the temperature does.

Qualitatively, similar anomalous behaviour is seen in two 10 nm barrier devices, with an upturn below 0.5 K that may be followed by a downturn or sign reversal at the lowest temperatures, for the lowest densities (Figures 10 and 14). The magnitude of the upturn differs by a factor of ten between devices (for the $n = p = 9 \times 10^{10}$ cm^{-2} at 300 mK, Figures 9 and 10), with the high-temperature drag ($\sim T^2$) agreeing well. This would suggest that sample-dependent factors such as disorder might be important in the anomalous regime. Anomalous behaviour also occurs at larger layer separations (25 nm barrier), consistent with the

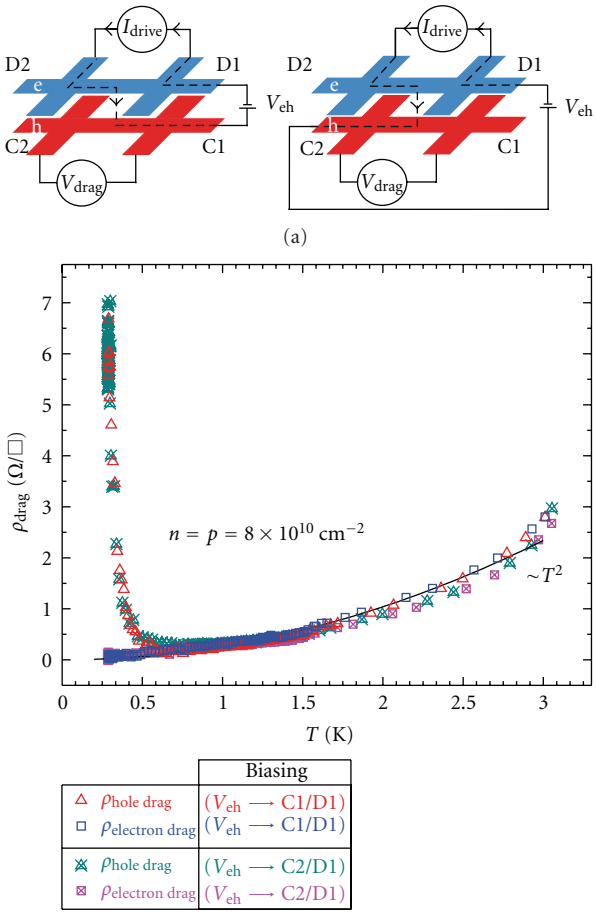

FIGURE 16: (a) Diagram showing that a sign reversal of the error in drag due to the excitation current leaking between layers is expected when biasing points (named C1, C2, D1, and D2) are altered, as the leakage current direction in the drag layer is changed. (b) Electron and hole drags for the two interlayer biasing configurations, for $n = p = 8 \times 10^{10}$ cm^{-2}. (Device: B138/C4-2-10 nm Barrier).

findings of Seamons et al. (2009) [51], where a small upturn was found in 20 nm barrier samples but not for 30 nm.

Third-order corrections to the interlayer interaction by Levchenko and Kamenev [58], showed that nonzero drag at $T = 0$ was possible, and so does not necessarily indicate the presence of strong interlayer correlations. However, the effect they find is small ($\sim 10^{-4}\,\Omega$/W), particularly for high-mobility samples, and cannot explain the anomalous drag seen ($\sim 1\,\Omega$/W).

The deviation is too large to be caused by a plasmon or phonon enhancement [28, 36], which would be peaked at matched densities and higher temperatures. Plasmon enhancement is expected at $T \sim 0.2T_F$ ($T_{F,e} > 16$ K, $T_{F,h} \gtrsim 3$ K), while below the Bloch-Grüneisen temperature (~ 1 K), the phonon contribution is heavily suppressed.

6.1. Coulomb Drag Upturn. The upturn in the Coulomb drag (Figure 9) at the lowest temperature, may be a signature of an increased interlayer coupling due to the formation of excitons. This coupling is not suppressed by the falling phase space with temperature, restricting scattering at the Fermi surfaces. Within the exciton regime, distinct Fermi surfaces no longer exist when the binding energy exceeds k_BT, lifting this phase-space restriction.

The transition temperature for an excitonic superfluid state (assuming a 2D Kosterlitz-Thouless type transition), is expected to increase with exciton density (in 2D $T_c = n_{ex}\hbar^2/0.71m^*_{ex}k_B$, (1)), where n_{ex} is the exciton density. Seamons et al. [51] attempted to identify the temperature of the minimum in the drag as the transition temperature, arguing that this point occurs at higher temperatures for larger densities. It is possible to see the same trend in Figures 9 and 11, though in the latter the deviation from T^2 clearly occurs at a higher temperature for the lower-density data ($n = p = 9 \times 10^{10}$ cm^{-2}). This point of deviation may be more significant than the drag minimum.

However, the upturn is far smaller than that predicted for an excitonic state [6, 8, 10]. The drag is anticipated to reach a value approaching the single-layer resistivities, with a sharp change (discontinuity) signifying the phase transition (unless only a small fraction of electrons and holes enter a paired state). Hu [8] predicted an enhancement due to electron-hole pair fluctuations above the transition rising as $\sim T^2/\log(T/T_c)$. Fitting this to an upturn to obtain T_c is possible (Morath et al. (2009) [52]), but it cannot explain the subsequent downturn seen in Figures 11 and 12. The prefactor to the expression predicted by Hu [8], is larger (by a factor of $\sim$1000) than the upturn measured [52]. For the drag at mismatched densities (Figure 14), the peak expected at $n = p$ is not seen. The peak in the figure is not sharp enough and is asymmetric. As discussed earlier, it is unclear whether $n = p$ or k_Fd plays a role in the peak. Crucially, matched densities are not necessary to see the upturn.

Other indicators for an excitonic phase could include a temperature dependent Hall voltage, since neutral excitons would not feel the Lorentz force. The authors had looked for this effect, but not observed it in their experiments.

6.2. Coulomb Drag Sign Reversal. At the lowest temperatures, in 10 nm and 25 nm barrier samples, a sign reversal of the drag resistivity has been seen. In this situation, driving the current in one layer in one direction causes particles in the other layer to move in the *opposite* direction. Sign reversal has been seen for drag between layers at large filling factors (moderate magnetic fields) in the quantum Hall regime [59–63]. Partly filled Landau levels, possess electron and hole character. If the highest Landau levels in the drag and drive layers have opposite deviation from half filling, then ρ_{drag} is negative (electron-hole like) at low temperatures. At higher temperatures when k_BT is larger than the disorder broadened width of the Landau level ($\hbar/\tau$), then the drag returns to the zero magnetic field (positive) sign. For nonzero drag, the excitations at the Fermi surface must not have particle-hole symmetry [60, 63]. At the centre of a disorder broadened Landau level, this symmetry is acquired and the drag goes to zero. Varying the magnetic field will change the Landau level

populations and a complex series of positive and negative drag oscillations results.

Figure 12 shares many of the features seen in the temperature dependence of magnetodrag in an electron-electron bilayer [63] at $\nu = 7.7, 9.5$, where a peak is followed by a downturn. It is not immediately clear how the banding (density of states) required for this would occur at zero magnetic field. For 2DHG and 2DEG, $E(k)$ is expected to be continuous and the concept of disorder broadening cannot be applied.

Alkauskas et al. (2002) [64] have proposed that a sign reversal in the drag resistivity may result from the inclusion of an in-plane periodic potential, with wavelength much greater than that of the underlying atomic lattice. This extra periodicity creates an additional Bragg plane and the formation of minibands, with a bandgap at much smaller k, at the Brillouin zone boundary corresponding to the large wavelength of this additional potential. They found that as the density was increased, a sign reversal would occur. Normally, particles exist within the parabolic bottom of the band and are scattered before they reach the zone boundary. If the Brillouin zone is smaller, then the point at which $\partial^2 E/\partial k^2$ $(= \hbar^2/m^*)$ changes sign is attainable at experimental densities, leading to a sign change in the effective mass and a sign reversal in the drag resistivity. But for this to be relevant, a periodic solid-like phase must appear in the EHBL. Candidates for this include the Wigner crystal, where one or both layers has crystallised into a periodic array overlaying each other [65] or a spontaneous periodic modulation in charge density, known as a charge density wave [55]. These possibilities would be discussed further in the context of the single-layer resistivity measurements.

6.3. Drag Reciprocity. It is expected that for measurements in the linear regime, the hole and electron drag resistivities should be equal [54, 66, 67]. At the lowest temperatures, where the deviation from T^2 is found, a Nonreciprocity between $\rho_{\mathrm{drag},e}$ and $\rho_{\mathrm{drag},h}$ is observed, despite the measurements appearing to be in the linear regime. The measurement circuit is not the cause of the Nonreciprocity as the drag is reciprocal at higher temperatures. The effect of interlayer leakage was discussed before as a possible source of error, but in our experiments, we have verified that this gives no noticeable contribution (Figure 16).

Measurements of Coulomb drag down to 300 mK on EHBLs has been performed by Seamons et al. (2009) [51, 52], on samples with 20 nm and 30 nm barriers and similar densities. For the narrower barrier, a small upturn is found only in the drag measured on the holes ($\sim 0.4\,\Omega$/W). This Nonreciprocity was explained as a result of additional Joule heating caused by passing current through the more resistive hole layer for the electron drag configuration. They report saturation in the electron Shubnikov-de Haas oscillations at about 1 K, when the same current used for drag is passed through the hole layer. Single-layer measurements reported by Seamons et al. on the hole layer require a much smaller current than that used for drag, so heating was avoided.

Joule heating cannot explain the Nonreciprocity found in this work. Heating will be a nonlinear effect ($\sim I^2$R), but no nonlinearity is found in the I-V traces of the drag resistivity. For the data taken in Figure 9 at $n = p = 9\times10^{10}$ cm^{-2}, at the lowest temperature, the two-probe resistance of the electron and hole layers differed by a factor of 9 (hole 2-probe 62 kΩ, electron 2-probe 7.2 kΩ). The two and four-probe (single-layer) resistances of the hole and electron layers are shown in Figure 17 as a function of temperature. Reducing the current by a factor of three will give the same Joule heating for the electron drag configuration as for the hole drag. But nonlinearities are not seen in this range (Figure 9). Indeed the same currents were used for single-layer measurements as for drag and no saturation of Shubnikov-de Haas amplitude with temperature was seen.

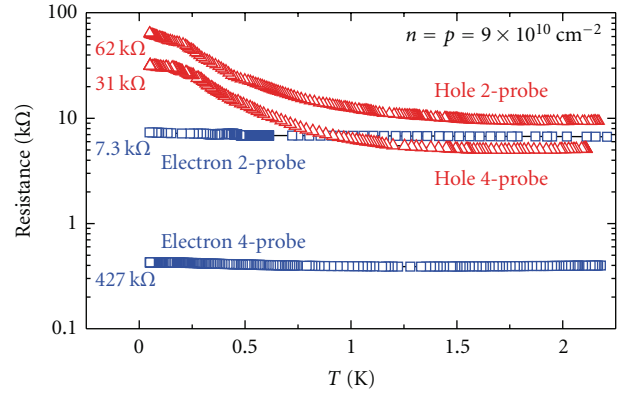

Figure 17: Two-probe and four-probe resistance of the electron (blue squares) and hole (red triangles) layers versus temperature, at $n = p = 9 \times 10^{10}$ cm^{-2}. (Device: B138/C4-1-10 nm Barrier).

7. Features in Single-Layer Resistivity: An Interaction-Driven Insulating State

In our EHBL devices it is possible to perform experiments with only the 2DHG present. This is achieved by keeping the interlayer bias below the threshold for electron accumulation ($V_{\mathrm{eh}} \approx 1.55$ V) and biasing both backgates negatively to induce holes in the QW. The hole density can then be controlled with the central backgate V_{bg}. The temperature dependence (0.3 to 1.5 K) of the single-layer resistivity of the holes is shown in Figure 18(a). As the density is lowered, there is a transition from metallic to insulating behaviour between 5 and 6×10^{10} cm^{-2}. These features are consistent with results from several 2DMIT studies of Silicon MOSFETs and GaAs/AlGaAs-based devices. The crossover occurs as expected close to $\rho_{xx} \approx h/e^2$ or equivalently to $k_F\ell = 1$, with $d\rho_{xx}/dT > 0$ for $\rho_{xx} < 25.8\,\mathrm{k\Omega}/\square$ and $d\rho_{xx}/dT < 0$ for $\rho_{xx} > 25.8\,\mathrm{k\Omega}/\square$. At $k_F\ell = 1$, the mean free path (ℓ) is approximately equal to the interparticle separation (l). Non-monotonic behaviour is observed for the $p = 6 \times 10^{10}$ cm^{-2} trace, which is insulating above $T \sim 0.8$ K and metallic below. This has been observed before in 2DHGs [68] and in an EHBL with a 30 nm barrier [57] and can be explained within Fermi liquid theory [69].

Most striking is the change in behaviour of the hole layer with the addition of the electron layer (kept in an

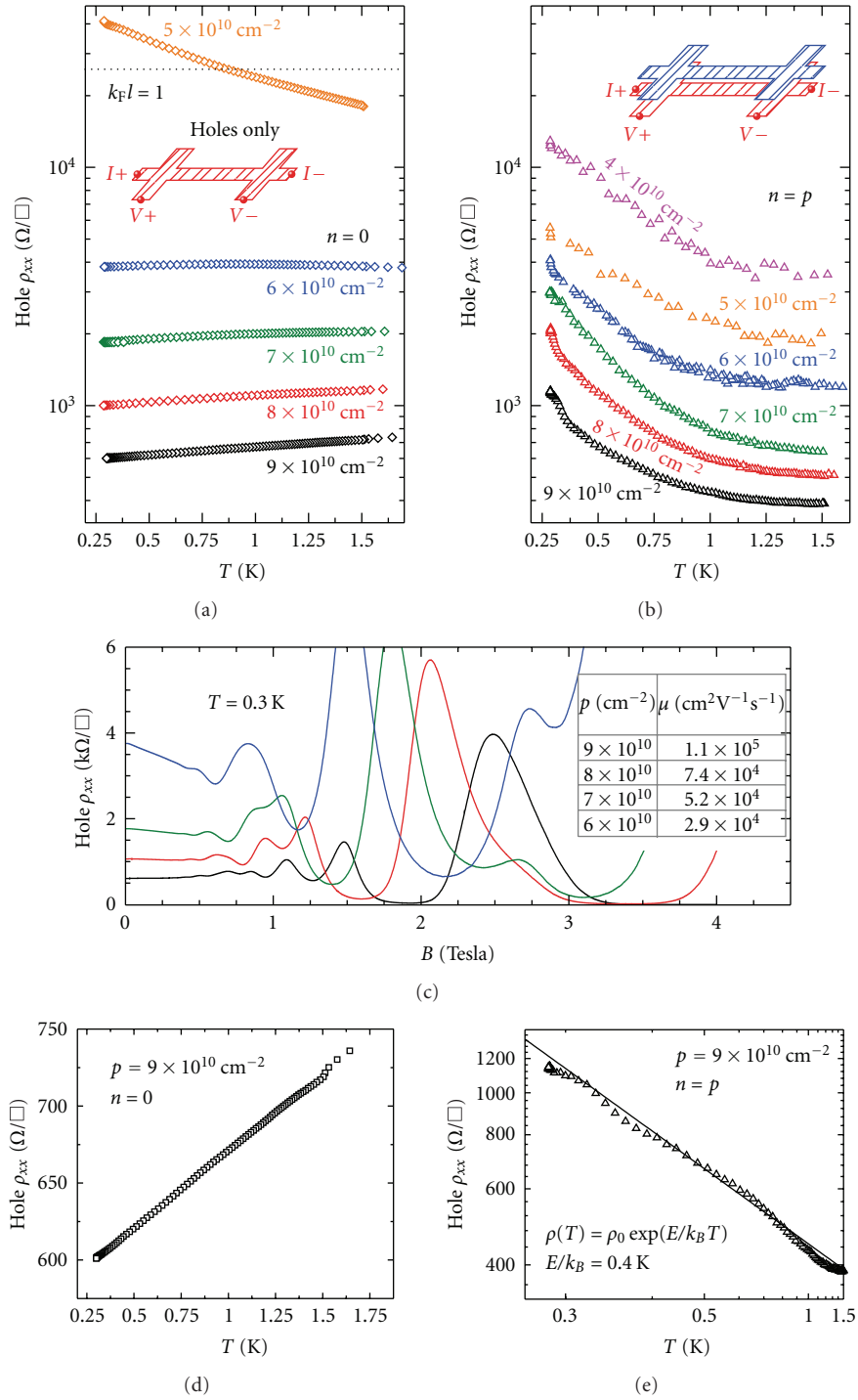

FIGURE 18: Resistivity of hole layer versus temperature for $p = 5, 6, 7, 8, 9 \times 10^{10}$ cm^{-2} at $B = 0$, (a) without electrons ($n = 0$) and (b) with electrons ($n = p$). (c) Magnetoresistance $\rho_{xx}(B)$ of hole layer for $p = 6, 7, 8, 9 \times 10^{10}$ cm^{-2} with no electrons present ($n = 0$), at $T = 0.3$ K. (d) "Metallic" hole layer $\rho_{xx}(T)$ for $p = 9 \times 10^{10}$ cm^{-2}, $n = 0$. (e) Arrhenius plot ($\ln(\rho)$ against $1/T$) for "insulating" hole layer $\rho_{xx}(T)$ with $n = p = 9 \times 10^{10}$ cm^{-2}, showing good fit to an exponential rise. (Device: B138/C4-2-10 nm Barrier).

open-circuit configuration), [70, 71] shown in Figure 18(b). All traces are now clearly insulating by $T \sim 1$ K, *even* those that had been metallic. This insulating state is occurring at $k_F \ell > 50$, with resistivity at $T = 1.5$ K far below the regime where a transition to insulating behaviour is expected. Localisation due to background disorder (impurities/dopants/defects) cannot account for this because the 2DHG sees the same disorder with and without the 2DEG present. Placing a plane of mobile charge next to the 2DHG is expected to improve the hole mobility. Adding

the electrons does result in a significant three-fold increase in hole mobility at $T = 1.5$ K; for $p = 6\times10^{10}$ cm^{-2}, $\rho_{xx,\mathrm{hole}}(n = 0) = 3808\,\Omega/\square$ falls to $\rho_{xx,\mathrm{hole}}(n = p) = 1203\,\Omega/\square$. This is consistent with the results of Morath et al. [57], from a 30 nm barrier EHBL device, where the dependence of the hole mobility with electron density was explored. The effect is much larger here, possibly due to the smaller barrier.

Improvement of the high-temperature mobility is likely to be the result of several processes. Background impurities will be screened by the presence of the 2DEG. Inducing the electrons requires a large electric field across the barrier, and then to reach matched densities ($n = p$) a depleting backgate bias is also required. Both of these cause the wavefunction to be "squeezed" against the AlGaAs barrier, improving the screening as the holes become more greatly confined (though also potentially harming the mobility due to increased interface roughness scattering and the higher level of background impurities found in AlGaAs). In this regime, the hole mobility is limited by remote ionised impurity scattering caused by the intentional p-dopants (verified by comparison to undoped structures). The interlayer bias will pull the holes towards the barrier and increase the effective spacer thickness (between the 2DHG and dopants) and accordingly improve the mobility.

Placing a conducting electron layer close to the 2DHG will also improve the screening, as image charges will form in this layer. If the interlayer separation is d, then the dipolar field (charge and its image) will drop faster than $\sim 1/r$ at distances greater than $\sim d$. This effect has been studied in gated 2DEGs [72] and in double QW structures (2x2DHG) with $d \sim 50$ nm [73].

While the change at $T = 1.5$ K can be accounted for by a combination of effects, the insulating behaviour at low temperature is unexpected as these arguments always improve the intralayer screening and lower the effective r_s. Matthiessen's rule-based addition of scattering rates cannot explain the increase in mobility [74] at $T = 1.5$ K. Adding the contribution of the interlayer scattering rate to the impurity scattering rate will cause a reduction in mobility. Going from the situation of a single hole gas ($1/\mu_h^{sl}$) (where $\mu = e\tau/m^*$), whose mobility is primarily dictated by impurity scattering ($1/\mu_h^{\mathrm{imp}}$), to the mobility of the holes with the addition of the electron layer (bilayer configuration) ($1/\mu_h^{bl}$) must introduce a term corresponding to the presence of the electron layer ($1/\mu_h^{C}$) and so

$$\frac{1}{\mu_h^{sl}} = \frac{1}{\mu_h^{\mathrm{imp}}} \longrightarrow \frac{1}{\mu_h^{bl}} = \frac{1}{\mu_h^{\mathrm{imp}}} + \frac{1}{\mu_h^{C}}. \tag{9}$$

This must mean that $1/\mu_h^{\mathrm{imp}}$ is changing in the presence of the second layer. Note that $1/\mu_h^{C} = en\rho_{\mathrm{drag}}$ [74], where n is the density of the electron layer. The anomalous drag cannot account for the increase in $\rho_{xx}(T)$ at lower temperatures, as it is too small. This suggests that a new single-layer scattering mechanism has emerged due to the presence of the electron layer.

The insulating state is *also* seen in the electron layer. Figure 19 shows both electron and hole layer resistivities down to ~50 mK. Both layers exhibit a similar behaviour,

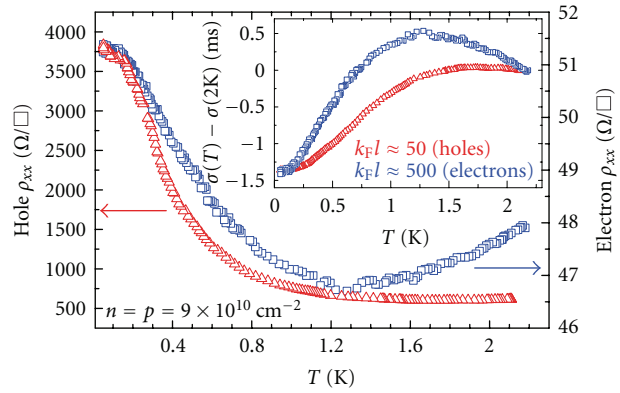

Figure 19: Resistivities of hole and electron layers versus temperature for $n = p = 9\times10^{10}$ cm^{-2}, down to $\approx$ 50 mK in a dilution refrigerator. At $T = 1.5$ K, $\mu_e = 1.5\times10^6$ cm^{2}V^{-1}s^{-1} and $\mu_h = 1.1\times10^5$ cm^{2}V^{-1}s^{-1}). (Inset) Change in conductivity relative to σ_{xx} ($T = 2$ K). (Device: B138/C4-1-10 nm Barrier).

though the relative change in resistance appears to be much larger in the hole layer. However, the loss of conductivity in both layers between 2 K and 50 mK (inset Figure 19) is similar (~0.2 mS), over which the insulating behaviour is seen. This is much larger than the change weak localisation (quantum interference) can account for ($\Delta\sigma_{xx} \approx 40\,\mu$S) [75]. Weak localisation predicts that $\Delta\sigma_{xx}(T) = (e^2/2\pi^2\hbar)\ln(\tau_i/\tau_0)$, where τ_i and τ_0 are the temperature-dependent lifetimes for eigenstates of energy and momentum, respectively. The insulating state was also seen in a third device (B141/C5-2) that had been processed with a shorter hall bar (250 μm as opposed to 500 μm), and the effect was found to be independent of the length to width ratio.

Figure 18(e) is an Arrhenius plot ($\ln\rho$ versus $1/T$) for $n = p = 9\times10^{10}$ cm^{-2}, and the resistivity shows a good fit to an activated behaviour (It is difficult to distinguish between a power law and an exponential rise as the insulating phase occurs over a small temperature range, less than one order of magnitude.) ($\rho_{xx}(T) = \rho_0 e^{E/k_BT}$), yielding an energy gap of $E/k_B = 0.4$ K. Similar analysis for the corresponding electron trace (data not shown) gives a far smaller gap of $E/k_B = 0.02$ K. As the density is lowered (Figure 18) and the interaction strength is increased (larger r_s), the fit to an exponential rise becomes poorer. But the traces are expected to be (weakly) insulating for $p < 6\times10^{10}$ cm^{-2}, regardless of the presence of the electrons. The important result is the emergence of a strongly insulating state at *large* $k_F\ell$ ($\rho_{xx} \ll h/e^2$). In Figure 19, $\rho_{xx}(T)$ for both layers appears to saturate at the lowest temperatures. This is likely to an artefact of the electron temperature not reaching the thermometry temperature (Shubnikov-de Haas oscillation amplitude had saturated by ~100 mK, in this measurement run).

7.1. Mismatched Densities. Matching the densities is not crucial to achieving the insulating state. In Figure 21, the hole density was held at $p = 1.6\times10^{11}$ cm^{-2} with the electron density varied ($n = 4, 6, 8\times10^{10}$ cm^{-2}). This was chosen so that for the lowest electron density $n = 4\times10^{10}$ cm^{-2},

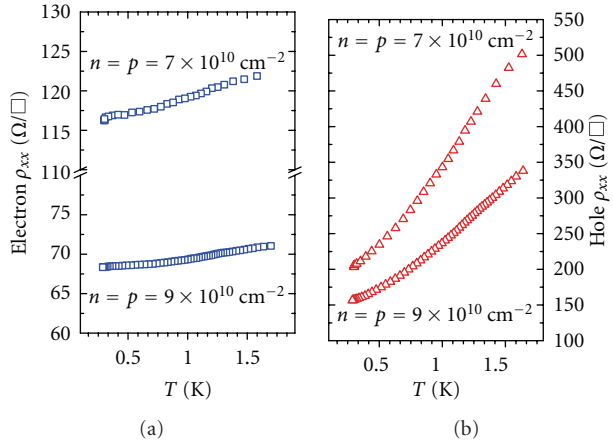

FIGURE 20: Resistivities of hole and electron layers versus temperature for $n = p = 7, 9 \times 10^{10}$ cm^{-2}, with 25 nm $Al_{0.3}Ga_{0.7}$ As barrier. (Device: B135/C3-4-25 nm Barrier).

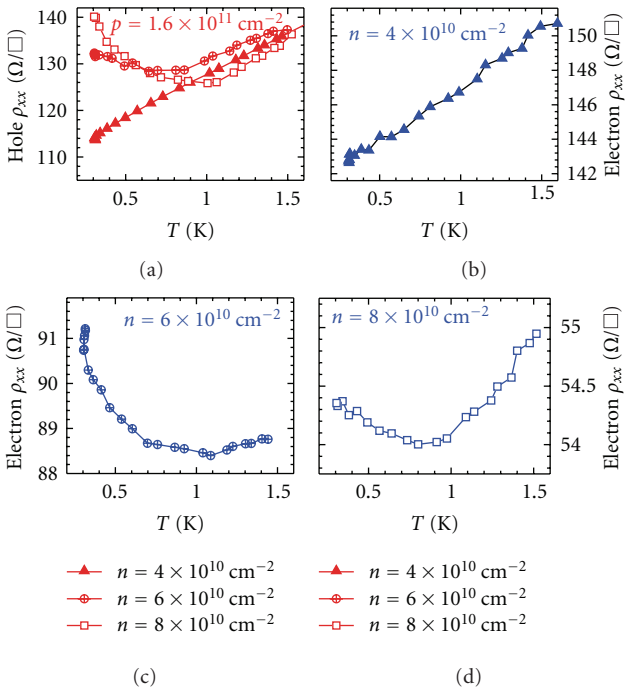

FIGURE 21: Resistivities of the hole (a) and electron layer (b), (c), and (d), versus temperature for fixed hole density $p = 1.6 \times 10^{11}$ cm^{-2}, and varied electron density $n = 4, 6, 8 \times 10^{10}$ cm^{-2}. (Device: B138/C4-1-10 nm Barrier).

both layers have similar resistivities at $T = 1.5$ K. As the electron density is *increased*, both layers undergo a transition from metallic to insulating behaviour. The transition occurs between 4 and 6×10^{10} cm^{-2} when $p \approx 3n$ in this instance, far from matched densities. A transition to insulating behaviour as the density is raised is very striking and incompatible with a disorder-driven mechanism; this strengthens the argument for an interlayer interaction-driven effect.

A similar experiment was performed (down to 50 mK) where n was fixed at 2×10^{10} cm^{-2} and p was varied

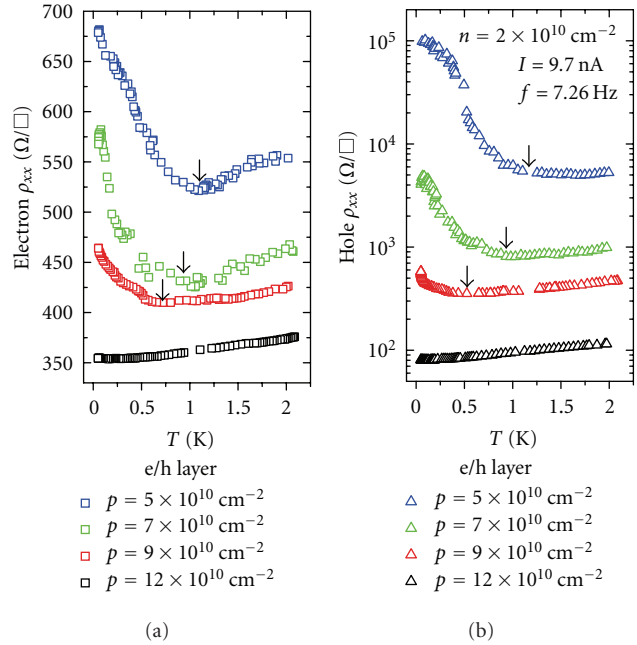

FIGURE 22: Resistivity of electron (a) and hole (b) layers versus temperature, for constant electron density ($n = 2 \times 10^{10}$ cm^{-2}) and different hole densities ($p = 5, 7, 9, 12 \times 10^{10}$ cm^{-2}). Arrows indicate approximate points of transition to insulating behaviour. (Device: B138/C4-2-10 nm Barrier).

(Figure 22). For the largest hole density ($p = 1.2 \times 10^{11}$ cm^{-2}), both layers are metallic, and as the hole density was lowered, both become insulating. Some degree of matching appears to be required for the insulating state to occur, though one would expect that in the limit of p becoming large relative to n (and the hole screening improving accordingly), they would behave as two isolated gases. Arrows in Figure 22 indicate the approximate points of transition to insulating behaviour, suggesting that there may be no abrupt transition as the density is lowered, but a shift in transition temperature.

As the hole density is varied with the electron density held constant ($n = 8.6 \times 10^{10}$ cm^{-2}), $\rho_{xx}(T)$ varies monotonically for both layers across $n = p$ (Figure 23) within the insulating regime at 300 mK. The electron resistance does increase slightly as the hole density is lowered. Matching the densities exactly does not appear to play a significant role. In all the experiments performed, the insulating state appeared to occur in both layers simultaneously, though at higher densities $\rho_{xx}(T)$ has little temperature dependence over the range measured.

7.2. Inhomogeneity. It is important to determine whether the emergent insulating state in the hole layer at large $k_F\ell$ can be attributed to (device-driven) density inhomogeneity. If the hole gas were highly inhomogeneous, the average resistance might be determined by high-density (low-resistance) regions, while the temperature dependence was dominated by low-density insulating regions. It can be established that without the electron gas present, the hole

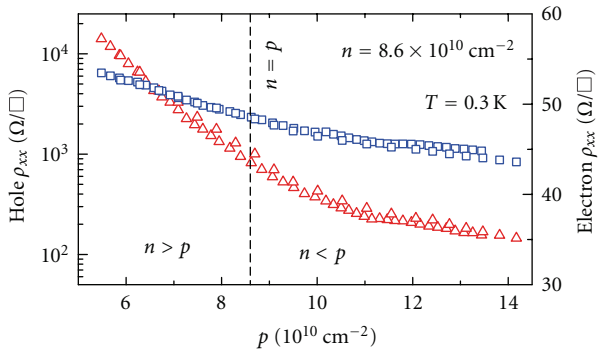

FIGURE 23: Resistivity of electron (blue squares) and hole (red triangles) layers versus hole density, with electron density fixed ($n = 8.6 \times 10^{10}$ cm^{-2}) at $T = 300$ mK. (Device: B138/C4-1-10 nm Barrier).

gas is homogeneous, from the hole layer magnetoresistance (Figure 18). The Shubnikov-de Haas oscillations are periodic in $1/B$ and the reciprocal of the carrier density. A variation in carrier density over the Hall bar region would smear the oscillation. In Figure 18, magnetoresistance traces are shown for four carrier densities, which clearly show well-pronounced oscillations with minima that go to zero for the higher densities. At lower densities, the larger sheet resistance and shorter transport lifetime broaden the Landau levels, requiring lower temperatures for them to be as clearly resolved. Considering only the higher two densities (8 and 9×10^{10} cm^{-2}), the resolution of the oscillations is consistent with the densities measured by the Hall probes at each end of the Hall bar, which record a difference of $\sim 1 \times 10^9$ cm^{-2}.

With the introduction of the electrons, verifying the homogeneity of the 2DHG with magnetoresistance is no longer possible. Indeed, if the insulating state corresponds to a density-modulated phase, then it might be expected that the Shubnikov-de Haas oscillations would no longer be resolved due to the inherent spatial density-variation. Indeed, there are no strong oscillations at 300 mK in the hole layer, but normal oscillations persist in the electron layer at low fields.

If in-built inhomogeneity is the source of the insulating behaviour, it must only be present when the electrons are induced across the barrier. Variation in the thickness of a 10 nm barrier will cause spatial density fluctuations due to a change in interlayer capacitance. MBE growth is capable of producing interfaces that are smooth to a couple of monolayers (0.3 nm for GaAs), giving a possible variation of ~1 nm in the barrier width. This results in a density fluctuation of $\lesssim$10%. (This is an overestimate as the appropriate distance corresponding to the interlayer capacitance is ~25 nm for a 10 nm barrier) and cannot force regions to become insulating ($p < 6 \times 10^{10}$ cm^{-2}) if the average density is 9×10^{10} cm^{-2}. Such inhomogeneity would also be mirrored equally in the electron layer and detectable in the 2DEG magnetoresistance as described above. However, even in the insulating regime the Shubnikov-de Haas oscillations are clearly resolved at 50 mK in the electron layer.

To go from $p, n = 0$ to $n = p$ requires (as well as an increase in interlayer bias) a depleting backgate bias as opposed to an inducing one. It is unclear how backgate action (50 μm away) can produce density variation on the short-length scale required (<60 μm, width of Hall bar/probes). The disagreement in density taken from the Hall slope at each end of the Hall bar is no worse with the electron layer present, (still about 1×10^9 cm^{-2}).

7.3. Two Component Plasma and the Significance of Unequal Electron and Hole Masses. Most of the early theoretical (and numerical) work on the EHBL made the simplifying assumption that the effective masses of the electrons and holes are equal. qSTLS was used by Moudgil et al. 2002 [76] to study the ground state of electron-electron and electron-hole bilayers ($m_e^* = m_h^*$). For the EHBL, a divergence for χ_+ at small q (CDW) was found for $r_s < 10$ with a crossover to the WC state above ($d \sim 4a_B^*$). Unlike [17], a divergence in $\chi_-(q)$ was found for the electron-electron bilayer. They found that the local fields in the electron-electron bilayer are weaker than the EHBL, and the density-modulated phases require larger r_s and smaller d. The results were compared with diffusion Monte Carlo simulations performed on the EHBL by De Palo et al. [65], who were able to show a transition to an excitonic condensate state (BCS-like state) and WC. The WC transition was in good agreement with the qSTLS data. However the CDW state was not considered by De Palo et al. [65].

Subsequent qSTLS work by Moudgil [77] studied the mass-asymmetric EHBL, with $m_h^*/m_e^* = 7$ (appropriate to GaAs) and included the finite widths of the electron and hole gases. The mass-asymmetry pushes the CDW and WC transitions to higher density, though the WC is found to exist only at an intermediate well separation, with the CDW favoured for smaller separations. The larger $r_{s,h}$ in the hole layer is found to be significant, with Wigner crystallisation predicted at $r_{s,e} = 2.4$. Interestingly, the correlation in the hole layer ($g_{hh}(r)$) for the density-modulated phases is found to be *stronger* than in the electron layer ($g_{ee}(r)$). Including a finite QW width was found to lower the critical density for Wigner crystallisation to $r_{s,e} = 3.75$.

More recent work implemented Monte Carlo methods for studying mass-asymmetric EHBLs, with the mass ratio varied [78] between 1 and 100, with the interlayer separation (d) fixed. Electron densities studied corresponded to $r_s \approx 10 - 20$, but for a large layer separation ($d = 20a_B^* \approx 200$ nm in GaAs). They found that by increasing the mass ratio, the hole layer evolves from a homogeneous to a localised state (WC), with the electron layer remaining in a relatively homogeneous state. Periodic structure in $g_{hh}(r)$ exists by $m_h = 5m_e$, a ratio appropriate to GaAs. While these particle densities are considerably lower than those achieved in these experiments, the d/l ratios are similar at ~1.

These results provide a large contrast to the low densities predicted to be required for a WC to occur in a single 2D gas, $r_s = 37 \pm 5$ by Tanatar and Ceperley (1989) [79]. This corresponds to an electron density of $\sim 2 \times 10^8$ cm^{-2}; this is difficult to achieve experimentally in GaAs while maintaining a high mobility such that localisation due to Coulomb

repulsion can be distinguished from that driven by disorder. Hole densities as low as $6 \times 10^8\,\mathrm{cm}^{-2}$ (in GaAs/AlGaAs) have been reported [80], where a much larger r_s is reached (relative to electrons), but at these densities, the 2DHG is in the insulating regime. But in the EHBL, the density-modulated phases are predicted at experimentally accessible r_s that lie within the "metallic" regime.

8. Conclusion

The idea of an excitonic condensate was put forward nearly forty years ago by Blatt et al. [81] and Moskalenko and Snoke [82]. But excitonic phases were initially thought to be necessarily insulating and not accessible by transport because they consisted of charge neutral particles. However, the key experimental development that has radically changed this perspective is the ability to make independent ohmic contacts to the electron-like and the hole-like parts of a system. Experimentally, 2x2DEGs, and 2x2DHGs in a magnetic field have shown striking evidence of transport by neutral objects driven by counterflow currents [33–35]. More recently, electron-hole bilayers in zero magnetic field have shown evidence of an emerging non-Fermi liquid phase [51–53, 70]. In these systems, excitonic phases and collective modes, characteristic of a 2-component plasma, may be competing in determining the ground state. It is very likely that this field will lead to exciting experimental and theoretical results in near future.

Acknowledgments

The work reported here was funded by EPSRC (UK) under the Grants *EP/D008506/1* and *EP/H017720/1*. A. F. Croxall acknowledges Trinity College for a fellowship. I. Farrer acknowledges Toshiba for support. The authors acknowledge several useful discussions with D. Neilson and A. R. Hamilton.

References

[1] Yu. E. Lozovik and V. I. Yudson, "A new mechanism for superconductivity: pairing between spatially separated electrons and holes," *Soviet Physics Journal of Experimental and Theoretical Physics*, vol. 44, p. 389, 1976.

[2] Yu. E. Lozovik and V. I. Yudson, "Feasibility of superfluidity of paired spatially separated electrons and holes; a new superconductivity mechanism," *Journal of Experimental and Theoretical Physics Letters*, vol. 22, p. 274, 1975.

[3] P. J. Price, "Hot electron effects in heterolayers," *Physica B+C*, vol. 117-118, no. 2, pp. 750–752, 1983.

[4] M. B. Pogrebinskii, "Mutual drag of carriers in a semiconductor-insulator-semiconductor system," *Soviet Physics: Semiconductors*, vol. 11, no. 4, pp. 372–376, 1977.

[5] A. P. Jauho and H. Smith, "Coulomb drag between parallel two-dimensional electron systems," *Physical Review B*, vol. 47, no. 8, pp. 4420–4428, 1993.

[6] G. Vignale and A. H. MacDonald, "Drag in paired electron-hole layers," *Physical Review Letters*, vol. 76, no. 15, pp. 2786–2789, 1996.

[7] S. Conti, G. Vignale, and A. H. MacDonald, "Engineering superfluidity in electron-hole double layers," *Physical Review B*, vol. 57, no. 12, pp. R6846–R6849, 1998.

[8] B. Y. K. Hu, "Prospecting for the superfluid transition in electron-hole coupled quantum wells using Coulomb drag," *Physical Review Letters*, vol. 85, no. 4, pp. 820–823, 2000.

[9] A. V. Balatsky, Y. N. Joglekar, and P. B. Littlewood, "Dipolar superfluidity in electron-hole bilayer systems," *Physical Review Letters*, vol. 93, no. 26, Article ID 266801, 2004.

[10] Y. N. Joglekar, A. V. Balatsky, and M. P. Lilly, "Excitonic condensate and quasiparticle transport in electron-hole bilayer systems," *Physical Review B*, vol. 72, no. 20, Article ID 205313, 6 pages, 2005.

[11] P. B. Littlewood and X. Zhu, "Possibilities for exciton condensation in semiconductor quantum-well structures," *Physica Scripta*, vol. T68, p. 56, 1996.

[12] J. Hubbard, "The description of collective motions in terms of many-body perturbation theory II. The correlation energy of a free electron gas," *Proceedings of the Royal Society of London A*, vol. 243, p. 336, 1958.

[13] K. S. Singwi, M. P. Tosi, R. H. Land, and A. Sjölander, "Electron correlations at metallic densities," *Physical Review*, vol. 176, no. 2, pp. 589–599, 1968.

[14] K. S. Singwi and M. P. Tosi, "Correlations in electron liquids," in *Solid State Physics: Advances in Research and Applications*, H. Ehrenreich, Ed., vol. 36, pp. 177–266, Academic Press, New York, NY, USA, 1981.

[15] L. Zheng and A. H. MacDonald, "Correlation in double-layer two-dimensional electron-gas systems: Singwi-Tosi-Land-Sjölander theory at B=0," *Physical Review B*, vol. 49, no. 8, pp. 5522–5530, 1994.

[16] L. Świerkowski, J. Szymański, and Z. W. Gortel, "Coupled electron-hole transport: beyond the mean field approximation," *Physical Review Letters*, vol. 74, no. 16, pp. 3245–3248, 1995.

[17] L. Liu, L. Świerkowski, D. Neilson, and J. Szymański, "Static and dynamic properties of coupled electron-electron and electron-hole layers," *Physical Review B*, vol. 53, no. 12, pp. 7923–7931, 1996.

[18] L. Liu, L. Świerkowski, and D. Neilson, "Exciton and charge density wave formation in spatially separated electron - Hole liquids," *Physica B*, vol. 249–251, pp. 594–597, 1998.

[19] U. Sivan, P. M. Solomon, and H. Shtrikman, "Coupled electron-hole transport," *Physical Review Letters*, vol. 68, no. 8, pp. 1196–1199, 1992.

[20] B. E. Kane, J. P. Eisenstein, W. Wegscheider, L. N. Pfeiffer, and K. W. West, "Separately contacted electron-hole double layer in a GaAs/Al_xGa_{1-x}As heterostructure," *Applied Physics Letters*, vol. 65, no. 25, pp. 3266–3268, 1994.

[21] H. Rubel, A. Fischer, W. Dietsche, K. von Klitzing, and K. Eberl, "Fabrication of indepedently contacted and tuneable 2D electron-hole systems in GaAs-AlGaAs double quantum wells," *Materials Science and Engineering B*, vol. 51, p. 205, 1998.

[22] M. Pohlt, M. Lynass, J. G. S. Lok et al., "Closely spaced and separately contacted two-dimensional electron and hole gases by in situ focused-ion implantation," *Applied Physics Letters*, vol. 80, no. 12, p. 2105, 2002.

[23] J. A. Keogh, K. Das Gupta, H. E. Beere, D. A. Ritchie, and M. Pepper, "Fabrication of closely spaced, independently contacted electron-hole bilayers in GaAs-AlGaAs heterostructures," *Applied Physics Letters*, vol. 87, no. 20, Article ID 202104, 3 pages, 2005.

[24] J. A. Seamons, D. R. Tibbetts, J. L. Reno, and M. P. Lilly, "Undoped electron-hole bilayers in a GaAs/AlGaAs double quantum well," *Applied Physics Letters*, vol. 90, no. 5, Article ID 052103, 2007.

[25] J. P. Eisenstein, L. N. Pfieffer, and K. W. West, "Independently contacted 2-dimensional electron systems in double quantum wells," *Applied Physics Letters*, vol. 57, p. 2324, 1990.

[26] A. F. Croxall, K. Das Gupta, C. A. Nicoll et al., "Patterned backgating using single-sided mask aligners: application to density-matched electron-hole bilayers," *Journal of Applied Physics*, vol. 104, no. 11, Article ID 113715, 2008.

[27] M. V. Weckwerth, J. A. Simmons, N. E. Harff et al., "Epoxy bond and stop-etch (EBASE) technique enabling backside processing of (AI)GaAs heterostructures," *Superlattices and Microstructures*, vol. 20, no. 4, pp. 561–567, 1996.

[28] N. P. R. Hill, J. T. Nicholls, E. H. Linfield et al., "Correlation effects on the coupled plasmon modes of a double quantum well," *Physical Review Letters*, vol. 78, no. 11, pp. 2204–2207, 1997.

[29] M. Prunnila, S. J. Laakso, J. M. Kivioja, and J. Ahopelto, "Electrons and holes in Si quantum well: a room-temperature transport and drag resistance study," *Applied Physics Letters*, vol. 93, no. 11, Article ID 112113, 2008.

[30] K. Takashina, K. Nishiguchi, Y. Ono et al., "Electrons and holes in a 40 nm thick silicon slab at cryogenic temperatures," *Applied Physics Letters*, vol. 94, no. 14, Article ID 142104, 2009.

[31] I. Farrer, A. F. Croxall, K. D. Gupta et al., "MBE growth and patterned backgating of electron-hole bilayer structures," *Journal of Crystal Growth*, vol. 311, no. 7, pp. 1988–1993, 2009.

[32] J. P. Eisenstein and A. H. MacDonald, "Bose-Einstein condensation of excitons in bilayer electron systems," *Nature*, vol. 432, no. 7018, pp. 691–694, 2004.

[33] M. Kellogg, J. P. Eisenstein, L. N. Pfeiffer, and K. W. West, "Vanishing hall resistance at high magnetic field in a double-layer two-dimensional electron system," *Physical Review Letters*, vol. 93, no. 3, Article ID 036801, 2004.

[34] L. Tiemann, J. G. S. Lok, W. Dietsche et al., "Exciton condensate at a total filling factor of one in Corbino two-dimensional electron bilayers," *Physical Review B*, vol. 77, no. 3, Article ID 033306, 2008.

[35] E. Tutuc, M. Shayegan, and D. A. Huse, "Counterflow measurements in strongly correlated GaAs hole bilayers: evidence for electron-hole pairing," *Physical Review Letters*, vol. 93, no. 3, Article ID 036802, 2004.

[36] T. J. Gramila, J. P. Eisenstein, A. H. MacDonald, L. N. Pfeiffer, and K. W. West, "Mutual friction between parallel two-dimensional electron systems," *Physical Review Letters*, vol. 66, no. 9, pp. 1216–1219, 1991.

[37] M. C. Bønsager, K. Flensberg, B. Y. K. Hu, and A. H. MacDonald, "Frictional drag between quantum wells mediated by phonon exchange," *Physical Review B*, vol. 57, no. 12, pp. 7085–7102, 1998.

[38] A. Yurtsever, V. Moldoveanu, and B. Tanatar, "Many-body effects in the Coulomb drag between low density electron layers," *Solid State Communications*, vol. 125, no. 11-12, pp. 575–579, 2003.

[39] R. Asgari, B. Tanatar, and B. Davoudi, "Comparative study of screened interlayer interactions in the Coulomb drag effect in bilayer electron systems," *Physical Review B*, vol. 77, no. 11, Article ID 115301, 2008.

[40] S. Das Sarma and E. H. Hwang, "In-plane magnetodrag in dilute bilayer two-dimensional systems: a Fermi-liquid theory," *Physical Review B*, vol. 71, no. 19, Article ID 195322, 5 pages, 2005.

[41] E. H. Hwang and S. Das Sarma, "Transport and drag in undoped electron-hole bilayers," *Physical Review B*, vol. 78, no. 7, Article ID 075430, 2008.

[42] F. Stern, "Polarizability of a two-dimensional electron gas," *Physical Review Letters*, vol. 18, no. 14, pp. 546–548, 1967.

[43] L. Świerkowski, J. Szymański, and Z. W. Gortel, "Linear-response theory for multicomponent fermion systems and its application to transresistance in two-layer semiconductor structures," *Physical Review B*, vol. 55, no. 4, pp. 2280–2292, 1997.

[44] S. Das Sarma and A. Madhukar, "Collective modes of spatially separated, two-component, two-dimensional plasma in solids," *Physical Review B*, vol. 23, no. 2, pp. 805–815, 1981.

[45] B. Y. K. Hu and J. W. Wilkins, "Two-stream instabilities in solid-state plasmas caused by conventional and unconventional mechanisms," *Physical Review B*, vol. 43, no. 17, pp. 14009–14029, 1991.

[46] M. Kellogg, J. P. Eisenstein, L. N. Pfeiffer, and K. W. West, "Evidence for 2k electron-electron scattering processes in Coulomb drag," *Solid State Communications*, vol. 123, no. 12, pp. 515–519, 2002.

[47] E. H. Hwang, S. Das Sarma, V. Braude, and A. Stern, "Frictional drag in dilute bilayer 2D hole systems," *Physical Review Letters*, vol. 90, no. 8, Article ID 086801, 4 pages, 2003.

[48] R. Pillarisetty, H. Noh, D. C. Tsui, E. P. De Poortere, E. Tutuc, and M. Shayegan, "Frictional drag between two dilute two-dimensional hole layers," *Physical Review Letters*, vol. 89, no. 1, Article ID 016805, 2002.

[49] C. Hodges, H. Smith, and J. W. Wilkins, "Effect of fermi surface geometry on electron-electron scattering," *Physical Review B*, vol. 4, no. 2, pp. 302–311, 1971.

[50] L. Zheng and A. H. MacDonald, "Coulomb drag between disordered two-dimensional electron-gas layers," *Physical Review B*, vol. 48, no. 11, pp. 8203–8209, 1993.

[51] J. A. Seamons, C. P. Morath, J. L. Reno, and M. P. Lilly, "Coulomb drag in the exciton regime in electron-hole bilayers," *Physical Review Letters*, vol. 102, no. 2, Article ID 026804, 2009.

[52] C. P. Morath, J. A. Seamons, J. L. Reno, and M. P. Lilly, "Density imbalance effect on the Coulomb drag upturn in an undoped electron-hole bilayer," *Physical Review B*, vol. 79, no. 4, Article ID 041305, 2009.

[53] A. F. Croxall, K. Das Gupta, C. A. Nicoll et al., "Anomalous coulomb drag in electron-hole bilayers," *Physical Review Letters*, vol. 101, no. 24, Article ID 246801, 2008.

[54] H. B. G. Casimir, "On Onsager's principle of microscopic reversibility," *Reviews of Modern Physics*, vol. 17, no. 2-3, pp. 343–350, 1945.

[55] J. Szymański, L. Wierkowski, and D. Neilson, "Correlations in coupled layers of electrons and holes," *Physical Review B*, vol. 50, no. 15, pp. 11002–11007, 1994.

[56] M. J. Kellogg, *Evidence for excitonic superfluidity in a two dimensional electron system*, Ph.D. thesis, California Institute of Technology, 2005.

[57] C. P. Morath, J. A. Seamons, J. L. Reno, and M. P. Lilly, "Layer interdependence of transport in an undoped electron-hole bilayer," *Physical Review B*, vol. 78, no. 11, Article ID 115318, 2008.

[58] A. Levchenko and A. Kamenev, "Coulomb drag at zero temperature," *Physical Review Letters*, vol. 100, no. 2, Article ID 026805, 2008.

[59] M. P. Lilly, J. P. Eisenstein, L. N. Pfeiffer, and K. W. West, "Coulomb drag in the extreme quantum limit," *Physical Review Letters*, vol. 80, no. 8, pp. 1714–1717, 1998.

[60] X. G. Feng, S. Zelakiewicz, H. Noh et al., "Negative electron drag and holelike behavior in the integer quantum hall regime," *Physical Review Letters*, vol. 81, no. 15, pp. 3219–3222, 1998.

[61] N. P. R. Hill, J. T. Nicholls, E. H. Linfield et al., "Electron-electron scattering between closely spaced two-dimensional electron gases," *Physica B*, vol. 249–251, pp. 868–872, 1998.

[62] J. G. S. Lok, S. Kraus, M. Pohlt et al., "Spin effects in the magnetodrag between double quantum wells," *Physical Review B*, vol. 63, no. 4, Article ID 041305, 4 pages, 2001.

[63] K. Muraki, J. G. S. Lok, S. Kraus et al., "Coulomb drag as a probe of the nature of compressible states in a magnetic field," *Physical Review Letters*, vol. 92, no. 24, Article ID 246801, 2004.

[64] A. Alkauskas, K. Flensberg, B. Y. K. Hu, and A. P. Jauho, "Sign reversal of drag in bilayer systems with in-plane periodic potential modulation," *Physical Review B*, vol. 66, no. 20, Article ID 201304, 2002.

[65] S. De Palo, F. Rapisarda, and G. Senatore, "Excitonic condensation in a symmetric electron-hole bilayer," *Physical Review Letters*, vol. 88, no. 20, Article ID 206401, 4 pages, 2002.

[66] L. Onsager, "Reciprocal relations in irreversible processes. I," *Physical Review*, vol. 37, no. 4, pp. 405–426, 1931.

[67] L. Onsager, "Reciprocal relations in irreversible processes. II," *Physical Review*, vol. 38, no. 12, pp. 2265–2279, 1931.

[68] A. P. Mills Jr., A. P. Ramirez, L. N. Pfeiffer, and K. W. West, "Nonmonotonic temperature-dependent resistance in low density 2D hole gases," *Physical Review Letters*, vol. 83, no. 14, pp. 2805–2808, 1999.

[69] S. Das Sarma and E. H. Hwang, "Calculated temperature-dependent resistance in low-density two-dimensional hole gases in GaAs heterostructures," *Physical Review B*, vol. 61, no. 12, pp. R7838–R7841, 2000.

[70] A. F. Croxall, K. Das Gupta, C. A. Nicoll et al., "Possible effect of collective modes in zero magnetic field transport in an electron-hole bilayer," *Physical Review B*, vol. 80, no. 12, Article ID 125323, 2009.

[71] A. F. Croxall, K. Das Gupta, C. A. Nicoll et al., "Towards the ground state of an electron-hole bilayer," *Physica E*, vol. 42, no. 4, pp. 1247–1250, 2010.

[72] J. Huang, D. S. Novikov, D. C. Tsui, L. N. Pfieffer, and K. W. West, "Interaction effects in the transport of two dimensional holes in GaAs," http://arxiv.org/abs/cond-mat/0610320.

[73] L. H. Ho, W. R. Clarke, A. P. Micolich et al., "Effect of screening long-range Coulomb interactions on the metallic behavior in two-dimensional hole systems," *Physical Review B*, vol. 77, no. 20, Article ID 201402, 2008.

[74] L. Świerkowski, J. Szymański, and Z. W. Gortel, "Intrinsic limits on carrier mobilities in double-layer systems," *Journal of Physics Condensed Matter*, vol. 8, no. 18, pp. L295–L300, 1996.

[75] G. Bergman, "Weak Localisation in thin films: a time of flight experiment with conduction electrons," *Physics Reports*, vol. 107, no. 1, pp. 1–58, 1984.

[76] R. K. Moudgil, G. Senatore, and L. K. Saini, "Dynamic correlations in symmetric electron-electron and electron-hole bilayers," *Physical Review B*, vol. 66, no. 20, Article ID 205316, 10 pages, 2002.

[77] R. K. Moudgil, "Coupled electron-hole quantum well structure: mass asymmetry and finite width effects," *Journal of Physics Condensed Matter*, vol. 18, no. 4, pp. 1285–1301, 2006.

[78] P. Ludwig, A. Filinov, YU. E. Lozovik, H. Stolz, and M. Bonitz, "Crystallization in mass-asymmetric electron-hole bilayers," *Contributions to Plasma Physics*, vol. 47, no. 4-5, pp. 335–344, 2007.

[79] B. Tanatar and D. M. Ceperley, "Ground state of the two-dimensional electron gas," *Physical Review B*, vol. 39, no. 8, pp. 5005–5016, 1989.

[80] J. Huang, D. S. Novikov, D. C. Tsui, L. N. Pfeiffer, and K. W. West, "Nonactivated transport of strongly interacting two-dimensional holes in GaAs," *Physical Review B*, vol. 74, no. 20, Article ID 201302, 2006.

[81] J. M. Blatt, K. W. Böer, and W. Brandt, "Bose-einstein condensation of excitons," *Physical Review*, vol. 126, no. 5, pp. 1691–1692, 1962.

[82] S. A. Moskalenko and D. W. Snoke, *Bose-Einstein Condensation of Excitons and Biexcitons and Coherent Nonlinear Optics with Excitons*, Cambridge University Press, Cambridge, UK, 2000.

Hindawi Publishing Corporation
Advances in Condensed Matter Physics
Volume 2011, Article ID 349362, 10 pages
doi:10.1155/2011/349362

Review Article

Coherence and Disorder in Bilayer Quantum Hall Systems

H. A. Fertig[1] and Ganpathy Murthy[2]

[1] *Department of Physics, Indiana University, Bloomington, IN 47405, USA*
[2] *Department of Physics and Astronomy, University of Kentucky, Lexington, KY 40506, USA*

Correspondence should be addressed to H. A. Fertig, hfertig@indiana.edu

Received 25 May 2010; Accepted 1 October 2010

Academic Editor: Melinda Kellogg

The quantum Hall bilayer at total filling factor $\nu = 1$ displays a number of properties akin to superfluidity, most clearly apparent in its very low dissipation in tunneling and counterflow transport. Theoretical descriptions in terms of quantum Hall ferromagnetism or thin-film superfluidity can be developed to explain these phenomena. In either case, merons can be identified as important low energy excitations. We demonstrate that a model in which puddles of merons induced by disorder, separated by narrow regions of interlayer coherence—*a coherence network*—can naturally explain many of the imperfect superfluid finite temperature properties that are observed in these systems. The periodic realization of this model shows that there can be low energy excitations beyond the superfluid mode. These are associated with transitions between states of different meron number in the puddles, where we argue that merons should be unbound at *any* temperature, and which can have important implications for the effect of quantum fluctuations on the system.

1. Introduction: Quantum Hall Bilayer as a Pseudospin System

The quantum Hall system at filling factor $\nu = 1$ supports a rich set of phenomena when discrete degrees of freedom can come into play at low energy. These are collectively known as quantum Hall ferromagnetism. Surprisingly, the spin degree of freedom in many such systems can be relevant in spite of the strong magnetic field in which the system is immersed, because the Landé g-factor is rather small in most two-dimensional electron gas systems based on GaAs. A description in terms of a spin-1/2 quantum ferromagnet turns out to be quite useful for this system, for example, suggesting that the basic charged excitations of this system are skyrmions [1, 2], excitations which carry a topological winding number in the spin and also turn out to be charged. Microscopic calculations [3–5] suggest these are indeed the low energy excitations in the clean limit, and several experimental results appear to confirm the presence of skyrmions [6, 7], although when disorder is taken into account such interpretations become less firm [8].

Quantum Hall ferromagnetism is also relevant in a very different context, the bilayer two-dimensional electron gas with total filling factor $\nu = 1$ [9]. This system can be artificially fabricated using molecular beam epitaxy, resulting in two high quality layers of electron gas very close to one another. A direct mapping between this and the real spin-1/2 quantum Hall system may be established if one labels one layer as "up" and the other "down." The layer index may thus be viewed as a pseudospin, and many of the ideas established for the spin behavior of the single layer quantum Hall system come into play for the bilayer, even if the real spin is fully polarized. (One can consider the situation in which both real spin and pseudospin are active degrees of freedom, leading to many possible states of the system [10]. In what follows we focus on the limit in which the Zeeman coupling polarizes the real spin. This has recently been realized experimentally, and qualitative features of the spin-polarized case are the same as at lower Zeeman couplings [11, 12].)

An important difference between the spin and the (bilayer) pseudospin degrees of freedom is the fact that interactions are not SU(2) invariant in the latter as they are in the former. This is because with finite layer separation d the Coulomb repulsion is larger for a pair of electrons in the same layer than it is for a pair in different layers with the same in-plane separation $\mathbf{r}$. The first and foremost

impact of this physics is that, in the absence of an external perpendicular electric field, the electron density will tend to be balanced between the layers. In the pseudospin language, this means that the effective spin-1/2 degree of freedom will favor an in-plane orientation. Even within this subspace of orientations, not all spin directions are equivalent. Interlayer tunneling energetically favors single particle states that are symmetric linear combinations of states in the two wells over antisymmetric combinations, which in the pseudospin language corresponds to spin oriented in the $\hat{x}$ direction. Real samples may be grown such that there is a wide range of possibilities for the scale of this term, from rather large so that all electrons are firmly in the symmetric state—essentially removing the layer degree of freedom from the problem—to very small, orders of magnitude below accessible temperatures. This latter situation has resulted in some of the most interesting and puzzling experimental observations on this system, which we will discuss in more detail below.

A crucial concept that applies to the bilayer system and to quantum Hall ferromagnets in general is known as *spin-charge coupling*. Because of the strong magnetic field, at filling factor $\nu = 1$ electrons will tend to reside almost solely in the lowest Landau level. However, restricting the *orbital* degrees of freedom to a single Landau level constrains the way in which spatially varying *spin* configurations may be realized. For configurations in which the direction of spin varies slowly on the scale of the magnetic length $\ell_0 = \sqrt{\hbar c/eB}$, with B the magnetic field, one may show [9] that charge and spin densities are tied together by the relation [1, 2]

$$q(\mathbf{r}) = -\frac{1}{8\pi}\varepsilon_{\mu\nu}\mathbf{m}\cdot\partial_\mu\mathbf{m}\times\partial_\nu\mathbf{m}, \tag{1}$$

where $\mathbf{m}(\mathbf{r})$ is a unit vector indicating the local direction of the spin. This relation may be applied somewhat more generally than just to states in the lowest Landau level; it works (with an appropriate overall constant) for any state with a quantized Hall conductivity σ_{xy} [13].

An effective energy functional for this pseudospin system which captures both the spin-charge coupling and the symmetry-breaking physics has the form [14]

$$\begin{aligned} E[\mathbf{m}] = {} & \frac{\rho_E}{2}\int d\mathbf{r}(\nabla m^\mu)^2 + \frac{1}{2}\int d\mathbf{r}d\mathbf{r}' q(\mathbf{r})v(\mathbf{r}-\mathbf{r}')q(\mathbf{r}) \\ & + \int d\mathbf{r}V(r)q(\mathbf{r}) - \frac{\Delta_{\mathrm{SAS}}}{4\pi\ell_0^2}\int d\mathbf{r}[m^x(d\mathbf{r})-1] \\ & + \Gamma\int d\mathbf{r}(m^z)^2 - \frac{e^2d^2}{16\pi\kappa}\int\frac{d\mathbf{q}}{4\pi^2}qm^z_{-\mathbf{q}}m^z_{\mathbf{q}} \\ & + \frac{\rho_A-\rho_E}{2}\int d\mathbf{r}(\nabla m^z)^2. \end{aligned} \tag{2}$$

The first three terms of the energy are SU(2) invariant contributions. The leading gradient term is the only one that appears in the nonlinear σ model for Heisenberg ferromagnets, and ρ_E is the spin stiffness in the $\hat{x}$-$\hat{y}$ plane. The second term describes the SU(2) invariant Hartree energy corresponding to the charge density associated with spin textures in quantum Hall ferromagnets. $v(r)$ is the Coulomb interaction screened by the dielectric constant κ of the host semiconductor. The third term incorporates interactions of the charge density with an external potential, for example, due to disorder. The fourth term describes the loss in tunneling energy when electrons are promoted from symmetric to antisymmetric states; here Δ_{SAS} is the single-particle splitting between symmetric and antisymmetric states.

The last three terms are the leading interaction anisotropy terms at long wavelengths. The term proportional to Γ implements the electrostatic energy cost of having a net charge imbalance between the layers. The $(\nabla m^z)^2$ term accounts for the anisotropy of the spin stiffness. Pseudospin order in the $\hat{x}$-$\hat{y}$ plane physically corresponds to interlayer phase coherence so that $\rho_A - \rho_E$ will become larger with increasing d. The sum of the first and seventh terms in (2) gives an XY-like anisotropic nonlinear σ model. However, this gradient term is not the most important source of anisotropy at long wavelengths. The fifth term produces the leading anisotropy and is basically the capacitive energy of the double-layer system. The sixth term appears due to the long-range nature of the Coulomb interaction; its presence demonstrates that a naive gradient expansion of the anisotropic terms is not valid. ($\mathbf{m}_q$ is the Fourier transform of the unit vector field $\mathbf{m}$.) Equation (2) can be rigorously derived from the Hartree- Fock approximation in the limit of slowly varying spin textures [15], and explicit expressions are obtained for ρ_E (which is due in this approximation entirely to interlayer interactions), ρ_A (due to intralayer interactions), and Γ. Quantum fluctuations will alter the values of these parameters from those implied by the Hartree-Fock theory.

Equation (2) is an energy functional for an easy-plane ferromagnet. As such one expects this system to support vortex excitations. In this context these are called *merons*, of which there are two for each vorticity—one in which the local spin vector $\mathbf{m}$ points in the positive $\hat{z}$ direction in the vortex core center and the other with $\mathbf{m}$ in the negative $\hat{z}$ direction. Due to the spin-charge relation (1), this means that vortices and antivortices *each* may have charge $\pm e/2$. In clean systems at low temperatures, we expect vortices and antivortices to be bound into pairs. Such *bimerons* then become the basic charged quasiparticles of the system [14], carrying charge e. Interestingly, such a bimeron is topologically equivalent to a skyrmion, confirming our understanding of the close relation between the real spin and the bilayer pseudospin system.

For $\Delta_{\mathrm{SAS}} = 0$, it is clear that above the Kosterlitz-Thouless temperature the meron pairs will unbind. Renormalization group calculations and simulation studies suggest that such unbinding can still occur if Δ_{SAS} is sufficiently small, either from thermal fluctuations [16] or disorder [17, 18]. The presence of unbound merons in the system has profound physical implications and may explain a number of remarkable phenomena that have been observed in experiments, as we now explain.

2. Analogy with Two-Dimensional Superfluidity

The analogy with easy-plane ferromagnetism suggests a different way to interpret the energy functional in (2). If Γ is sufficiently large then out of plane fluctuations will be strongly suppressed, and in a first approximation one may ignore m_z as a dynamical degree of freedom. Writing $m_x + im_y = e^{i\theta}$, to lowest order in gradients the energy functional may be written in the simple form

$$E_{SF} = \int d\mathbf{r}\left[\frac{\rho_s}{2}(\nabla\theta)^2 - \frac{\Delta_{\mathrm{SAS}}}{4\pi\ell_0^2}\cos\theta\right] \tag{3}$$

in the absence of an external potential $V(\mathbf{r})$. For $\Delta_{\mathrm{SAS}} = 0$ (i.e., negligible tunneling), this has exactly the form expected for a two-dimensional thin film superfluid, with θ the condensate wavefunction phase and ρ_s an effective two-dimensional "superfluid stiffness." In this case one expects the system to have a linearly dispersing "superfluid mode" which is analogous to the spin wave of an easy-plane ferromagnet. The presence of such a mode has been verified in microscopic calculations using the underlying electron degrees of freedom [19]. This suggests the possibility that one might observe some form of superfluidity in this system. To see exactly what this means, it is convenient to consider momentarily a wavefunction for the groundstate of the system in terms of the electron degrees of freedom

$$|\Psi_{ex}\rangle = \Pi_X\left[u_X + v_X c_{T,X}^{\dagger} c_{B,X}\right]|\mathrm{Bot}\rangle, \tag{4}$$

where $|\mathrm{Bot}\rangle$ represents the state in which all the single particle states of the bottom layer in the lowest Landau level, created by $c_{B,X}^{\dagger}$, have been filled. For a state with uniform density and equal populations in each well, $u_X = v_X = 1/\sqrt{2}$. More generally, one can represent an imbalanced state, obtained physically with an electric field applied perpendicular to the bilayer, by taking $u_X = \sqrt{\nu_T}$ and $v_X = \sqrt{\nu_B}$, with $\nu_T + \nu_B = 1$. The constants ν_T and ν_B represent the filling fractions in each of the layers, and the situation where $\nu_T \neq \nu_B$ turns out to be quite interesting, as we will discuss below.

Equation (4) is an excellent trial wavefunction for the groundstate, provided the layer separation d is not too large [20]. It shows that in the ideal (clean) limit, this system has a coherence much akin to that of a superconductor and that the condensed objects in the groundstate are *excitons*, particle-hole pairs with each residing in a different layer. This immediately implies that the superfluidity in the this system will be in *counterflow* transport, where electric current in each layer runs in opposite directions.

Something much like this has been observed in experiments where electrical contact is made separately with each layer [21, 22]. In such studies current flows in opposite directions in the two layers. Such a current can be sustained by exciton flow, since the charge of the two constituents of the exciton have opposite sign. By measuring the voltage drop in a single layer along the direction of current, one may learn about dissipation in this exciton flow. In the experiments [21, 22], the dissipation is nonvanishing at any temperature $T > 0$, but apparently extrapolates to zero as $T \to 0$.

Another type of experiment takes advantage of the fact that Δ_{SAS}, while very small (typically several tens of microKelvin), is not zero. When the last term in (3) is included, the energy functional has a form very similar to that of a Josephson junction, suggesting that this system supports a Josephson effect [23]. In tunneling experiments, where one separately contacts to each layer such that current must tunnel between them, the tunneling I-V is nearly vertical near zero interlayer bias [24], which appears very similar to a Josepshon I-V characteristic.

Another similarity between Josephson junction physics and the quantum Hall bilayer is the existence of a critical current. Josephson junctions can pass dissipationless currents only up to a limit that scales as $\sqrt{\Delta_{\mathrm{SAS}}}$ in the model of (3). Above this current, a voltage sets in, and the system behaves dissipatively. Again, behavior reminiscent of this has been observed experimentally [25], although in the quantum Hall bilayer one should note carefully that the critical current separates a low from a high dissipation regime, rather than a zero from a nonzero dissipation regime. A number of theories have addressed this issue in the clean [26–28] and dirty [29] limits, which give very different behaviors with respect to how the critical current should scale with respect to the sample area. Interestingly, it is the latter which seems to agree best with experiment.

While these results look quite similar to what one might expect for exciton superfluidity, it is important to recognize that these results clearly are *not* genuine superfluid behavior. If the condensate could truly flow without dissipation, one would expect zero dissipation at any finite temperature below the Kosterlitz-Thouless transition, where vortex-antivortex pairs unbind. In experiment this truly dissipationless flow appears to emerge, if at all, only in the zero temperature limit. Similarly, the Josepshon effect should be truly dissipationless, whereas in experiment there is always a measurable tunneling resistance at zero bias. The superfluidity in this system is *imperfect*. What kind of state can be nearly superfluid in this way? The answer likely involves disorder, which as mentioned above can cause the meron-antimeron pairs to unbind at arbitrarily low temperature. We next discuss a model which seems to capture much of the physics found in experiment.

3. The Coherence Network Model

One important way in which skyrmions and merons of the $\nu = 1$ quantum Hall system are different than those of more standard ferromagnets is that they carry charge. This means that they couple to electric potential fluctuations due to disorder. In these systems, disorder is ubiquitous because electrons are provided to the layers by dopants, which leave behind charged centers. The resulting potential fluctuations are extremely strong, and in fact divergent at long length-scales. In the Efros picture, the system screens nonlinearly by creating large puddles of positive and negative charge, separated by narrow strips of incompressible Hall fluid with local filling factor near $\nu = 1$ [30, 31]. For the bilayer system, the charge flooding the puddles should take the form of merons and antimerons, whose high density

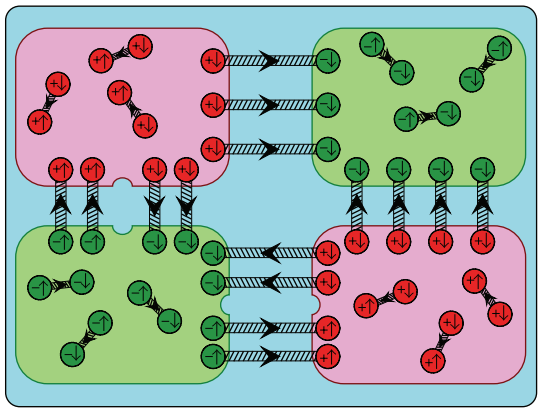

Figure 1: Representation of coherence network. Links and nodes separate puddles of merons (circles). Meron charge and electric dipole moments indicated inside circles, as are strings of overturned phase connecting meron-antimeron pairs. Reproduced from [18].

spoils the interlayer coherence. The coherence however will remain strongest in the regions separating the puddles, even though some meron-antimeron pairs will likely straddle them. Thus one forms a network structure for the regions where the coherence is strong, and these should dominate the "superfluid" properties of the system. A schematic picture of the system is illustrated in Figure 1.

The key assumption in this model is that with such dense puddles, merons are able to diffuse independently through the system. This is supported by a renormalization group analysis, which suggests that there exists a state in which disorder enters as an effective temperature, so that one would likely be above any meron-antimeron unbinding transition for such strong disorder [18]. Motion of the merons is then limited by energy barriers for them to cross the coherent links between puddles. The tendency for dissipationless counterflow to emerge only at zero temperature now becomes very natural. When condensed excitons flow down the system, these produce a force on the merons perpendicular to that current [32]. The resulting meron current is limited by the activation energy to hop over the coherent links and vanishes rapidly but only completely when the temperature drops to zero. This meron current induces a voltage drop in the direction of the exciton current via the Josephson relation, rendering the counterflow current dissipative. True superfluid response in this system can only occur at zero temperature.

Dissipation in the tunneling geometry also emerges naturally in this model [18]. Since the current flows into (say) the top layer on the left and leaves via the bottom layer on the right, the current in the system must be decomposed into a sum of symmetric "coflow" and antisymmetric counterflow (CF). The former is likely carried by edge currents which are essentially dissipationless in the quantum Hall state. To obtain the correct current geometry, the CF current must point in opposite directions at the two ends of the sample. Thinking of the network as a Josephson array, the current of excitons—that is, CF current—is proportional to $\nabla\theta$. In order to inject CF currents in opposite directions at each end of the sample, the phase angle at the sample edges should be rotated in the *same* direction. This means that the phase angle throughout the system will tend to rotate at a uniform rate, which is limited by the $(\Delta_{\mathrm{SAS}}/4\pi\ell_0^2)\cos\theta$ term in (3). This is most effective at the nodes of the network, where the coherence is least compromised by the disorder-induced merons.

The dynamics of a typical node with phase angle θ may be described by a Langevin equation

$$\Gamma\frac{d^2\theta}{dt^2} = \sum_{\mathrm{links}} F_{\mathrm{link}} - \gamma_0\frac{d\theta}{dt} - h\,\sin\theta + \xi(t). \tag{5}$$

The quantities F_{link} represent the torque on an individual "rotor" (*i.e.*, θ variable) due its neighbors, transmitted through the links. Γ is the effective moment of inertia of a rotor, proportional to the capacitance of the node, $h = \Delta_{\mathrm{SAS}}/4\pi\ell_0^2$, ξ is a random (thermal) force, and γ_0 is the viscosity due to dissipation from the other node rotors in the system. For a small driving force, the node responds viscously, and the resulting rotation rate has the form $\gamma\dot{\theta} = \sum F_{\mathrm{link}}$. The Josephson relation $V = (\hbar/e)(d\theta/dt)$ then implies that the viscosity γ is proportional to the tunneling *conductance* σ_T of the system. For $k_BT \gg h$ one may show the viscosity for an individual node to be [33]

$$\gamma = \gamma_0 + \Delta\gamma = \gamma_0 + \sqrt{\frac{\pi}{2\Gamma}}\frac{h^2}{(k_BT)^{3/2}}. \tag{6}$$

As each node contributes the same amount to the total viscosity, the *total* response of the system to the injected CF current obeys

$$I_{\mathrm{CF}} \propto N_{\mathrm{nodes}}\Delta\gamma\frac{e^2V_{\mathrm{int}}}{\hbar} = \sigma_T V_{\mathrm{int}}. \tag{7}$$

Note that because the nodes respond viscously, the tunneling conductance is proportional to the area of the bilayer. This is a nontrivial prediction of the model discussed here, which has been confirmed in experiment [34]. The proportionality of the tunneling conductance to Δ_{SAS}^2 is another nontrivial prediction which appears to be consistent with experimental data, and which contrasts with the result one expects in the absence of disorder, for which $\sigma_T \propto \Delta_{\mathrm{SAS}}$.

4. Drag Experiments and Interlayer Bias

When an electric field is applied perpendicular to the layers, the density in the two layers becomes imbalanced. The effect of this can be incorporated into the model, (2), by replacing $\Gamma\int d\mathbf{r}(m^z)^2$ with $\Gamma\int d\mathbf{r}(m^z - m_0)^2$, with $m_0 = \nu_T\text{-}\nu_B$. The imbalance has interesting consequences for merons: since the pseudospin field $\mathbf{m}$ does not drop back into the $\hat{x}-\hat{y}$ plane as one moves out from the center of meron, the spin-charge relation (1) indicates that the four types of merons will have four different charges. These charges are specifically given by $q_{s,T(B)} = -s\,\sigma\nu_{B(T)}$, where $s = \pm 1$ is the vorticity of the meron, and the $T(B)$ subscript reflects the layer in which the magnetization at the core of the meron—its polarization—resides. The index σ indicates a sign associated with the

polarizations: $\sigma = 1$ for $\mathbf{m}$ in the meron center oriented in the top layer, $\sigma = -1$ for merons where it resides in the bottom layer.

The connection between polarization and charge has very interesting consequences for another type of transport experiment specific to bilayers, known as drag. In these experiments, one drives a current through only a single layer and measures voltage drops either in the drive layer or the drag layer. Within the coherence network model, the activation barrier for merons to hop across incompressible strips will clearly depend on the relative orientation of the meron polarization and the applied bias. Naively one would think that at low temperature, transport will be dominated by only the smallest activation energy, so that a measurement of resistance will reveal an activation energy that is symmetric around zero bias, which drops as the bias increases.

But this is not what is seen in experiment. The activation energy as measured in the drive layer is highest when the density is biased into the drive layer and decreases monotonically as the imbalance is changed so that more density is transferred to the drag layer. In the drag layer, the measured voltage drops turn out to be much smaller than in the drive layer, and are symmetric, but *increase* as the layer is imbalanced [35].

A careful analysis of the situation requires a method for determining voltage drops in individual layers, not just the interlayer voltage difference, which is what the Josephson relation applied above actually reveals. This can be accomplished [36] by adopting a "composite boson" description of the $\nu = 1$ quantum Hall state [1, 37]. The idea is to model electrons as *bosons*, each carrying a single magnetic flux quantum in an infinitesimally thin solenoid. The Aharonov-Bohm effect then implements the correct phase (minus sign) when two of these objects are interchanged [37]. By orienting the flux quanta opposite to the direction of the applied magnetic field, on average the field is canceled, and in mean-field theory the system may be modeled as a collection of bosons in zero field. The quantum Hall state is then equivalent to a Bose condensate of these composite bosons. For the coherent bilayer state, there is an additional sense in which the bosons are condensed: they carry a pseudospin with an in-plane ferromagnetic alignment.

Because merons carry physical charge, they will carry a quantity of magnetic flux proportional to this charge. In analogy with a thin-film superconductor [32], this means that a net current in the bilayer (i.e., a coflow) creates a force on the meron perpendicular to the current. This has to be added to the force due to a counterflow component. Together, these yield a net force which may be shown to be [36]

$$\mathbf{F}_T = \frac{es}{2}\Phi_0[(1+\sigma)\mathbf{J}_B - (1-\sigma)\mathbf{J}_T] \times \hat{z}, \tag{8}$$

where $\mathbf{J}_{T(B)}$ is the current density in the top (bottom) layer. As is clear from this expression, merons with only one of the possible polarizations are subject to a force in a drag experiment, since one of the two current densities vanishes.

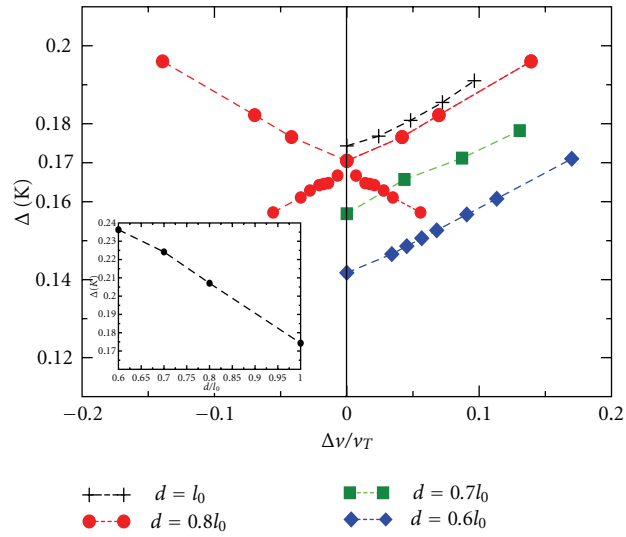

Figure 2: Expected activation energy Δ as a function of relative density imbalance between the layers, $\Delta\nu/\nu_T$. For voltage drop measured in the drive layer, the results are asymmetric with around $\Delta\nu = 0$, as shown explicitly for $d = 0.8\ell_0$ (see text). For measurements in the drag layer, the data is reflected around $\Delta\nu = 0$; the measured result would follow the higher of the two activation energies, yielding a result symmetric in bias. Inset: activation energy at zero bias versus layer separation. Reproduced from [36].

The force $F_{s,\sigma}$ on merons of vorticity s and polarization σ will cause them to flow with a velocity $u_{s,\sigma} = \mu_{s,\sigma}F_{s,\sigma}$, where $\mu_{s,\sigma}$ is an effective mobility, which we expect to be thermally activated, with a bias dependence of the activation energy as discussed above. The resulting motion of the vortices induces voltages in two ways. The first is through the Josepshon relation for the interlayer phase, yielding the relation [36]

$$\Delta V = \Delta V_T - \Delta V_B = -\frac{2\pi h}{e} y_0 \sum_{s,\sigma} n_{s\sigma} s u_{s\sigma} \tag{9}$$

for the voltage drops between ΔV_σ between two points a distance y_0 apart along the direction of electron current, in layer σ, where $n_{s,\sigma}$ is the meron density. The second is due to the effective magnetic flux moving with the merons, which induces a voltage drop between electrons at different points along the current flow that is independent of the layer in which they reside. This contribution is given by [36]

$$(\nu_T \Delta V_T + \nu_B \Delta V_B) = -\frac{h}{e} y_0 \sum_{s,\sigma} n_{s\sigma} q_{s\sigma} u_{s\sigma}. \tag{10}$$

In a drag geometry we have, for example, $J_B = 0$ and $\mathbf{J}_T = (I/W)\hat{y}$, with I the total current and W the sample width. Combining (9) and (10), we obtain $\Delta V_B = 0$ and

$$\frac{\Delta V_T}{I} = \frac{y_0}{W} h\Phi_0 (n_{1,-1}\mu_{1,-1} + n_{-1,-1}\mu_{-1,-1}). \tag{11}$$

Notice that the final result depends on the mobility of *only*

merons with polarization $\sigma = -1$. It immediately follows that the voltage drop in the drive layer is asymmetric with respect to bias, precisely as observed in experiment.

In order to explain the voltage drop in the drag layer ($\Delta V_L \neq 0$), we must identify how forces on the $\sigma = +1$ merons might arise. A natural candidate for this is the attractive interaction between merons with opposite vorticities, which in the absence of disorder binds them into pairs at low meron densities. Assuming that driven merons crossing incompressible strips will occasionally be a component of these bimerons, a voltage drop in the drag layer will result. The mobility of such bimerons is limited by the energy barrier to cross an incompressible strip. These strips are likely to be narrow compared to the size scale of the constituents of the bimeron [36], so we expect the activation energy to be given approximately by the maximum of the activation energies for merons of the two polarizations $\sigma = \pm 1$. This leads to a drag resistance much smaller than that of the drive layer, with an activation energy that is *symmetric* with respect to and increases with bias. These are the behaviors observed in experiment [35]. Figure 2 illustrates the expected activation energy from a microscopic model implementing this physics [36] as a function of relative density imbalance between the layers, $\Delta\nu/\nu_T$, where $\Delta\nu = \nu_T - \nu_B$ and $\nu_T = 1$, for different layer separations. For voltage drop measured in the drive layer, the results are asymmetric around $\Delta\nu = 0$, as shown explicitly for $d = 0.8\ell_0$. For the drive layer, the large circles represent the activation energy found from a voltage drop measurement when it has a higher density than the drag layer, and the small circles the activation energy when it has the smaller density. Thus a measurement on the drive layer while continuously adjusting the density imbalance from positive through zero to negative results in a line from the large circles to the small circles as zero is crossed, yielding an asymmetric result. For measurements in the drag layer, the result would follow the higher of the two activation energies, yielding a result symmetric in bias.

This result followed from the precise cancellation between the counterflow current force on the vorticity of merons of a particular polarization and the Lorentz force associated with meron charge and its associated effective flux. The experiments thus provide indirect evidence that the meron charges vary in precisely the way one expects from the spin-charge relation, (1), verifying this unique property of quantum Hall ferromagnetism.

5. Periodic Models of the Quantum Hall Bilayer

As explained in Section 3, disorder has a nonperturbative effect on the incompressible quantum Hall state. True disorder is extremely difficult to treat theoretically. In analogy with superfluid systems [38], and one-component quantum Hall systems near a plateau transition [39–42], one may hope that a periodic potential captures some of the nonperturbative effects of disorder. Once one has obtained a second-order phase transition, one then adds disorder or other perturbations and examines their relevance/irrelevance [43]. This approach has been very fruitful in the past.

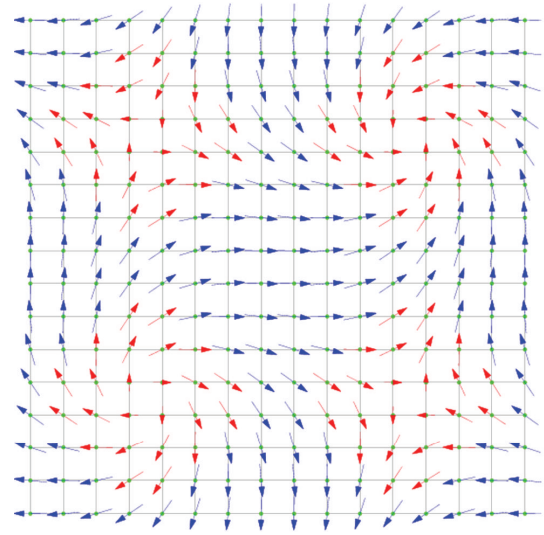

Figure 3: (*Color online*) The ground state configuration for a 16×16 unit cell with the strength of the periodic potential (in units, where $J = 1$) being $V = 3.0$, and the Hubbard interaction is $U = 8.0$. The lengths of the spins denote their planar projection. Note a vortex/antivortex at the center of each puddle.

As a first attempt, one of us (G. Murthy) and Subir Sachdev [13] examined the Composite Boson theory [1] near a putative Superfluid/Mott Insulator transition [38]. The primary difference between the neutral system and this one is that the Composite Boson is charged and is minimally coupled to both the external gauge field and the statistical field which attaches flux. There are two natural phases: a Bose-condensed Higgs phase in which all excitations are massive and the system can be shown to have a quantized Hall conductivity and a Mott Insulating phase in which all conductivities vanish [13].

In the large-N approximation, one can integrate out the bosons, leaving behind an effective theory of gauge fluctuations. The phase transition turns out to be second-order in the large-N limit, with the critical point having the conductivities [13]

$$\sigma_{xx}^*(0,\omega) = \frac{e^2}{h}\frac{\pi/8}{1+(\pi/8)^2}, \qquad \sigma_{xy}^* = \frac{\pi}{8}\sigma_{xx}^*. \tag{12}$$

The XY-angle θ also acquires an imaginary part of the self-energy at the critical point which vanishes as ω^7 for zero interlayer tunneling and ω^5 when interlayer tunneling is nonzero [13].

While this model is fully quantum, it is overly simplistic in assuming that only a single phase transition exists between the uniform superfluid and a Mott Insulator.

Recently, the present authors in collaboration with Jianmin Sun and Noah Bray-Ali have taken some steps towards building a more realistic model [44]. In this model, fermions are assumed to be gapped out, and the real spin is assumed to be fully polarized, leaving dynamics only in the pseudospin. We put the system on a square lattice with

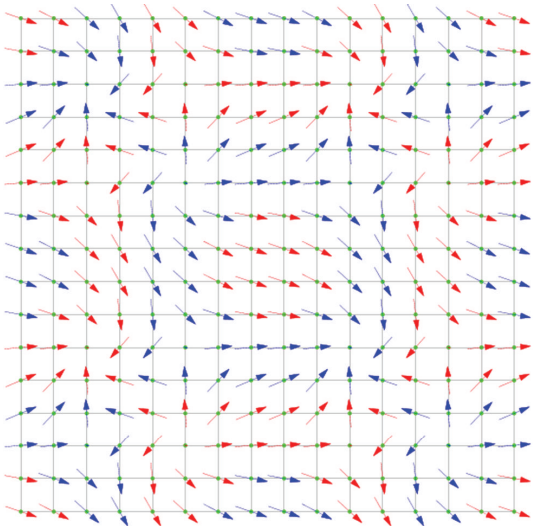

Figure 4: (*Color online*) The ground state configuration for $V = 7.0$ and $U = 8.0$.

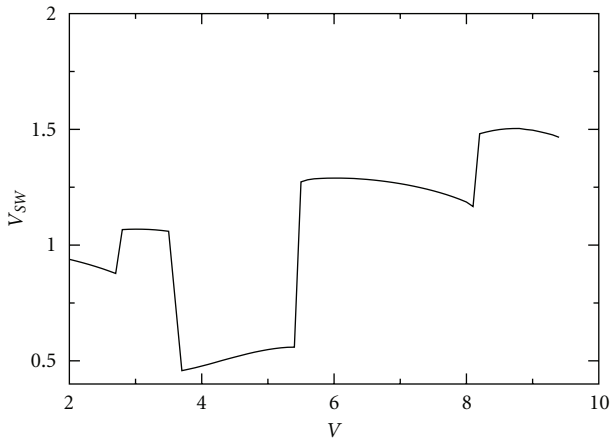

Figure 5: The spin wave velocity of the G-mode as a function of V. Note that it never vanishes, but that it can vary by a factor of three, and have significant discontinuities at transitions.

lattice constant $a = l_0\sqrt{2\pi}$, so that there is one electron per site. There is a periodic potential with period $L = Na$ in each direction coupling to the charge associated with pseudospin textures, which assumes the following form for a triplet of spins on the lattice [45]:

$$\delta Q_{123} = \frac{e}{2\pi}\tan^{-1}\left(\frac{\mathbf{n}_1 \cdot \mathbf{n}_2 \times \mathbf{n}_3}{1 + \mathbf{n}_1 \cdot \mathbf{n}_2 + \mathbf{n}_2 \cdot \mathbf{n}_3 + \mathbf{n}_3 \cdot \mathbf{n}_1}\right). \quad (13)$$

The usual spin-stiffness, planar anisotropy, and interlayer tunneling terms are present. Finally, to model the Coulomb interaction between pseudospin textures, we introduce a Hubbard interaction for the charge on each plaquette $\square$.

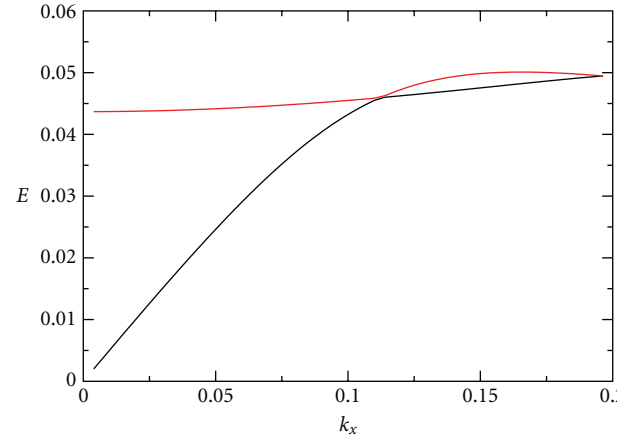

Figure 6: The lowest-lying modes for $V = 4.3$ and $U = 18$. The system is very close to a ground state transition. Note the almost gapless Q-mode.

Thus, the Hamiltonian is

$$\mathcal{H} = -J\sum_{\langle \mathbf{r}\mathbf{r}'\rangle}\left(n_x(\mathbf{r})n_x(\mathbf{r}') + n_y(\mathbf{r})n_y(\mathbf{r}')\right) + \frac{\Gamma}{2}\sum_{\mathbf{r}}(n_z(\mathbf{r}))^2 - h\sum_{\mathbf{r}}n_x(\mathbf{r}) - V\sum_{\square}f(X,Y)\delta Q_{\square} + H_U[\delta Q^2]. \quad (14)$$

Here V is the strength of the periodic potential living on the dual lattice, and $f(X, Y)$ its functional form. We choose the simple form $f = \sin(2\pi X/L)\sin(2\pi Y/L)$, resulting in each unit cell having four puddles, two each being positive and negative. We show results for $J = \Gamma$ and measure all energies in units of J. We find the ground states (really saddle point configurations of the spins) numerically by simulated annealing. For small V the uniform ferromagnetic state is the ground state, but as V increases the ground state nucleates more and more merons/antimerons in each of the puddles. An example is shown Figure 3.

As the strength of the periodic potential increases, more merons/antimerons are nucleated to screen the potential, as exemplified by Figure 4.

The phase transitions between these ground states are generically first order, though occasionally they can become weakly first order or even second order. Various physical quantities, such as the spin stiffness (without vortex corrections) and spin wave velocity, also exhibit jumps at these transitions, as shown in Figure 5.

We note an important qualitative difference between the models with and without the periodic potential as a function of interlayer coupling. In the clean model, with no potential, the interlayer tunneling strength h is strongly relevant, and thus systems with weak and strong h at the microscopic scale are expected to behave similarly at large length scales. However, in the model with a periodic potential, as h increases, the system undergoes transitions in which merons/antimerons are lost from the puddles, ending at very large h in the uniform ferromagnetic state. Thus, the

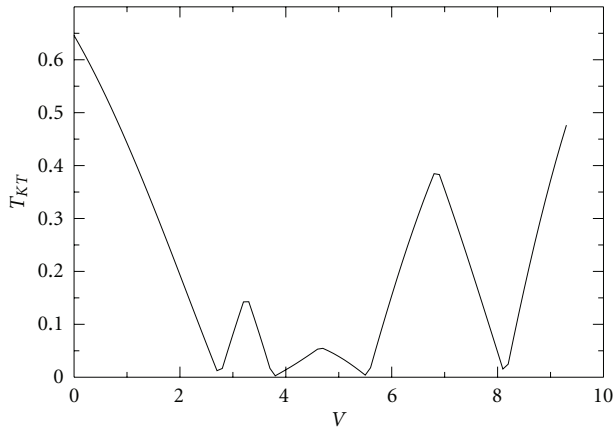

FIGURE 7: T_{KT} in units of J/k_B as a function of V for a 16×16 unit cell at $U = 8$. Dramatic decreases in the transition temperature T_{KT} separating the low-temperature ferromagnetic phase from high-temperature paramagnetic phase occur due to changes in the topological density of the ground-state at critical potential strengths.

weak and strong h systems are in different phases, and there is no reason to expect similar behavior from them. Indeed, experimentally one sees the puzzling features only in systems with a tiny h.

Secondly, we examined the collective mode spectrum, and found that when the transition is weakly first order there is a new, quadratically dispersing, mode which becomes low in energy and can be even lower in energy than the linearly dispersing Goldstone mode (or G-mode). We call this new mode the Q-mode. Examining the wave functions of the Q-mode reveals that it represents vortex motion within the puddle. An example of the low-energy part of the collective mode dispersions is shown in Figure 6.

The presence of first-order ground state phase transitions results in the strong suppression of the Berezinskii-Kosterlitz-Thouless transition temperature T_{KT} near the V_0 corresponding to the transition. This can be seen in a simple way as follows. The ground state transition occurs between states having different numbers of merons/antimerons in each puddle. The simplest picture is when the ground state on one side of the transition has no merons/antimerons while the ground state on the other side has a checkerboard pattern of merons/antimerons. Integrating out the spin waves, the difference in ground state energy can be modelled as arising from a Coulomb gas energy of the form

$$E[\{m(\mathbf{R}\,\}] = \frac{1}{2}\sum_{\mathbf{R}\neq\mathbf{R}'} \mathcal{K}_s m(\mathbf{R}) m(\mathbf{R}') \log\left(\frac{|\mathbf{R}-\mathbf{R}'|}{\xi}\right) - E_c(V)\sum_{\mathbf{R}} (m(\mathbf{R}))^2, \tag{15}$$

where $E_c(V)$ is a core energy that depends on the potential strength, $m(\mathbf{R})$ is the vorticity at the dual lattice site $\mathbf{R}$, and ξ is a cutoff which can be tuned so that the groundstate goes through the transition seen to occur at V_c in the simulation. Near the transition the difference in ground state energies behaves as $\alpha(V - V_c)$. Attributing this difference to the difference in vortex/antivortex core energies, we can extract $E_c \approx (\alpha/4)|V - V_c|$. Note that the vortex and the absence of a vortex interchange roles as the excitation as one goes through the transition. As the core energy of a vortex/antivortex vanishes, they proliferate and disorder the system. One can solve the renormalization group equations to find T_{KT} as one varies V. We find that T_{KT} is typically suppressed by an order of magnitude compared to Hartree-Fock estimates, as shown in Figure 7.

Now consider the suppression of interlayer tunneling near a ground state transition with a nearly gapless Q-mode. It is important to note that the XY angle θ couples to both the G- and Q-modes, and for small deviations, can be written as a linear combination of them. To see the effect of the Q-mode, one decomposes the tunneling term as

$$h\cos(\theta) \simeq h\left(e^{i\theta_G} e^{i\theta_Q} + c.c\right) \tag{16}$$

and integrates out the Q-mode at nonzero temperature T. Assuming a quadratic dispersion $\omega_Q(\mathbf{k}) = E_{Q0} + \gamma\mathbf{k}^2$, after integrating the Q-mode one obtains a renormalized h

$$h_R \approx h e^{-Tl^2 \log(\Lambda/E_{Q0})/\gamma}. \tag{17}$$

Here Λ is a cutoff, and it can be seen that as the gap E_{Q0} of the Q-mode vanishes, $h_R \to 0$.

One of the most important open questions is whether, and how much of, the phenomenology of the system with the periodic potential survives in the system with true disorder. Our expectation is that the qualitative difference between weak and strong tunneling will survive, as will the fact that the ground state has topological content. One can expect the disorder to smooth the first-order transitions into second-order ones with a gapless mode at the transition [46–48]. In such a case, near a transition one expects the suppression of interlayer tunneling to survive as well. Furthermore, an important effect of disorder is to create large rare regions in which the system is close to critical (the Griffiths phase [49]), and thus even for a *generic* disorder strength one expects low-energy modes to exist in the system. However, whether interlayer tunneling is thus suppressed for generic disorder strength is not clear.

6. Conclusion

Quantum Hall bilayers have natural descriptions in the languages of ferromagnetism and thin film superconductivity. Both these descriptions suggest that the system should have vortex-like excitations, called merons, which can play a key role in the dissipative properties of the system. Real bilayer systems are inevitably subject to disorder, which is likely to be strong, and to induce such vortices in the groundstate, forming a "coherence network" which surrounds puddles of merons. We have discussed how the motion of merons accounts for the deviation of the system from perfect superfluid behavior and how the model naturally explains dissipation at finite temperatures in in counterflow, tunneling, and drag geometries. To better

understand quantum effects in this system, one can consider a simpler model in which the puddles are periodically arranged and study the low energy collective modes of the system. In this case we found a series of first-order zero temperature transitions separating states of different meron occupations in the puddles and argued that the Kosterlitz-Thouless temperature should drop to zero at these transitions. Approaching these transitions, the collective mode spectrum may develop a low energy mode associated with vortex motion which can greatly suppress the effect of tunneling on the system.

There is much yet to understand about this rich and fascinating system, including how quantum effects impact the zero temperature state and its transport properties, whether there is any attainable limit in which true counterflow superfluidity could be observed, and whether the competing effects of tunneling and disorder can lead to further exotic states. We anticipate that this system will remain a subject of keen interest for years to come.

Acknowledgments

The authors have benefited from discussions and collaborations with many colleagues in the course of the research described here. They would like in particular to thank Noah Bray-Ali, Luis Brey, René Côté, Jim Eisenstein, Allan MacDonald, Kieran Mullen, Bahman Roostaei, Subir Sachdev, Steve Simon, Joseph Straley, and Jianmin Sun. The work described here was supported by the NSF through Grants nos. DMR-0704033 (H. A. Fertig) and DMR-0703992 (G. Murthy).

References

[1] D.-H. Lee and C. L. Kane, "Boson-vortex-Skyrmion duality, spin-singlet fractional quantum hall effect, and spin-1/2 anyon superconductivity," *Physical Review Letters*, vol. 64, no. 12, pp. 1313–1317, 1990.

[2] S. L. Sondhi, A. Karlhede, S. A. Kivelson, and E. H. Rezayi, "Skyrmions and the crossover from the integer to fractional quantum Hall effect at small Zeeman energies," *Physical Review B*, vol. 47, no. 24, pp. 16419–16426, 1993.

[3] E. H. Rezayi, "Reversed-spin excitations of the fractionally quantized Hall effect from finite-size calculations," *Physical Review B*, vol. 36, no. 10, pp. 5454–5457, 1987.

[4] E. H. Rezayi, "Wave functions and other properties of spin-reversed quasiparticles at =1/m Landau-level occupation," *Physical Review B*, vol. 43, no. 7, pp. 5944–5949, 1991.

[5] H. A. Fertig, L. Brey, R. Côté, and A. H. MacDonald, "Charged spin-texture excitations and the Hartree-Fock approximation in the quantum Hall effect," *Physical Review B*, vol. 50, no. 15, pp. 11018–11021, 1994.

[6] S. E. Barrett, G. Dabbagh, L. N. Pfeiffer, K. W. West, and R. Tycko, "Optically pumped NMR evidence for finite-size Skyrmions in GaAs quantum wells near Landau level filling ν=1," *Physical Review Letters*, vol. 74, no. 25, pp. 5112–5115, 1995.

[7] A. Schmeller, J. P. Eisenstein, L. N. Pfeiffer, and K. W. West, "Evidence for skyrmions and single spin flips in the integer quantized hall effect," *Physical Review Letters*, vol. 75, no. 23, pp. 4290–4293, 1995.

[8] G. Murthy, "Effects of disorder on the $\nu = 1$ quantum hall state," *Physical Review B*, vol. 64, no. 24, Article ID 241309, 4 pages, 2001.

[9] A. H. MacDonald, S. M. Girvin, S. Das Sarma, and A. Pinczuk, *Perpspectives in Quantum Hall Effects*, John Wiley & Sons, New York, NY, USA, 1996.

[10] J. Bourassa, B. Roostaei, R. Côté, H. A. Fertig, and K. Mullen, "Pseudospin vortex-antivortex states with interwoven spin textures in double-layer quantum Hall systems," *Physical Review B*, vol. 74, no. 19, Article ID 195320, 14 pages, 2006.

[11] P. Giudici, K. Muraki, N. Kumada, Y. Hirayama, and T. Fujisawa, "Spin-dependent phase diagram of the $\nu_T = 1$ bilayer electron system," *Physical Review Letters*, vol. 100, no. 10, Article ID 106803, 4 pages, 2008.

[12] A. D.K. Finck, J. P. Eisenstein, L. N. Pfeiffer, and K. W. West, "Quantum hall exciton condensation at full spin polarization," *Physical Review Letters*, vol. 104, no. 1, 2010.

[13] G. Murthy and S. Sachdev, "Quantum hall to insulator transition in the bilayer quantum hall ferromagnet," *Physical Review Letters*, vol. 101, no. 22, Article ID 226801, 4 pages, 2008.

[14] L. Brey, H. A. Fertig, R. Côté, and A. H. MacDonald, "Charged pseudospin textures in double-layer quantum Hall systems: bimerons and meron crystals," *Physical Review B*, vol. 54, no. 23, pp. 16888–16902, 1996.

[15] K. Moon, H. Mori, K. Yang et al., "Spontaneous interlayer coherence in double-layer quantum Hall systems: charged vortices and Kosterlitz-Thouless phase transitions," *Physical Review B*, vol. 51, no. 8, pp. 5138–5170, 1995.

[16] H. A. Fertig, "Deconfinement in the two-dimensional XY model," *Physical Review Letters*, vol. 89, no. 3, Article ID 035703, 4 pages, 2002.

[17] H. A. Fertig and J. P. Straley, "Deconfinement and dissipation in quantum hall Josephson tunneling," *Physical Review Letters*, vol. 91, no. 4, Article ID 046806, 4 pages, 2003.

[18] H. A. Fertig and G. Murthy, "Coherence network in the quantum hall bilayer," *Physical Review Letters*, vol. 95, no. 15, Article ID 156802, 4 pages, 2005.

[19] H. A. Fertig, "Energy spectrum of a layered system in a strong magnetic field," *Physical Review B*, vol. 40, no. 2, pp. 1087–1095, 1989.

[20] A. H. MacDonald, H. A. Fertig, and L. Brey, "Skyrmions without sigma models in quantum hall ferromagnets," *Physical Review Letters*, vol. 76, no. 12, pp. 2153–2156, 1996.

[21] M. Kellogg, J. P. Eisenstein, L. N. Pfeiffer, and K. W. West, "Vanishing hall resistance at high magnetic field in a double-layer two-dimensional electron system," *Physical Review Letters*, vol. 93, no. 3, Article ID 036801, 4 pages, 2004.

[22] E. Tutuc, M. Shayegan, and D. A. Huse, "Counterflow measurements in strongly correlated GaAs hole bilayers: evidence for electron-hole pairing," *Physical Review Letters*, vol. 93, no. 3, Article ID 036802, 4 pages, 2004.

[23] X. G. Wen and A. Zee, "Tunneling in double-layered quantum Hall systems," *Physical Review B*, vol. 47, no. 4, pp. 2265–2270, 1993.

[24] I. B. Spielman, J. P. Eisenstein, L. N. Pfeiffer, and K. W. West, "Resonantly enhanced tunneling in a double layer quantum hall ferromagnet," *Physical Review Letters*, vol. 84, no. 25, pp. 5808–5811, 2000.

[25] L. Tiemann, Y. Yoon, W. Dietsche, K. Von Klitzing, and W. Wegscheider, "Dominant parameters for the critical tunneling current in bilayer exciton condensates," *Physical Review B*, vol. 80, no. 16, Article ID 165120, 2009.

[26] J.-J. Su and A. H. MacDonald, "Critical tunneling currents in quantum Hall superfluids: pseudospin-transfer torque theory," *Physical Review B*, vol. 81, no. 18, Article ID 184523, 11 pages, 2010.

[27] D. V. Fil and S. I. Shevchenko, "Josephson vortex motion as a source for dissipation of superflow of e-h pairs in bilayers," *Journal of Physics Condensed Matter*, vol. 21, no. 21, Article ID 215701, 2009.

[28] M. Abolfath, A. H. MacDonald, and L. Radzihovsky, "Critical currents of ideal quantum Hall superfluids," *Physical Review B*, vol. 68, no. 15, Article ID 155318, 16 pages, 2003.

[29] P. R. Eastham, N. R. Cooper, and D. K. K. Lee, "Vortex states of a disordered quantum Hall bilayer," *Physical Review B*, vol. 80, no. 4, Article ID 045302, 5 pages, 2009.

[30] A. L. Efros, "Density of states of 2D electron gas and width of the plateau of IQHE," *Solid State Communications*, vol. 65, no. 11, pp. 1281–1284, 1988.

[31] A. L. Efros, F. G. Pikus, and V. G. Burnett, "Density of states of a two-dimensional electron gas in a long-range random potential," *Physical Review B*, vol. 47, no. 4, pp. 2233–2243, 1993.

[32] A. J. Leggett, *Quantum Liquids*, Oxford University Press, New York, NY, USA, 2006.

[33] W. Dieterich, I. Peschel, and W. R. Schneider, "Diffusion in periodic potentials," *Zeitschrift für Physik B Condensed Matter and Quanta*, vol. 27, no. 2, pp. 177–187, 1977.

[34] A. D. K. Finck, A. R. Champagne, J. P. Eisenstein, L. N. Pfeiffer, and K. W. West, "Area dependence of interlayer tunneling in strongly correlated bilayer two-dimensional electron systems at $\nu_T = 1$," *Physical Review B*, vol. 78, no. 7, Article ID 075302, 5 pages, 2008.

[35] R. D. Wiersma, J. G.S. Lok, S. Kraus et al., "Activated transport in the separate layers that form the $\nu_T = 1$ Exciton condensate," *Physical Review Letters*, vol. 93, no. 26, Article ID 266805, 4 pages, 2004.

[36] B. Roostaei, K. J. Mullen, H. A. Fertig, and S. H. Simon, "Theory of activated transport in hilayer quantum Hall systems," *Physical Review Letters*, vol. 101, no. 4, Article ID 046804, 4 pages, 2008.

[37] S. C. Zhang, T. H. Hansson, and S. Kivelson, "Effective-field-theory model for the fractional quantum hall effect," *Physical Review Letters*, vol. 62, no. 1, pp. 82–85, 1989.

[38] M. P. A. Fisher, P. B. Weichman, G. Grinstein, and D. S. Fisher, "Boson localization and the superfluid-insulator transition," *Physical Review B*, vol. 40, no. 1, pp. 546–570, 1989.

[39] W. Chen, M. P. A. Fisher, and Y.-S. Wu, "Mott transition in an anyon gas," *Physical Review B*, vol. 48, no. 18, pp. 13749–13761, 1993.

[40] X.-G. Wen and Y.-S. Wu, "Transitions between the quantum Hall states and insulators induced by periodic potentials," *Physical Review Letters*, vol. 70, no. 10, pp. 1501–1504, 1993.

[41] L. P. Pryadko and S.-C. Zhang, "Duality and universality for the Chern-Simons bosons," *Physical Review B*, vol. 54, no. 7, pp. 4953–4955, 1996.

[42] J. Ye and S. Sachdev, "Coulomb interactions at quantum hall critical points of systems in a periodic potential," *Physical Review Letters*, vol. 80, no. 24, pp. 5409–5412, 1998.

[43] A. W. W. Ludwig, M. P. A. Fisher, R. Shankar, and G. Grinstein, "Integer quantum Hall transition: an alternative approach and exact results," *Physical Review B*, vol. 50, no. 11, pp. 7526–7552, 1994.

[44] J. Sun, G. Murthy, H. A. Fertig, and N. Bray-Ali, "Bilayer quantum Hall ferromagnet in a periodic potential," *Physical Review B*, vol. 81, no. 19, Article ID 195314, 13 pages, 2010.

[45] S. Sachdev and K. Park, "Ground states of quantum antiferromagnets in two dimensions," *Annals of Physics*, vol. 298, no. 1, pp. 58–122, 2002.

[46] Y. Imry and S.-K. Ma, "Random-field instability of the ordered state of continuous symmetry," *Physical Review Letters*, vol. 35, no. 21, pp. 1399–1401, 1975.

[47] M. Aizenman and J. Wehr, "Rounding of first-order phase transitions in systems with quenched disorder," *Physical Review Letters*, vol. 62, no. 21, pp. 2503–2506, 1989.

[48] K. Hui and A. N. Berker, "Random-field mechanism in random-bond multicritical systems," *Physical Review Letters*, vol. 62, no. 21, pp. 2507–2510, 1989.

[49] R. B. Griffiths, "Nonanalytic behavior above the critical point in a random ising ferromagnet," *Physical Review Letters*, vol. 23, no. 1, pp. 17–19, 1969.

Hindawi Publishing Corporation
Advances in Condensed Matter Physics
Volume 2011, Article ID 792125, 7 pages
doi:10.1155/2011/792125

Research Article

Breakdown of Counterflow Superfluidity in a Disordered Quantum Hall Bilayer

D. K. K. Lee,[1] P. R. Eastham,[2] and N. R. Cooper[3]

[1] *Blackett Laboratory, Imperial College London, London SW7 2AZ, UK*
[2] *School of Physics, Trinity College, Dublin 2, Ireland*
[3] *Cavendish Laboratory, University of Cambridge, Cambridge CB3 0HE, UK*

Correspondence should be addressed to D. K. K. Lee, dkk.lee@imperial.ac.uk

Received 1 September 2010; Accepted 12 January 2011

Academic Editor: Yogesh Joglekar

We present a theory for the regime of coherent interlayer tunneling in a disordered quantum Hall bilayer at total filling factor one, allowing for the effect of static vortices. We find that the system consists of domains of polarized superfluid phase. Injected currents introduce phase slips between the polarized domains which are pinned by disorder. We present a model of saturated tunneling domains that predicts a critical current for the breakdown of coherent tunneling that is extensive in the system size. This theory is supported by numerical results from a disordered phase model in two dimensions. We also discuss how our picture might be used to interpret experiments in the counterflow geometry and in two-terminal measurements.

1. Introduction

In a quantum Hall bilayer at total Landau level filling $\nu_T = 1$, Coulomb interactions induce a state with interlayer phase coherence [1, 2]. This state is expected to be approximately the Halperin [111] state [3], which can be understood as a Bose-Einstein condensate of interlayer excitons [4, 5]. The motion of excitons corresponds to counterflowing electrical currents in the layers so that excitonic supercurrents can give dissipationless electrical transport. The superfluid properties of the [111] state have been demonstrated theoretically by Wen and Zee [6, 7].

This counterflow superfluidity can be probed in tunneling experiments. In the tunneling geometry (Figure 1), a current I_t is injected into the top layer at one corner and removed from the bottom layer at the opposite corner. These current flows may be written as superpositions of layer-symmetric and layer-antisymmetric currents

$$I_{\text{in(out)}} = \frac{1}{2} I_t \left[\begin{pmatrix} 1 \\ 1 \end{pmatrix} \pm \begin{pmatrix} 1 \\ -1 \end{pmatrix} \right], \tag{1}$$

where the two components refer to currents in the two layers. Thus, the tunneling experiment corresponds to a flow of layer-symmetric current, with equal counterflow currents $I_{\text{CF}} = I_t/2$ injected by both the electron source and drain. The symmetric component is transported by a dissipationless edge state, which does not penetrate the bulk due to an energy gap to charged excitations. However, the bulk can carry the counterflow component as a charge-neutral excitonic supercurrent. Since both these channels are dissipationless, we expect dissipationless electrical transport. In particular, a finite interlayer current I at negligible interlayer voltage V has been predicted [8, 9]. This has been recently confirmed by four-terminal measurements by Tiemann and coworkers [10, 11]. This phenomenon can be regarded as a form of the Josephson effect [7]. Note that thermally activated quasiparticles and contact effects [12] can give rise to complications in actual experiments.

The Josephson-like regime persists for interlayer currents up to a critical value I_c. Above I_c, interlayer transport becomes dissipative. Nevertheless, interlayer coherence can still be detected in the interlayer IV characteristics of the system. A strong peak is observed at zero bias in the differential interlayer conductivity. This is followed at low bias by a regime with negative differential conductivity [13, 14]. This regime can be studied theoretically treating the interlayer tunneling as a perturbation [15–17].

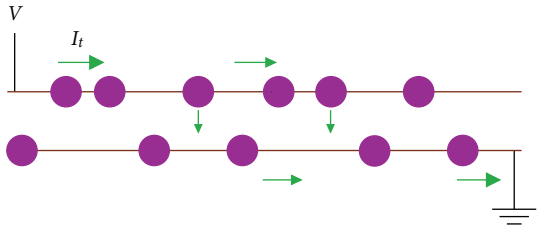

Figure 1: Schematic diagram of tunneling experiment.

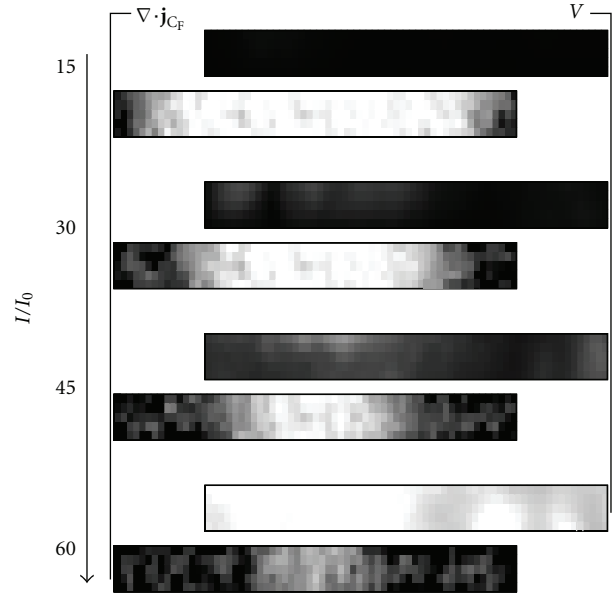

Figure 2: Spatial distribution of tunneling currents (left column) and interlayer voltages (right column), in a lattice model of 200 × 20 sites, with current injection at the two lower corners. The injected counterflow currents are $I/I_0 = 15, 30, 45, 60$ for the four pairs of plots. Dark colours, left column: high current. Dark colours, right column: low voltage. $t\xi^2/\rho_s = 0.6$. Results are averaged over 500 realizations; tunneling currents are summed over blocks of 3 × 3 sites.

In this paper, we focus on the Josephson regime below the critical current and present a physical picture of its breakdown. We have previously presented, in a short paper [18], a theory of this breakdown based on numerical results on a one-dimensional model. The aim of the present paper is to present numerical results for a two-dimensional model, which directly demonstrate the breakdown mechanism in a realistic geometry. The key motivation of our work is to understand the observation [11] that the critical current I_c is proportional to the sample area. (Area scaling is also observed in the zero-bias peak of the interlayer conductivity [19]. We will discuss this in Section 6.) The source and drain contacts for the applied current are located at opposite ends of the system. If one models this system as a clean homogeneous bilayer using reasonable estimates of the tunnel splitting, one finds that the injected current should have tunneled across the bilayer within a few microns of the source contact (λ_J in (6)). Such a current profile would suggest that the critical value of the interlayer current should *not* depend on the sample length in the direction of the current [12, 20, 21]. Put another way, the area scaling of the critical current could only be explained by a clean model of the bilayer if one accepts a tunnel splitting that is anomalously small by several orders of magnitude [12].

A similar puzzle is found in the original observation of dissipationless counterflow [22, 23] in the counterflow geometry (Figure 3). Again, counterflow currents apparently traverse the system over distances orders of magnitude further than expected. We will return to this geometry in the final section.

The resolution of this puzzle lies in the presence of disorder. We shall see (Figure 2) that in the presence of static phase disorder (pinned vortices), the supercurrent profile can be pinned by disorder. The time-independent supercurrents can then penetrate into the sample over indefinitely large distances, limited only by the finite size of the sample. In fact, we find that dissipation only appears when supercurrents completely fill the sample. This mechanism gives a critical current (11) which is proportional to the area of the sample. The magnitude of this critical current agrees with experiments, using reasonable estimates of the parameters [18].

This paper is organized as follows. We will discuss the origin of disorder in the bilayer in Section 2. Then, in Section 3, we will introduce the phase Hamiltonian for the excitonic superfluid that describes the interlayer-coherent phase of the quantum Hall bilayer. In Section 4, we discuss how quenched vortices in the superfluid affect the ground state of the system and its response to injected currents. Then, in Section 5, we present the results of a numerical simulation of the bilayer in the tunneling configuration to support the prediction of our theory. In the final section, we discuss how our picture can be used to interpret experiments for the bilayer in other configurations.

2. Model of Disorder

Weak disorder, such as a spatially varying tunneling splitting, does not affect the tunneling properties of the system dramatically [24]. A tunneling mechanism based on a disordered edge has been proposed by Rossi et al. [25]. However, such a theory predicted linear scaling with the sample length but not its area.

We consider here a bilayer with charge disorder in the bulk. One common source for this disorder is the electrostatic potential due to disordered dopant layers. We expect the incompressible quantum Hall phase to occupy only a fraction of the sample, with the remainder occupied by puddles of compressible electron liquid. Thus, the incompressible phase forms a network of channels separating puddles of size $\xi \approx d_d \approx 200$ nm, the distance to the dopants. We suppose that the width of the channels is of the order of the magnetic length $\ell_B \sim 20$ nm. This coherent network model was first studied in the context of the quantum Hall bilayer by Fertig and Murthy [26].

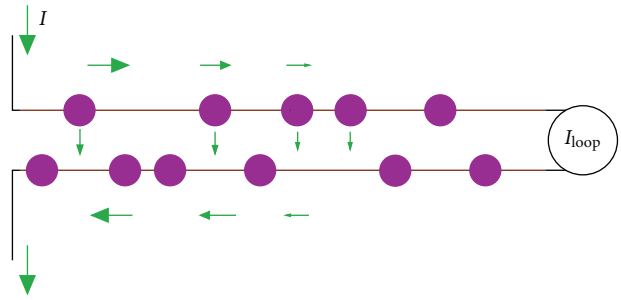

Figure 3: Schematic diagram of a counterflow experiment with a short circuit to complete current loop for counterflow. I_{loop} measures current through the short circuit. Diagram depicts the Josephson regime where the loss of counterflow current through tunneling means that $I_{\text{loop}} = 0$. The current-carrying region penetrates to the right as the injected current I is increased, eventually reaching the other end at I_c.

In a quantum Hall superfluid, excess charge nucleates vortices in the exciton superfluid [16, 17, 26–28]. For a balanced bilayer with individual layer fillings $\nu_1 = \nu_2 = 1/2$ these vortices are merons of charge $\pm e/2$. (In an unbalanced bilayer, the charges are [29] $\pm e\nu_{1(2)}$.) In previous work [27], we have studied how the vortex density is determined by a competition between the superfluid energy cost of the vortex and the charging energy of each puddle. We found that the bilayer can be strongly disordered in the current experimental regimes. This suggests that the random field due to the pinned vortices has an exponentially decaying correlation function in space.

The above scenario provides a specific physical model for quenched vortices with short-ranged correlations in the exciton superfluid. The theory we present below depends on the existence of trapped fractional $e/2$ charges to create these vortices but does not depend crucially on the details of the disorder distribution. Our results should be valid as long as the vortices are dense enough that their separation ($\sim\xi$) is smaller than the clean tunneling length scale λ_J (6).

3. Phase Model

In the previous section, we have outlined a model of disorder which induced quenched vortices in a quantum Hall state. To describe this exciton superfluid with quenched vortices, we start with an effective Hamiltonian for the phase θ of the superfluid. We separate out the component, θ^0, of the phase field that is due to the quenched vortices. The remaining component, $\phi \equiv \theta - \theta^0$, would have no vorticity in the ground state but may acquire vorticity in the presence of injected currents and other external perturbations. It can be shown that the effective Hamiltonian can be written as a random field XY model

$$H_{\text{eff}} = \int \left[\frac{\rho_s}{2} (\nabla\phi)^2 - t\cos(\phi + \theta^0) \right] d^D\mathbf{r}, \tag{2}$$

which describes the low-energy phase fluctuations of a bilayer containing pinned vortices. This form is a simple extension of the form for a clean model [8]. The first term describes the superfluid stiffness to phase twists, while the second describes the interlayer tunneling. We will assume that the quenched phase field θ^0 has a correlation length of ξ.

In the Josephson regime, there is no quasiparticle flow at zero temperature. All currents are accounted for by superflow and coherent tunneling. The counterflow supercurrent density above the ground state, $\mathbf{j}_{\text{CF}}$, and the interlayer tunneling current density, J_t, are related to the phase field by

$$\mathbf{j}_{\text{CF}} = \frac{e\rho_s}{\hbar}\nabla\phi, \qquad J_t = \frac{et}{\hbar}\sin(\phi + \theta^0). \tag{3}$$

A time-varying superfluid phase $\phi(t)$ gives rise to an interlayer voltage difference V via the Josephson relation

$$V = \frac{\hbar\dot{\phi}}{e}. \tag{4}$$

Therefore, a state with a finite interlayer current at zero interlayer voltage is time-independent, corresponding to a local minimum of the energy (2). The stationary equation is simply the continuity equation stating that the loss of counterflow current is accounted for by interlayer tunneling $\nabla \cdot \mathbf{j}_{\text{CF}} = J_t$. This can be written as

$$-\rho_s\nabla^2\phi + t\sin(\phi + \theta^0) = 0. \tag{5}$$

All states with zero interlayer voltage obey this equation. The dependence on the injected current arises as the boundary conditions at the source and drain specifying the injected counterflow component $\mathbf{j}_{\text{CF}}$. In terms of the phase field, this is a boundary condition on $\nabla\phi$.

We expect that the counterflow current injected at the boundary will decay into the sample because interlayer tunneling will recombine electrons and holes across the two layers, as depicted in Figure 3. In the clean case ($\theta^0 = 0$), one expects [20, 30] the static solution to show all the injected counterflow current tunneling across the bilayer over a "Josephson length" of

$$\lambda_J = \sqrt{\frac{\rho_s}{t}}. \tag{6}$$

This length scale is estimated to be of the order of a few microns using realistic parameters.

Since the phase angle is compact, this implies a maximum injected current density of $\rho_s|\nabla\phi| \sim \pi\rho_s/\lambda_J$. For higher injected currents, phase slips enter and propagate through the system. This gives rise to a time-varying phase and hence a nonzero interlayer voltage *via* the Josephson relation (4).

Note that this picture of current penetration into the clean system gives a penetration depth as a microscopic length scale independent of the injected current. We will see below that the disordered system behaves qualitatively differently—the current can penetrate into an indefinitely large area of the system. The reason is that injected phase slips are pinned by disorder, and therefore, a static solution to (5) can persist to higher injected currents. In the next section, we will discuss this picture of pinning.

4. Pinned Superfluid

We will now review the heuristic theory of pinning presented in our previous work [18] in order to provide the context to interpret our simulation results. The quenched vortices play a crucial role for the critical current. They pin any injected supercurrents and sustain dissipationless states. This is reminiscent of how disorder pins magnetic flux in superconductors [31–33] or charge in charge-density waves [34]. However, we emphasize that there is a significant difference in the bilayer compared with these other systems. In the superconductor, the depinning force arises from the Lorentz force on the flux lines due to the bulk transport current. In charge-density-wave systems, depinning originates from the electric field in the bulk which is an insulator when the charge density cannot slide. In the quantum Hall bilayer, depinning arises from the injected charge current which is applied *only* at the sample boundary. Thus, in this case, the critical current will depend on how the depinning "forces" are transmitted through the system. In such a geometry, it is not immediately obvious how the critical current I_c would scale with the area of the whole sample.

We will borrow from the Fukuyama-Lee theory [34] of disordered charge density waves and the Imry-Ma theory [35] for ferromagnets in random fields. We recall the form of the ground states of the random field XY model, (2), in the weak disorder regime $\xi \ll \lambda_J$ relevant for the bilayer. In this regime, it is energetically costly for the phase ϕ to follow the random field θ^0 which varies over the scale of the correlation length ξ. The ground state consists of domains of polarized phase. These domains cannot be arbitrarily large, because the energy cost of the mismatch between the phase and random field grows with the domain size. The energy cost for a phase twist that varies over the scale l is $E_s(l) \sim \rho_s l^{D-2}$ in D dimensions. The typical tunneling energy of a polarized region of size l is obtained by summing random energies in the range $\pm t\xi^D$ for its $(l/\xi)^D$ correlation areas, giving $E_t(l) \sim t\xi^D(l/\xi)^{D/2}$. The phases will twist when $E_t(l)$ exceeds $E_s(l)$. Therefore, the ground state consists of domains of size L_d determined by

$$E_s(L_\mathrm{d}) \sim E_t(L_\mathrm{d}). \tag{7}$$

This "Imry-Ma scale" for the domain is

$$L_\mathrm{d} \sim \left(\frac{\rho_s}{t\xi^{D/2}}\right)^{2/(4-D)} = \left(\frac{\lambda_J^2}{\xi^{D/2}}\right)^{2/(4-D)}. \tag{8}$$

In this ground state of polarized domains, the average coarse-grained phase over a domain is chosen such that the tunneling energy H_t of each domain is minimized. Since $\delta H_t/\delta\phi(\mathbf{r})$ is the tunneling current at position $\mathbf{r}$, the total tunneling current over the domain vanishes.

In two dimensions, $L_\mathrm{d} = \lambda_J^2/\xi$. We see that in the experimentally relevant regime of $\lambda_J \gg \xi$, this new disorder-induced length scale is much larger than the Josephson length. This is the length scale controlling current penetration into the sample. However, as we see below, this should not be interpreted simply as a renormalized length scale for how far counterflow currents penetrate into the sample.

Consider now the effect of an injected counterflow which imposes a phase twist at the boundary. The phase will therefore twist away from its equilibrium configuration. We assume that the domain at the boundary remains polarized at short distances and so will rotate uniformly on the scale of L_d. This generates a tunneling current which reduces the counterflow current. The residual counterflow currents will be transmitted further into the sample, causing the domains there to rotate in a similar way.

This picture allows us to average over each domain. The total tunneling current in a domain consists of a similar random sum to that for the tunneling energy, E_t, and is given by $I_\mathrm{d} f(\overline{\phi})$, where

$$I_\mathrm{d} = \frac{eE_t(L_\mathrm{d})}{\hbar} = \frac{e\rho_s}{\hbar} L_\mathrm{d}^{D-2}, \tag{9}$$

$\overline{\phi}$ is the deviation of the coarse-grained phase from its equilibrium value, and the range of $f(\overline{\phi})$ is typically $[-1, 1]$. To minimize the region pushed out of equilibrium by the injected current, each domain will rotate so as to minimize the counterflow current transmitted into the sample. This maximizes the tunneling current and is achieved if we choose $|f| \sim 1$. Thus, we argue that forcing at a boundary leads to a self-organized critical state, in which the driven part of the system is saturated at the threshold $|f| \sim 1$. This means that the area S_t of the system driven out of equilibrium to provide coherent tunneling is simply proportional to the number of domains necessary to carry the injected current I. Each domain can support a current of I_d, and so

$$\frac{S_t(I)}{L_\mathrm{d}^D} \approx \frac{I}{I_\mathrm{d}}. \tag{10}$$

The critical current is reached when all domains in the sample are saturated: $S = S_t(I_c)$ for a 2D sample of area S. Therefore, the critical current for a sample of area S is

$$I_c \sim I_\mathrm{d} \frac{S}{L_\mathrm{d}^D} = \frac{e\rho_s}{\hbar} \frac{S}{L_\mathrm{d}^2}. \tag{11}$$

This formula also applies to the 1D case with S being the sample length.

5. Numerical Results

We will now present numerical results to support the theory in the previous section. Our numerical results are obtained using the dissipative model

$$-\lambda\dot{\phi} = \frac{\delta H_\mathrm{eff}}{\delta\phi} = -\rho_s\nabla^2\phi + t\sin(\phi + \theta^0), \tag{12}$$

whose stationary solutions $\dot{\phi} = V = 0$ are the local minima of (2). This is performed on a lattice model. The phase field θ_i^0 at site i is uncorrelated with the phase field at any other site. This corresponds to taking the lattice spacing to be the correlation length ξ of the original continuum model. The natural unit of current is $I_0 = e\rho_s/\hbar$. The results that we present below are the results for a 200×20 lattice,

averaged over 500 realizations of the disorder. For this illustration, we take the ratio of the tunneling strength to the superfluid stiffness to be $t\xi^2/\rho_s = 0.6$. This corresponds to a Josephson depth λ_J of the order of a lattice spacing and a domain size L_d of 2 lattice spacings. Although this is not deep in the weak-disorder regime considered in the previous section, our results appear to support the conclusions in that section.

The boundary conditions for (2) are determined by the current flows through the sample [12]. We consider a tunneling geometry in which, as seen in Figure 2, a current I_t is injected into the top layer at the bottom left corner and removed from the bottom layer at the bottom right corner. As already discussed in (1), the counterflow component of the currents corresponds to equal counterflow currents I_{CF} injected by *both* the electron source and drain.

The ground state of the system is found by evolving from a random state using the dissipative dynamics (12) with the boundary condition of no injected current. From (3), this corresponds to $\hat{\mathbf{n}} \cdot \nabla\phi = 0$ everywhere on the boundary with $\hat{\mathbf{n}}$ being the normal to the boundary. To model the current injection in a tunneling experiment, we then slowly increase the counterflow current at the source and drain sites (1 and 2) to the final values $\xi\hat{\mathbf{n}} \cdot \nabla\phi|_1 = -\xi\hat{\mathbf{n}} \cdot \nabla\phi|_2 = I/I_0$. For the low values of the injected current I, the dynamics reach a static solution, corresponding to the Josephson regime with vanishing interlayer voltages. At higher currents, these time-independent solutions break down and the phase winds continuously in time. This corresponds to the breakdown of the d.c. Josephson regime and the appearance of a state with finite interlayer voltages.

We expect that the counterflow current injected at the boundary will decay into the sample, because interlayer tunneling will recombine electrons and holes across the two layers. We find that the manner in which this occurs is qualitatively different in clean and disordered bilayers. As mentioned in Section 1, the penetration depth of the injected current is simply the Josephson length λ_J in the clean case. We see in Figure 2 that for the disordered case, the current penetrates further and further into the sample as we increase the injected current from the two ends. We see from the border of the regions with finite tunneling ($\nabla \cdot \mathbf{j}_{CF} \neq 0$) that the counterflow region increases linearly in area (S_t) with the injected current. This is consistent with the prediction (10) for S_t as a function of the injected current from our theory.

At a high enough injected current ($I/I_0 \simeq 50$), the current profiles from the contacts (lower left and right corners) will meet in the middle of the lattice. Beyond this point, further increases in current cannot be accommodated by coherent tunneling and an interlayer voltage develops.

We emphasize that this interpretation of the threshold for the breakdown of the stationary solutions is qualitatively different from the clean case. In the clean model, the breakdown can be understood in terms of the injection of phase solitons at the boundary [20, 36] when the injected current exceeds the superflow that can be supported by a static phase twist $|\nabla\phi| \sim \pi/\lambda_J$. These phase solitons propagate through the sample. Thus, the phase at any point varies in time, and the system develops an interlayer voltage by the a.c. Josephson effect. In this language, we can say that these injected solitons can be pinned by disorder so that stationary solutions exist even when there are many solitons in the system.

6. Discussion

We have so far focused our discussion on the bilayer in the tunneling geometry. Finally, we will discuss how two other experimental situations can be interpreted in our theory. The first setup is the transport in the bilayer in a counterflow geometry, where the source and drain contacts are on the same side of the bilayer, while the other end is short-circuited to allow the current to flow from the top layer to bottom without the need for tunneling. This is depicted schematically in Figure 3. This was first investigated by Tutuc et al. [22] and Kellogg et al. [23]. A large current (I_{loop} in figure) was found passing through the short circuit that join the top and bottom layers. This seems to imply that there is no leakage by tunneling across hundreds of microns. As we discussed in Section 1 for the case of the tunneling geometry, a realistic estimate of the tunneling rate based on a clean bilayer predicts that the injected current would have tunneled across the bilayer within a micron and that *no* current should remain at the far end.

In our theory, this situation can be simulated by solving (12) with injected counterflow current at one end only, say the left end of Figure 2. We expect the tunneling domains to saturate successively from this end, and the current profile is the same as that found in Figure 2 for this side of the sample. There will be no current flow on the right side. In other words, we expect to see zero current in the short-circuit loop ($I_{loop} = 0$) in the Josephson regime. As we increase the injected current I to I_c, the current-carrying region reaches the other end of the sample. Any further currents will pass through the short circuit. For an ideal loop, we expect $I_{loop} = I - I_c$. However, the short circuit itself should have a finite resistance. Therefore, the presence of a nonzero I_{loop} implies a small interlayer voltage at the end of the sample. In the phase theory, the Josephson relation (4) means that the superfluid phase must wind in time. Thus, a static solution to (12) becomes impossible anywhere in the system, and the whole sample develops an interlayer voltage. We expect that the phase dynamics will be complex and chaotic. The nature of the steady state would depend on details of the damping mechanisms. This provides a zero-temperature picture of the counterflow geometry and is consistent with the recent experiments of Yoon et al. [37], in which the loop current I_{loop} is negligible for tunnel currents below a critical value. A broadly similar scenario for these experiments has been recently suggested by Gilbert [38]. We should keep in mind that at finite temperatures, there may be in-plane resistances associated with the flow of vortices and thermally activated quasiparticles. Thermal effects have been considered by many authors [26, 39]. Most recently, Hyart and Rosenow have modeled this with a decoherence rate that crosses over from a thermally activated form at high temperatures to a power law form at lower temperatures [40].

The second situation we wish to discuss is the two-terminal measurements of zero-bias interlayer conductance, $G(0)$, by Finck et al. [19]. Within our theory, this could be interpreted as the dissipative regime (i.e., no static solutions for the phase) above the critical current. We note that these measurements were performed close to the phase boundary between the excitonic superfluid with interlayer coherence and the incoherent $\nu = 1/2$ liquids. We expect the critical current to vanish near the phase boundary [11, 18]. Therefore, it is easy to exceed the critical current in this region of the phase diagram. Then, we see in Figure 2 that a nonzero interlayer voltage develops across the whole sample, and the tunneling current exists over the whole sample. In other words, $G(0)$ should be proportional to the area of the sample, as seen by Finck et al. We point out that whereas this interpretation gives an intrinsic zero-temperature source of a finite conductance, there may be other sources of dissipation. Even below I_c there could be a finite dissipation due to contact resistances and thermally activated vortex motion [39, 40]. Fluctuations in the pinning energies could also lead to very weakly pinned regions in large samples [41], which may lead to dissipation below I_c even at $T = 0$.

In summary, we have presented a theory of the Josephson regime of coherent tunneling in a disordered quantum Hall bilayer with static pinned vortices. We find that in the tunneling geometry, there are two current-carrying regions emanating separately from the source and drain contacts. In these regions, coherent tunneling is saturated. All injected counterflow current is lost by tunneling by the edge of these regions. The area of the saturated region S_t grows linearly with the injected current I. This linear relation is predicted by our theory and is confirmed by the numerical results presented here. This is analogous to the Bean critical state for flux penetration into a disordered superconductor.

This picture tells us that the system reaches the critical current when the whole sample is saturated with coherent tunneling. This results in a critical current that is extensive for sufficiently large samples that contain many domains of polarized phase. In contrast, the clean limit [12] sees area scaling for I_c only for small samples (small compared to the Josephson length).

Theoretically, our results are qualitatively different from clean theories [12] because of the existence of these pinned polarized domains. The size L_d of these domains is a disorder-induced length scale that emerges in our theory (8). This scale has no counterpart in the clean system. It would, therefore, be useful if this length scale can be probed in experiments. We note that for the area-scaling formula (11) to apply, the sample should be large enough to include many complete domains. For sample dimensions smaller than L_d, the system should cross over to a regime where I_c scales with the square-root of the sample dimension [18]

$$\begin{aligned} I_c &\sim \frac{e\rho_s}{\hbar}\sqrt{\frac{L_x}{L_d}}\frac{L_y}{L_d} \quad \left(\text{quasi-1D: } L_x \ll L_d \ll L_y\right) \\ &\sim \frac{e\rho_s}{\hbar}\sqrt{\frac{L_xL_y}{L_d^2}} \quad \left(\text{for } L_x, L_y \ll L_d\right). \end{aligned} \tag{13}$$

This crossover provides an experimental probe of the domain size L_d.

Acknowledgments

The authors thank P. B. Littlewood for helpful discussions. This work was supported by EPSRC-GB (EP/C546814/01) and Science Foundation Ireland (SFI/09/SIRG/I1592).

References

[1] S. Q. Murphy, J. P. Eisenstein, G. S. Boebinger, L. N. Pfeiffer, and K. W. West, "Many-body integer quantum Hall effect: evidence for new phase transitions," *Physical Review Letters*, vol. 72, no. 5, pp. 728–731, 1994.

[2] T. S. Lay, Y. W. Suen, H. C. Manoharan, X. Ying, M. B. Santos, and M. Shayegan, "Anomalous temperature dependence of the correlated ν=1 quantum Hall effect in bilayer electron systems," *Physical Review B*, vol. 50, no. 23, pp. 17725–17728, 1994.

[3] B. I. Halperin, "Theory of the quantized hall conductance," *Helvetica Physica Acta*, vol. 56, p. 75, 1983.

[4] H. A. Fertig, "Energy spectrum of a layered system in a strong magnetic field," *Physical Review B*, vol. 40, no. 2, pp. 1087–1095, 1989.

[5] J. P. Eisenstein and A. H. MacDonald, "Bose-Einstein condensation of excitons in bilayer electron systems," *Nature*, vol. 432, no. 7018, pp. 691–694, 2004.

[6] X. G. Wen and A. Zee, "Neutral superfluid modes and magnetic monopoles in multilayered quantum Hall systems," *Physical Review Letters*, vol. 69, no. 12, pp. 1811–1814, 1992.

[7] X. G. Wen and A. Zee, "Superfluidity and superconductivity in double-layered quantum Hall state," *International Journal of Modern Physics B*, vol. 17, no. 25, pp. 4435–4446, 2003.

[8] X. G. Wen and A. Zee, "Tunneling in double-layered quantum Hall systems," *Physical Review B*, vol. 47, no. 4, pp. 2265–2270, 1993.

[9] Z. F. Ezawa and A. Iwazaki, "Lowest-Landau-level constraint, Goldstone mode, and Josephson effect in a double-layer quantum Hall system," *Physical Review B*, vol. 48, no. 20, pp. 15189–15197, 1993.

[10] L. Tiemann, W. Dietsche, M. Hauser, and K. von Klitzing, "Critical tunneling currents in the regime of bilayer excitons," *New Journal of Physics*, vol. 10, Article ID 045018, 2008.

[11] L. Tiemann, Y. Yoon, W. Dietsche, K. von Klitzing, and W. Wegscheider, "Dominant parameters for the critical tunneling current in bilayer exciton condensates," *Physical Review B*, vol. 80, no. 16, Article ID 165120, 2009.

[12] J.-J. Su and A. H. MacDonald, "Critical tunneling currents in quantum Hall superfluids: pseudospin-transfer torque theory," *Physical Review B*, vol. 81, no. 18, Article ID 184523, 11 pages, 2010.

[13] I. B. Spielman, J. P. Eisenstein, L. N. Pfeiffer, and K. W. West, "Resonantly enhanced tunneling in a double layer quantum Hall ferromagnet," *Physical Review Letters*, vol. 84, no. 25, pp. 5808–5811, 2000.

[14] J. P. Eisenstein, "Evidence for spontaneous interlayer phase coherence in a bilayer quantum Hall exciton condensate," *Solid State Communications*, vol. 127, no. 2, pp. 123–130, 2003.

[15] R. L. Jack, D. K. K. Lee, and N. R. Cooper, "Dissipation and tunneling in quantum Hall bilayers," *Physical Review Letters*, vol. 93, no. 12, Article ID 126803, 4 pages, 2004.

[16] A. Stern, S. M. Girvin, A. H. MacDonald, and N. Ma, "Theory of interlayer tunneling in bilayer quantum Hall ferromagnets," *Physical Review Letters*, vol. 86, no. 9, pp. 1829–1832, 2001.

[17] L. Balents and L. Radzihovsky, "Interlayer tunneling in double-layer quantum Hall pseudoferromagnets," *Physical Review Letters*, vol. 86, no. 9, pp. 1825–1828, 2001.

[18] P. R. Eastham, N. R. Cooper, and D. K.K. Lee, "Critical supercurrents and self-organization in quantum Hall bilayers," *Physical Review Letters*, vol. 105, no. 23, Article ID 236805, 4 pages, 2010.

[19] A. D. K. Finck, A. R. Champagne, J. P. Eisenstein, L. N. Pfeiffer, and K. W. West, "Area dependence of interlayer tunneling in strongly correlated bilayer two-dimensional electron systems at $\nu_T = 1$," *Physical Review B*, vol. 78, no. 7, Article ID 075302, 5 pages, 2008.

[20] D. V. Fil and S. I. Shevchenko, "Josephson vortex motion as a source for dissipation of superflow of e-h pairs in bilayers," *Journal of Physics Condensed Matter*, vol. 21, no. 21, Article ID 215701, 2009.

[21] M. Abolfath, A. H. MacDonald, and L. Radzihovsky, "Critical currents of ideal quantum Hall superfluids," *Physical Review B*, vol. 68, no. 15, Article ID 155318, 16 pages, 2003.

[22] E. Tutuc, M. Shayegan, and D. A. Huse, "Counterflow measurements in strongly correlated GaAs hole bilayers: evidence for electron-hole pairing," *Physical Review Letters*, vol. 93, no. 3, Article ID 036802, 4 pages, 2004.

[23] M. Kellogg, J. P. Eisenstein, L. N. Pfeiffer, and K. W. West, "Vanishing Hall resistance at high magnetic field in a double-layer two-dimensional electron system," *Physical Review Letters*, vol. 93, no. 3, Article ID 036801, 4 pages, 2004.

[24] O. G. C. Ros and D. K. K. Lee, "Effect of disorder and electron-phonon interaction on interlayer tunneling current in quantum Hall bilayer," *Physical Review B*, vol. 81, no. 7, Article ID 075115, 7 pages, 2010.

[25] E. Rossi, A. S. Núñez, and A. H. MacDonald, "Interlayer transport in bilayer quantum Hall systems," *Physical Review Letters*, vol. 95, no. 26, Article ID 266804, 4 pages, 2005.

[26] H. A. Fertig and G. Murthy, "Coherence network in the quantum Hall bilayer," *Physical Review Letters*, vol. 95, no. 15, Article ID 156802, 4 pages, 2005.

[27] P. R. Eastham, N. R. Cooper, and D. K. K. Lee, "Vortex states of a disordered quantum Hall bilayer," *Physical Review B*, vol. 80, no. 4, Article ID 045302, 5 pages, 2009.

[28] M. M. Fogler and F. Wilczek, "Josephson effect without superconductivity: realization in quantum Hall bilayers," *Physical Review Letters*, vol. 86, no. 9, pp. 1833–1836, 2001.

[29] B. Roostaei, K. J. Mullen, H. A. Fertig, and S. H. Simon, "Theory of activated transport in bilayer quantum Hall systems," *Physical Review Letters*, vol. 101, no. 4, Article ID 046804, 4 pages, 2008.

[30] P. Bak, "Commensurate phases, incommensurate phases and the devil's staircase," *Reports on Progress in Physics*, vol. 45, no. 6, pp. 587–629, 1982.

[31] M. Tinkham, *Introduction to Superconductivity*, McGraw-Hill, New York, NY, USA, 1996.

[32] A. I. Larkin and Y. N. Ovchinnikov, "Pinning in type II superconductors," *Journal of Low Temperature Physics*, vol. 34, no. 3-4, pp. 409–428, 1979.

[33] V. M. Vinokur and A. E. Koshelev, "Collective flux pinning in extended Josephson junctions," *Soviet Physics JETP*, vol. 70, p. 547, 1990.

[34] H. Fukuyama and P. A. Lee, "Dynamics of the charge-density wave—I. Impurity pinning in a single chain," *Physical Review B*, vol. 17, no. 2, pp. 535–541, 1978.

[35] Y. Imry and S. K. Ma, "Random-field instability of the ordered state of continuous symmetry," *Physical Review Letters*, vol. 35, no. 21, pp. 1399–1401, 1975.

[36] P. B. Littlewood and T. M. Rice, "Metastability of the Q vector of pinned charge- and spin-density waves," *Physical Review Letters*, vol. 48, no. 1, pp. 44–47, 1982.

[37] Y. Yoon, L. Tiemann, S. Schmult, W. Dietsche, K. von Klitzing, and W. Wegscheider, "Interlayer tunneling in counterflow experiments on the excitonic condensate in quantum Hall bilayers," *Physical Review Letters*, vol. 104, no. 11, Article ID 116802, 4 pages, 2010.

[38] M. J. Gilbert, "Finite-temperature pseudospin torque effect in graphene bilayers," *Physical Review B*, vol. 82, no. 16, Article ID 165408, 12 pages, 2010.

[39] D. A. Huse, "Resistance due to vortex motion in the $\nu = 1$ bilayer quantum Hall superfluid," *Physical Review B*, vol. 72, no. 6, Article ID 064514, 4 pages, 2005.

[40] T. Hyart and B. Rosenow, "Quantitative description of Josephson-liketunneling in $\nu_T = 1$ quantum Hall bilayers," preprint, http://arxiv.org/abs/1011.5684v1.

[41] S. N. Coppersmith, "Phase slips and the instability of the Fukuyama-Lee-Rice model of charge-density waves," *Physical Review Letters*, vol. 65, no. 8, pp. 1044–1047, 1990.

Hindawi Publishing Corporation
Advances in Condensed Matter Physics
Volume 2011, Article ID 614173, 5 pages
doi:10.1155/2011/614173

Research Article

p-Wave Pairing in Quantum Hall Bilayers

Z. Papić[1,2] and M. V. Milovanović[1]

[1] *Scientific Computing Laboratory, Institute of Physics, University of Belgrade, P.O. Box 68, 11 000 Belgrade, Serbia*
[2] *Laboratoire de Physique des Solides, UMR 8502, CNRS, Université Paris-Sud, 91405 Orsay Cedex, France*

Correspondence should be addressed to M. V. Milovanović, mima@ipb.ac.rs

Received 25 May 2010; Accepted 9 August 2010

Academic Editor: Emanuel Tutuc

We show that the wave functions that describe the ground states of putative p-wave-paired phases in quantum Hall bilayers, like the Pfaffian at $\nu_T = 1/2$ or the paired phase at $\nu_T = 1$, are more likely to describe the excited states of Fermi liquids at these filling factors. We point out to the close competition between Fermi liquid and paired phases, which leads to the conclusion that in the experiments only direct transitions from the correlated 111 and 331 states into Fermi liquid(s) are likely to be observed.

1. Introduction

The quantum Hall bilayer, which consists of two layers of 2D electron gases in the presence of strong magnetic field orthogonal to the layers, represents a stage for correlated states with an extra layer degree of freedom [1]. When the total filling factor is $\nu_T = 1/2$ and the distance d between the layers is on the order of the magnetic length, $d \sim l_B$, we expect the so-called 331 state, which can be viewed as a Cauchy determinant pairing among the underlying quasiparticles which are neutral fermions. This is a p-wave pairing between two species of neutral fermions belonging to different layers. The pairing or order parameter function should be an eigenstate of rotations in two dimensions and, in the p-wave case, assumes the form [2] $\Delta_{\mathbf{k}} = \Delta(k_x - ik_y)$, where $\mathbf{k}$ is the relative momentum of the Cooper pair and Δ a constant. Antisymmetrizing a Cauchy determinant leads to the Pfaffian wave function [3]. The physical question therefore is whether the tunneling in the quantum Hall bilayer can mimic the antisymmetrization between the two species of electrons. Tunneling would allow to reach a p-wave-paired state of electrons without the layer degree of freedom, that is, the Moore-Read state. Recent work [4] pointed out that this route to the Pfaffian may be obstructed by the intervening phase of the Fermi liquid of neutral fermions [5]. The latter is, for all that we know, the only stable phase of one-component neutral fermions at the filling factor $\nu = 1/2$ in the lowest Landau level (LLL) and would constitute a certain outcome of strong tunneling. On the other hand, for the quantum Hall bilayer at total filling factor $\nu_T = 1$ and for small distances we have a highly correlated excitonic 111 state [6, 7]. For large distances between the two layers, two separate Fermi liquids of neutral fermions are formed, each at the filling factor 1/2. Proposals [8–12] were made for an intervening p-wave-paired phase between electrons—neutral fermions, that belong to different layers at intermediate distances.

In this paper, by analytical and numerical means, we further address the relevance of the proposals for the p-wave phases: (a) Pfaffian in the context of bilayer at $\nu_T = 1/2$ and (b) the BCS-like (with two species) p-wave wave function for the bilayer at $\nu_T = 1$. In both cases, we assume the problem is defined by the usual Coulomb interaction. We point out to the close competition between Fermi liquid(s) and paired phases in these systems, suggesting that direct transitions from the correlated 111 and 331 states into Fermi liquid(s) are likely to take place in the experiments.

2. The Quantum Hall Bilayer and Its Model Wave Functions

In the following, we review some basic facts about the quantum Hall bilayer including its possible phases and the corresponding quantum Hall wave functions. We consider the quantum Hall bilayer in the presence of the vector

potential $\mathbf{A}$ that describes a strong magnetic field, $B\hat{z} = \nabla \times \mathbf{A}$, perpendicular to both layers. In the rotationally symmetric gauge, the lowest Landau level (LLL) eigenstates of an electron with the coordinate $z = x + iy$ in the plane and localized in the layer $\sigma \in \{\uparrow, \downarrow\}$ are given by

$$z^m \exp\left\{-\frac{|z|^2}{4l_B^2}\right\}\eta_\sigma, \quad m = 0, \ldots, N_\phi - 1, \tag{1}$$

where η_σ is the usual spinor wave function and the unit of length is given by the magnetic length, $l_B = \sqrt{\hbar c/eB}$. The number of flux quanta, N_ϕ, denotes the number of available states in the LLL. In the thermodynamic limit, the ratio of the total number of electrons N_e and the number of flux quanta N_ϕ defines the filling factor $\nu_T = N_e/N_\phi$. We focus on the filling factors $\nu_T = 1/2$ and $\nu_T = 1$.

The many-body interacting system of electrons is defined by the following Lagrangian density in the second quantized formulation:

$$\begin{aligned}\mathcal{L} = \sum_\sigma \Bigg\{ & \Psi_\sigma^\dagger \partial_\tau \Psi_\sigma - \Psi_\sigma^\dagger \frac{(\partial_{\mathbf{r}} + e\mathbf{A})^2}{2m}\Psi_\sigma - \Psi_\sigma^\dagger \frac{\Delta_{\mathrm{SAS}}}{2}\Psi_{-\sigma} \\ & + \frac{1}{2}\int d\mathbf{r}' \rho_\sigma(\mathbf{r}) V_c^{\mathrm{intra}}(\mathbf{r}-\mathbf{r}')\rho_\sigma(\mathbf{r}') \\ & + \frac{1}{2}\int d\mathbf{r}' \rho_\sigma(\mathbf{r}) V_c^{\mathrm{inter}}(\mathbf{r}-\mathbf{r}')\rho_{-\sigma}(\mathbf{r}') \Bigg\},\end{aligned} \tag{2}$$

where Ψ_σ is the electron field which carries the pseudospin (layer) index and Δ_{SAS} denotes the tunneling term. The interaction is defined by

$$V_c^{\mathrm{intra}}(r) = \frac{e^2}{\epsilon r} \tag{3}$$

and in general V_c^{inter} is different. When we model a quantum Hall bilayer,

$$V_c^{\mathrm{inter}}(r) = \frac{e^2}{\epsilon\sqrt{r^2 + d^2}}, \tag{4}$$

d has the meaning of distance between the two layers of 2D gases and it is of the order of l_B. (In the Lagrangian density (2) we set $\hbar = c = l_B = 1$.) Significant insight into the physics described by the Lagrangian (2) can be obtained using first-quantized trial wave functions for its ground states [13]. We now list several candidate wave functions that are expected to describe the ground state of (2) in different limits of Δ_{SAS} and d for the filling factors $\nu_T = 1/2$ and $\nu_T = 1$. Trial wave functions in the LLL are analytic in z variables and we will omit the omnipresent Gaussian factor for each electron as the one in (1).

In the small tunneling regime, the fractional quantum Hall (FQH) system at $\nu_T = 1/2$ is two-component, described by the 331 Halperin state for two distinguishable species of electrons, $z_{i\sigma}; \sigma = \uparrow, \downarrow;\ i = 1, \ldots, N_e/2$,

$$\Psi_{331} = \prod_{i<j}\left(z_{i\uparrow} - z_{j\uparrow}\right)^3 \prod_{k<l}(z_{k\downarrow} - z_{l\downarrow})^3 \prod_{p,q}\left(z_{p\uparrow} - z_{q\downarrow}\right). \tag{5}$$

Due to the fact that the correlation exponents between electrons of the same layer are bigger than those between electrons of the opposite layers, we expect the wave function (5) to be more appropriate for nonzero d, for example, in the range $d \sim l_B$.

As the tunneling strength Δ_{SAS} is increased, the electrons find it energetically favorable to be in the superposition of two layers, $\uparrow + \downarrow$, and the system loses its two-component character. The effective single-component state is characterized by full polarization in the x-direction. At $\nu = 1/2$ single layer in the LLL, a compelling candidate for the polarized state is Rezayi-Read composite Fermi liquid state [14]:

$$\Psi_{1/2} = \mathcal{P}_{\mathrm{LLL}}\left\{\mathcal{F}(\{z, \bar{z}\}) \cdot \prod_{i<j}\left(z_i - z_j\right)^2\right\}, \tag{6}$$

where $\mathcal{P}_{\mathrm{LLL}}$ is a projector to the LLL and $\mathcal{F} \equiv \det[e^{i\mathbf{k}_i \mathbf{r}_j}]$ represents the Slater determinant of free waves. Note that a single index suffices to label the electron coordinates as the pseudospin index is implicitly assumed to be $\uparrow + \downarrow$.

An alternative candidate for the polarized state at the half filling is the so-called Pfaffian state, which up to a normalization factor can be expressed as

$$\Psi_{\mathrm{Pf}} = \mathcal{A}\{\Psi_{331}\}. \tag{7}$$

The two-component state is made single-component under the action of the antisymmetrizer $\mathcal{A}$ between $\uparrow$ and $\downarrow$ electron coordinates. In the notation of (7), one can think of the Pfaffian originating from the two-component 331 state with the pairing represented by the Cauchy determinant because

$$\Psi_{331} \propto \Psi_{222} \det\left[\frac{1}{z_\uparrow - z_\downarrow}\right], \tag{8}$$

by virtue of the Cauchy identity. As a result, we can express the Pfaffian state in its more familiar form as

$$\begin{aligned}\Psi_{\mathrm{Pf}} \propto & \prod_{i<j}\left(z_i - z_j\right)^2 \\ & \times \sum_{\sigma \in S_n} \operatorname{sgn}\sigma \left\{\frac{1}{(z_{\sigma(1)} - z_{\sigma(2)})} \cdots \frac{1}{(z_{\sigma(N_e-1)} - z_{\sigma(N_e)})}\right\},\end{aligned} \tag{9}$$

where the sum represents a BCS wave function for spinless fermions that pair in the manner of a p-wave (see below). Pfaffian (7) is usually thought of as a candidate wave function to describe the half filling of the *second* Landau level, where the nature of the effective interaction facilitates the pairing between the electrons [15]. However, being an analytic wave function, Pfaffian is also a valid trial state for the LLL.

At $\Delta_{\mathrm{SAS}} = 0$ and in the small d regime, the FQH system at $\nu_T = 1$ is two-component, described by the 111 Halperin state for two distinguishable species of electrons,

$$\Psi_{111} = \prod_{i<j}\left(z_{i\uparrow} - z_{j\uparrow}\right)\prod_{k<l}(z_{k\downarrow} - z_{l\downarrow})\prod_{p,q}\left(z_{p\uparrow} - z_{q\downarrow}\right). \tag{10}$$

The correlation exponents are the same between the electrons belonging to the same and opposite layers, reflecting the excitonic nature [6] of the correlated state in the regime when the inter- and intrainteractions are about the same. As the distance between the layers is increased, it is expected that electrons find it energetically more favorable to correlate inside the layers and make two independent composite Fermi liquid states, each in the form of (6).

When we study the trial states on a spherical surface, we will make use of the fact that they are characterized by the topological number called the shift, $\mathcal{S} = N_e/\nu - N_\phi$. In the case of the 331 state $\mathcal{S} = 3$, for the 111 state $\mathcal{S} = 1$, and for the Fermi liquid state in (6) $\mathcal{S} = 2$. The shift is a distinctive feature of each FQH state on the sphere.

3. The Role of p-Wave Pairing for the Transitions from 331 and 111 State into Fermi Liquids

We start with the effective description of [16] of the p-wave-paired state in order to describe its instability towards the Fermi liquid. We will show how the paired wave function, from representing a ground state in the paired phase, ends up describing an excited state of the Fermi liquid after the transition. The BCS effective description near $\mathbf{k} = 0$ is given by

$$K_{\text{eff}} = \sum_{\mathbf{k}} \left\{ (\epsilon_{\mathbf{k}} - \mu) c_{\mathbf{k}}^{\dagger} c_{\mathbf{k}} + \left(\Delta_{\mathbf{k}} c_{\mathbf{k}}^{\dagger} c_{-\mathbf{k}}^{\dagger} + h.c. \right) \right\}, \tag{11}$$

where $\Delta_{\mathbf{k}} = \Delta(k_x - ik_y)$ and the diagonal term describes fermions with a quadratic dispersion in 2D. After the Bogoliubov transformation with operators in the form $\alpha_{\mathbf{k}} = u_{\mathbf{k}} c_{\mathbf{k}} - v_{\mathbf{k}} c_{-\mathbf{k}}^{\dagger}$, we obtain for the dispersion of the excitations above the ground state

$$E_{\mathbf{k}} = \sqrt{(\epsilon_{\mathbf{k}} - \mu)^2 + |\Delta_{\mathbf{k}}|^2}, \tag{12}$$

and the ground state is

$$\prod_{\mathbf{k}} \left(1 + g_{\mathbf{k}} c_{\mathbf{k}}^{\dagger} c_{-\mathbf{k}}^{\dagger} \right) |0\rangle, \tag{13}$$

where $g_{\mathbf{k}} = v_{\mathbf{k}}/u_{\mathbf{k}}$. For small $\mathbf{k}$ and $\mu > 0$, this becomes

$$\frac{v_{\mathbf{k}}}{u_{\mathbf{k}}} = -\frac{(E_{\mathbf{k}} - \epsilon_{\mathbf{k}} + \mu)}{\Delta_{\mathbf{k}}^{*}} \longrightarrow -\frac{2\mu}{\Delta_{\mathbf{k}}^{*}}, \tag{14}$$

which then in the real space yields asymptotically $g(\mathbf{r}) \sim 1/z$, that is, the p-wave Cooper pair pairing function. The antisymmetrization over a collection of these Cooper pairs leads to the Moore-Read state or the Pfaffian where the pairing is described by $1/z$ for all distances [16].

If $\mu > 0$ becomes large and $\Delta_{\mathbf{k}}$ stays about the same or decreases, then due to the simple expansion for small k the energy of excitations behaves as

$$E_{\mathbf{k}} \approx \mu - \epsilon_{\mathbf{k}} + \frac{|\Delta_{\mathbf{k}}|^2}{2\mu} \tag{15}$$

and the minimum around $\mathbf{k} = 0$ becomes a local maximum. Then we may think of this unstable point in the phase space as a description of an excited state of the system which finds itself, with high probability, in the state of Fermi liquid because the minimum for excitations has moved to $\mathbf{k} = \mathbf{k}_F$ from $\mathbf{k} = 0$. But the description of this unstable point, that is the excited state is still given by (13) and (14), that is, by a Pfaffian pairing function. Therefore Pfaffian may describe an excited state of the Fermi liquid.

In the following, we will discuss the two correlated systems, at $\nu_T = 1/2$ and $\nu_T = 1$, where the p-wave-paired state may occur as an excited state of the Fermi liquid.

331 Case. In the presence of tunneling, the 331 bilayer state can be transformed into a Fermi liquid of neutral or composite fermions in the LLL. This expectation is based on the fact that Pfaffian, as an alternative candidate, is not found in any polarized system (without an internal degree of freedom) in the LLL. BCS theory of the 331 system can be found in [4, 16]. There is a separation of the description into two sectors, the even and odd channel. Each channel is described by the Read-Green theory of the p-wave pairing of spinless fermions that we introduced above. With the increase of tunneling Δ_{SAS}, the number of electrons in the even channel increases and its effective chemical potential is modified as $\mu^e = \mu + \Delta_{\text{SAS}}/2$. The excitations of the even channel, by having μ^e instead of μ above as a parameter that enters the expression for their energies (12), become unstable unless there is an appropriate change in $\Delta_{\mathbf{k}}$, for example, the strengthening of the pairing. In the absence of this change, the system evolves into a Fermi liquid with a possibility that one of the excited states is described by the Pfaffian (13), as argued previously. Exact diagonalization calculations on the sphere, performed at the fixed value of $d = l_B$ and at the fixed shift $\mathcal{S} = 3$, characteristic of the Pfaffian state, give high overlaps for the Pfaffian with the increase of tunneling [4]. On the other hand, exact diagonalization on the torus [4], with the same fixed distance between the layers, does not find the characteristic degeneracy of the Pfaffian with the increase of tunneling [4]. A possible interpretation of the result on the sphere is that the true ground state of the system is found at a different shift $\mathcal{S}$, where the Pfaffian describes, to a high accuracy, an excited state of the system. This is corroborated by comparing the ground state energies on the sphere as a function of tunneling for the shifts $\mathcal{S} = 3$ (Pfaffian) and $\mathcal{S} = 2$ (the shift of the Fermi liquid); see Figure 1. We show the data for two systems of $N = 8$ and $N = 10$ electrons which do not suffer from the aliasing with Jain's composite fermion states [17]. The energies plotted in Figure 1 include the appropriate background charge and finite-size corrections [17]. We observe that the polarized state (for large Δ_{SAS}) is found at the Fermi liquid shift of $\mathcal{S} = 2$ whereas the excited state lying closely above it, at the shift of $\mathcal{S} = 3$, is the Moore-Read state as shown in [4].

111 Case. The increase of distance between the two layers transforms the 111 state at the bilayer total filling factor $\nu_T = 1$ into two Fermi liquids, each with a filling factor equal to

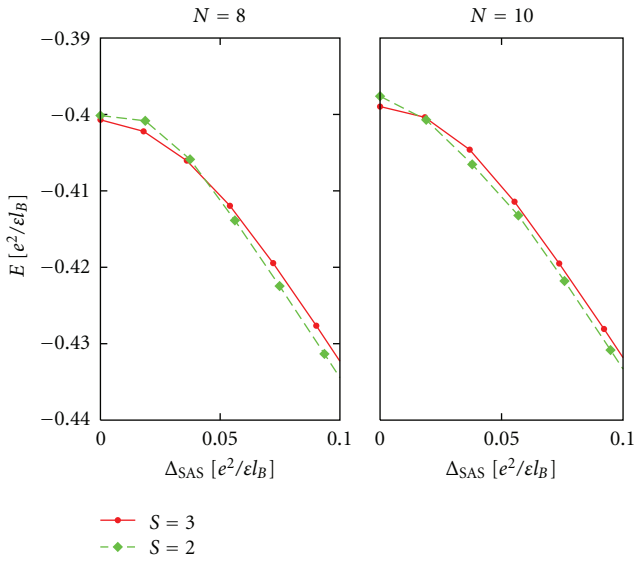

FIGURE 1: (color online) Ground state energies on the sphere as a function of tunneling for the filling factor $\nu_T = 1/2$ and the shifts $\mathcal{S} = 3$ and $\mathcal{S} = 2$. We show data for $N = 8$ and $N = 10$ electrons and the distance is fixed at $d = l_B$.

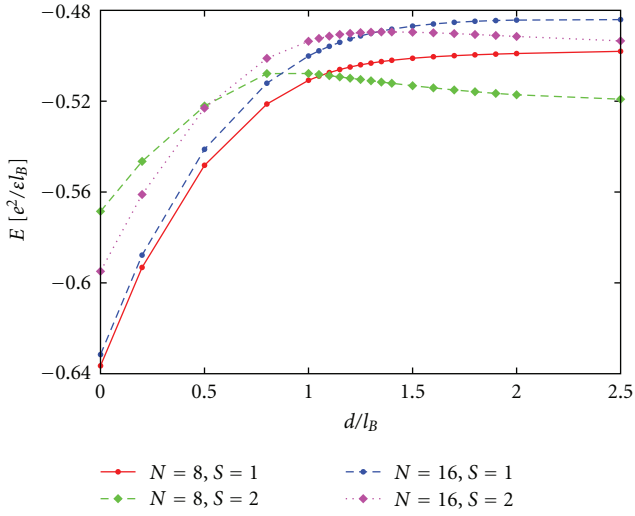

FIGURE 2: (color online) Ground state energies on the sphere as a function of distance for $N = 8$ and $N = 16$ electrons at the filling factor $\nu_T = 1$ and the shifts $\mathcal{S} = 1$ and $\mathcal{S} = 2$.

1/2. An intermediate state based on p-wave pairing between composite fermions of the two layers is a viable candidate, as shown by the numerical investigation in the spherical geometry [10, 11] and analytical work [12]. In the latter investigation the manner of superfluid disordering with the increasing distance was analyzed and implications for the form of the ground state that evolves with distance were derived. Based on the universal phonon correction [18, 19] for small distances, the nature of pairing in the ground state wave function was extrapolated. The most likely kind of pairing was found to be $g(\mathbf{r}) = \sqrt{z/z^*}$, that is, a pure phase that leads to very weak pairing in the opposite angular momentum channel. This result was derived following the long-distance, effective (Chern-Simons) argument with the universal phonon correction. It is different from what we are used to when considering the Pfaffian for which $g(\mathbf{r}) = 1/z$, because here we have the pairing for the opposite value of the angular momentum. The numerics [10, 11] confirms the value of the angular momentum for the pairing. However, as the numerics was done in the LLL, it also does not preclude the pairings of the same angular momentum like $g(\mathbf{r}) = 1/z^*$, which amounts to the same leading short-distance behavior $\tilde{g}(\mathbf{r}) \sim z$, in the LLL, which was determined by Möller et al. [10, 11]. In the following, we will consider only these two possibilities for the pairing, which is expected to be weak (as opposed to the extreme case of strong pairing when the Cooper pairs are exponentially bound).

The physical picture that emerges from these works and the proposal for mixed states of composite bosons and composite fermions in [20] is that, with increasing distance, composite fermions nucleate in the 111 (composite boson) condensate and they do that by pairing in the p-wave pairs. The number of composite fermions or, equivalently, neutral fermions increases with the increase of distance between the layers. Therefore, their chemical potential increases as well. In this case, we can apply the theory of Read and Green, generalized to two species (spinful pairing), which differs from the one we described earlier only by the degeneracy equal to two of the excitations. For $g(\mathbf{r}) = \sqrt{z/z^*}$ pairing, we have $|\Delta_{\mathbf{k}}| \sim |\mathbf{k}|^2$ (due to the very weak pairing), and the theory is always unstable, leading to a direct transition from 111 state into Fermi liquids. For $g(\mathbf{r}) = 1/z^*$, we have $|\Delta_{\mathbf{k}}| \sim |\mathbf{k}|$ and the considerations that we pointed out in the beginning follow. Because the chemical potential of composite fermions increases, we may expect the transition into two Fermi liquids at a finite distance. A comparison of the lowest energies in the spherical geometry for the shifts $\mathcal{S} = 1$ (the 111 state) and $\mathcal{S} = 2$ (the Fermi liquids) corroborates this expectation; see Figure 2. We show data for $N = 8$ and $N = 16$ electrons; the former represents the case where composite fermions in each layer form a filled shell, leading to a local energy minimum [21], while the latter is the largest system attainable by exact diagonalization. Further information on the finite-size scaling of the data, including the estimate for critical d_C, will be given elsewhere [21].

We thus conclude that, even in the clean system with translational invariance such as in Figure 2, we may have a direct transition between the 111 state and the decoupled Fermi liquids occurring at a finite d_C. This happens when the shift $\mathcal{S} = 2$ becomes energetically favorable. If one continues to study the system for $d > d_C$ at the fixed shift of $\mathcal{S} = 1$, a paired state is likely to have an excellent overlap but it will only describe the excited state of the system.

4. Conclusions and Discussion

We described a possible role of the p-wave-paired states in the transition of the 111 and 331 correlated states into Fermi liquids. In the case of the 111 state, we have a transition

into two Fermi liquids induced by increasing the distance between two layers and in the case of the 331 state the transition into a one-component Fermi liquid is induced by tunneling. The previous studies [4, 10, 11] have shown that the p-wave state is slowly nucleated in a correlated state and here we demonstrated that after the transition it may assume the role of an excited state of the Fermi liquid(s). Whether we have a case for a second-order transition in each of our two examples we cannot claim. However, this scenario will likely lead to the observance of smooth transitions into Fermi liquids in experiments as found in [22, 23] in the case of the 111 excitonic, correlated state. As we pointed out in the 331 case by changing the distance between layers, that is, fixing a parameter for the transition driven by tunneling, Pfaffian may indeed become a ground state in the place of the Fermi liquid state [4]. Unfortunately, it becomes so with a very small gap [4, 24] which would again lead to the observance of a smooth transition into a compressible thermodynamic phase in experiments if the beginning phase is the 331 correlated phase.

In the transitions we discussed that are followed by p-wave states, there is a mismatch between the shift numbers characteristic of the beginning of the correlated phase and the ending of the Fermi liquid phase. Quantum fluctuations in the correlated state produce the p-wave state which inherits and accommodates the shift of the correlated phase and therefore has to play a role at the transition into a new phase. Unfortunately, p-wave states are unstable or very weak and give a way to Fermi liquids.

Acknowledgments

The authors thank Y. Joglekar for discussions. This work was supported by the Serbian Ministry of Science under Grant no. 141035.

References

[1] B. I. Halperin, "Theory of the quantized Hall conductance," *Helvetica Physica Acta*, vol. 56, pp. 75–82, 1983.

[2] We follow the conventions of Ref. 16.

[3] G. Moore and N. Read, "Nonabeuons in the fractional quantum hall effect," *Nuclear Physics B*, vol. 360, no. 2-3, pp. 362–396, 1991.

[4] Z. Papić, M. O. Goerbig, N. Regnault, and M. V. Milovanović, "Tunneling-driven breakdown of the 331 state and the emergent Pfaffian and composite Fermi liquid phases," *Physical Review B*, vol. 82, Article ID 075302, 10 pages, 2010.

[5] B. I. Halperin, P. A. Lee, and N. Read, "Theory of the half-filled Landau level," *Physical Review B*, vol. 47, no. 12, pp. 7312–7343, 1993.

[6] I. B. Spielman, J. P. Eisenstein, L. N. Pfeiffer, and K. W. West, "Resonantly enhanced tunneling in a double layer quantum hall ferromagnet," *Physical Review Letters*, vol. 84, no. 25, pp. 5808–5811, 2000.

[7] K. Moon, H. Mori, K. Yang et al., "Spontaneous interlayer coherence in double-layer quantum Hall systems: charged vortices and Kosterlitz-Thouless phase transitions," *Physical Review B*, vol. 51, no. 8, pp. 5138–5170, 1995.

[8] N. E. Bonesteel, I. A. McDonald, and C. Nayak, "Gauge fields and pairing in double-layer composite fermion metals," *Physical Review Letters*, vol. 77, no. 14, pp. 3009–3012, 1996.

[9] Y. B. Kim, C. Nayak, E. Demler, N. Read, and S. Das Sarma, "Bilayer paired quantum Hall states and Coulomb drag," *Physical Review B*, vol. 63, no. 20, Article ID 205315, 2001.

[10] G. Möller, S. H. Simon, and E. H. Rezayi, "Paired composite Fermion phase of quantum hall bilayers at $\nu = 1/2 + 1/2$," *Physical Review Letters*, vol. 101, no. 17, Article ID 176803, 4 pages, 2008.

[11] G. Möller, S. H. Simon, and E. H. Rezayi, "Trial wave functions for $\nu = 1/2 + 1/2$ quantum Hall bilayers," *Physical Review B*, vol. 79, no. 12, Article ID 125106, 23 pages, 2009.

[12] M. V. Milovanović and Z. Papić, "Nonperturbative approach to the quantum Hall bilayer," *Physical Review B*, vol. 79, no. 11, Article ID 115319, 2009.

[13] R. B. Laughlin, "Anomalous quantum Hall effect: an incompressible quantum fluid with fractionally charged excitations," *Physical Review Letters*, vol. 50, no. 18, pp. 1395–1398, 1983.

[14] E. Rezayi and N. Read, "Fermi-liquid-like state in a half-filled Landau level," *Physical Review Letters*, vol. 72, no. 6, pp. 900–903, 1994.

[15] E. H. Rezayi and F. D. M. Haldane, "Incompressible paired Hall state, stripe order, and the composite fermion liquid phase in half-filled Landau levels," *Physical Review Letters*, vol. 84, no. 20, pp. 4685–4688, 2000.

[16] N. Read and D. Green, "Paired states of fermions in two dimensions with breaking of parity and time-reversal symmetries and the fractional quantum Hall effect," *Physical Review B*, vol. 61, no. 15, pp. 10267–10297, 2000.

[17] J. Jain, *Composite Fermions*, Cambridge University Press, Cambridge, UK, 2007.

[18] A. Lopez and E. Fradkin, "Fermionic Chern-Simons theory for the fractional quantum Hall effect in bilayers," *Physical Review B*, vol. 51, no. 7, pp. 4347–4368, 1995.

[19] L. Jiang and J. Ye, "Ground state, quasihole, a pair of quasihole wave functions, and instability in bilayer quantum Hall systems," *Physical Review B*, vol. 74, no. 24, Article ID 245311, 8 pages, 2006.

[20] S. H. Simon, E. H. Rezayi, and M. V. Milovanović, "Coexistence of composite bosons and composite fermions in $\nu = 1/2 + 1/2$ quantum hall bilayers," *Physical Review Letters*, vol. 91, no. 4, Article ID 046803, 2003.

[21] Z. Papić and M. V. Milovanović, "Coherent states in double quantum well systems," submitted to *Advances in Condensed Matter Physics*.

[22] A. D. K. Finck, J. P. Eisenstein, L. N. Pfeiffer, and K. W. West, "Quantum hall exciton condensation at full spin polarization," *Physical Review Letters*, vol. 104, Article ID 016801, 4 pages, 2010.

[23] P. Giudici, K. Muraki, N. Kumada, and T. Fujisawa, "Intrinsic gap and exciton condensation in the $\nu_T = 1$ bilayer system," *Physical Review Letters*, vol. 104, Article ID 056802, 4 pages, 2010.

[24] M. R. Peterson and S. Das Sarma, "Quantum Hall phase diagram of half-filled bilayers in the lowest and the second orbital Landau levels: abelian versus non-Abelian incompressible fractional quantum Hall states," *Physical Review B*, vol. 81, Article ID 165304, 17 pages, 2010.

Hindawi Publishing Corporation
Advances in Condensed Matter Physics
Volume 2011, Article ID 815169, 7 pages
doi:10.1155/2011/815169

Research Article

Trial Wavefunctions for the Goldstone Mode in $\nu = 1/2 + 1/2$ Quantum Hall Bilayers

Gunnar Möller[1] and Steven H. Simon[2]

[1] *TCM Group, Cavendish Laboratory, JJ Thomson Avenue, Cambridge CB3 0HE, UK*
[2] *Rudolf Peierls Centre for Theoretical Physics, Oxford University, Oxford OX1 3NP, UK*

Correspondence should be addressed to Gunnar Möller, gm360@cam.ac.uk

Received 12 September 2010; Accepted 28 October 2010

Academic Editor: Yogesh Joglekar

Based on the known physics of the excitonic superfluid or 111 state of the quantum Hall $\nu = 1/2 + 1/2$ bilayer, we create a simple trial wavefunction ansatz for constructing a low-energy branch of (Goldstone) excitations by taking the overall ground state and boosting one layer with respect to the other. This ansatz works extremely well for any interlayer spacing. For small d, this is simply the physics of the Goldstone mode, whereas for large d, this is a reflection of composite fermion physics. We find hints that certain aspects of composite fermion physics persist to low d whereas certain aspects of Goldstone mode physics persist to high d. Using these results, we show nonmonotonic behavior of the Goldstone mode velocity as a function of d.

The $\nu = 1/2 + 1/2$ quantum Hall bilayer is a remarkably rich system [1, 2]. At small enough spacing between the layers, d, the system is known to be an excitonic superfluid [3] known sometimes as the 111 phase [4]. At larger layer spacing, a phase transition or crossover is observed experimentally [5–11] leading to a compressible phase which is well described by two weakly coupled composite fermion Fermi liquids. The nature of this crossover, as well as whether there are intervening phases between small and large d, has been a matter of some debate in the community [12–20].

There are some results, however, that are extremely well established theoretically. In the limit where d becomes very small, it is known that the Halperin 111 trial wavefunction becomes exact [4]. In a more BCS-like language, this wavefunction can be expressed as [3]

$$|111\rangle = \prod_X \left(c^\dagger_{X,\uparrow} + c^\dagger_{X,\downarrow}\right)|0\rangle, \tag{1}$$

where $\uparrow$ and $\downarrow$ indicate the layer index (we assume the real spin is frozen throughout this paper) and X constitutes the orbital index within the lowest Landau level (chosen to be the x-directed momentum in Landau gauge, e.g.). (Strictly speaking this second quantized form of the wavefunction must be projected to fixed number of particles within each layer to generate a Halperin 111 wavefunction. However, in the thermodynamic limit these two descriptions are essentially equivalent.)

The BCS-like form of (1) allows one to consider long wavelength Goldstone excitations of the form [3, 21]

$$|111 - \text{excitation}, k\rangle = \prod_X \left(c^\dagger_{X,\uparrow} + e^{ikX} c^\dagger_{X,\downarrow}\right)|0\rangle. \tag{2}$$

These modes are expected to form a linearly dispersing low energy branch with energy proportional to k for small k. Physically, this Goldstone mode corresponds to superflow—one layer being boosted with respect to the other. Both a linearly dispersing mode [22] and excitonic superflow [7, 9, 23–25] were observed experimentally in this system. Some properties of the Goldstone mode were discussed in a numerical study on the torus [17].

Away from the $d \to 0$ limit, the form of the bilayer ground state is not known exactly. However, so long as we remain in the same phase of matter, there will continue to be a linearly dispersing Goldstone mode in the long wavelength limit. An approximate expression for this Goldstone mode can be obtained from the ground state wavefunction at any d simply by boosting one layer with respect to the other. One purpose of the current paper is to test this technique

of generating trial wavefunctions for the long wavelength Goldstone modes.

We note that this technique is not expected to be exact away from $d = 0$, but for small d is expected to be quite accurate. In a conventional picture of superfluidity, one might imagine that it would be better to find a way to boost the superfluid fraction while leaving the "normal" fraction unboosted (only at $d = 0$ is the system entirely super in some sense [13]). Nonetheless, our technique appears to work quite well even away from $d = 0$.

One might expect that once the system is no longer in the 111 phase of matter (roughly $d > 1.5$ magnetic lengths), our technique for generating excited states would fail. However, this turns out not to be the case. First of all, at intermediate d there may exist an interlayer paired state as discussed in [19]. Such a paired state would also have a Goldstone mode that could be generated from the ground state by boosting one layer in exactly the same way.

However, even at very large d when either such a pairing phase is absent or pairing is extremely weak, our scheme for generating excited states still works surprisingly well. To understand why this is so, we realize that at large enough d each layer is essentially independent. To the first approximation, each layer forms a composite fermion Fermi liquid, which for finite-size system has finite momentum (except when the number of electrons exactly fills a shell). The two Fermi liquids are weakly coupled and can combine their momenta to form an overall zero momentum ground state, but since the coupling between the two layers is weak, it costs very little energy to form a state of overall finite momentum instead—which can be interpreted as boosting one layer with respect to the other in comparison to the ground state.

In the absence of any superfluid order parameter (at large d), it is probably not strictly appropriate to refer to this low-energy mode as a Goldstone mode. However, since this mode may evolve continuously into the Goldstone mode at smaller d, we will abuse nomenclature and continue to call it a Goldstone mode (If, as conjectured in [19], the bilayer is actually paired out to large d, then the usage remains correct).

Throughout this paper we will work with a spherical geometry. In this case, boosting one layer with respect to the other corresponds to applying the angular momentum raising operator L_+ to one layer but not the other (call this operator $L_{+,\uparrow}$ meaning that it is applied to the $\uparrow$ layer only). In the appendix we show that if we start with any $L = 0$ state of the entire system, applying $(L_{+,\uparrow})^J$ generates a bilayer state with overall angular momentum $L = L_z = J$. Our technique is then to use exact diagonalization to generate the $L = 0$ ground state of the bilayer system, which is used to obtain the trial wavefunction for the excited state

$$|\text{Trial}(d) : L = J\rangle = (L_{+,\uparrow})^J |\text{Ground State}(d) : L = 0\rangle. \quad (3)$$

Despite the apparent asymmetry between spins $\uparrow$ and $\downarrow$, the trial state (3) has a distinct parity of $(-1)^J$ under spin reversal, as shown in the appendix. In turn, we compare this trial state to the exact excited states with angular momentum $L = J$.

Our numerical work is based on exact diagonalization of the Coulomb Hamiltonian for a bilayer system on the sphere [26]. We simplify the problem to exclude issues related to a finite tunneling amplitude between the layers, Landau level mixing, or spin (which we assume is polarized) and model each layer as an ideal 2D plane without considering its width into the third dimension. At fillings smaller than one per layer, the Hamiltonian is thus given by the projection of the Coulomb interaction into the lowest Landau level

$$\mathcal{H}[d] = \sum_{\substack{\sigma=\uparrow,\downarrow \\ i<j}} \frac{e^2}{\epsilon \left| r_{\sigma,i} - r_{\sigma,j} \right|} + \sum_{i,j} \frac{e^2}{\epsilon \sqrt{\left| r_{\uparrow,i} - r_{\downarrow,j} \right|^2 + d^2}}, \quad (4)$$

where sums run over all particles with the given pseudospin. The interactions are parametrized by the layer separation d that is measured in units of the magnetic length $\ell_0 = \sqrt{\hbar c/eB}$. All lengths given in this paper should be understood to be measured in units of ℓ_0, where this is not explicitly indicated.

In our exact diagonalization calculations, we focus specifically on the density-balanced bilayer system with $N_\uparrow = N_\downarrow = N/2$ and devote the majority of this paper to the discussion of the state at the shift of the 111 state, namely, $N_\phi = N - 1$. We have also tested the system at the neighbouring shifts of $N_\phi = N$ and $N_\phi = N - 2$ and found in these cases that the low-lying spectrum is very flat, and that the ground state may occur at finite L—unlike the behaviour expected from the collective modes of a condensate. We thus focus on $N_\phi = N - 1$, but we should caution that our analysis does not exclude the possibility that for large d a first-order phase transition into a state occurring at a different shift may occur. For our discussion, we obtain the two lowest-lying eigenvalues and eigenvectors in each sector of angular momentum. This is most easily achieved using a projected Lanczos algorithm [27] which uses an additional projection to the lowest energy subspace of minimal angular momentum after each multiplication with the Hamiltonian. In a given sector with fixed L_z, this procedure therefore directly yields eigenstates of L^2 with the eigenvalue $L = L_z$.

To assess the accuracy of the trial states (3) for the Goldstone mode, we consider their overlap with the lowest energy state in each sector of angular momentum L^2 and for layer separations $d = 0 \cdots 3\ell_0$, in steps of $(1/2)\ell_0$ (We will attempt to keep the convention of using the word "ground state" to indicate the absolute lowest energy state of the system, whereas the lowest energy state of an angular momentum sector will be referred to as such.) We note again that the the trial states are generated by applying the operator $(L_{+,\uparrow})^J$ to the exact ground state at $L = 0$. Only at $d = 0$ is an exact analytical expression of the ground state known: the 111 state. At other values of d, the numerical ground states from exact diagonalization are used, although very accurate trial wavefunctions are also known [20]. The results are summarized in Figure 1, which also indicates overlaps with the first excited state in addition to the overlaps with the lowest energy state in each sector. At $d = 0$, the ansatz

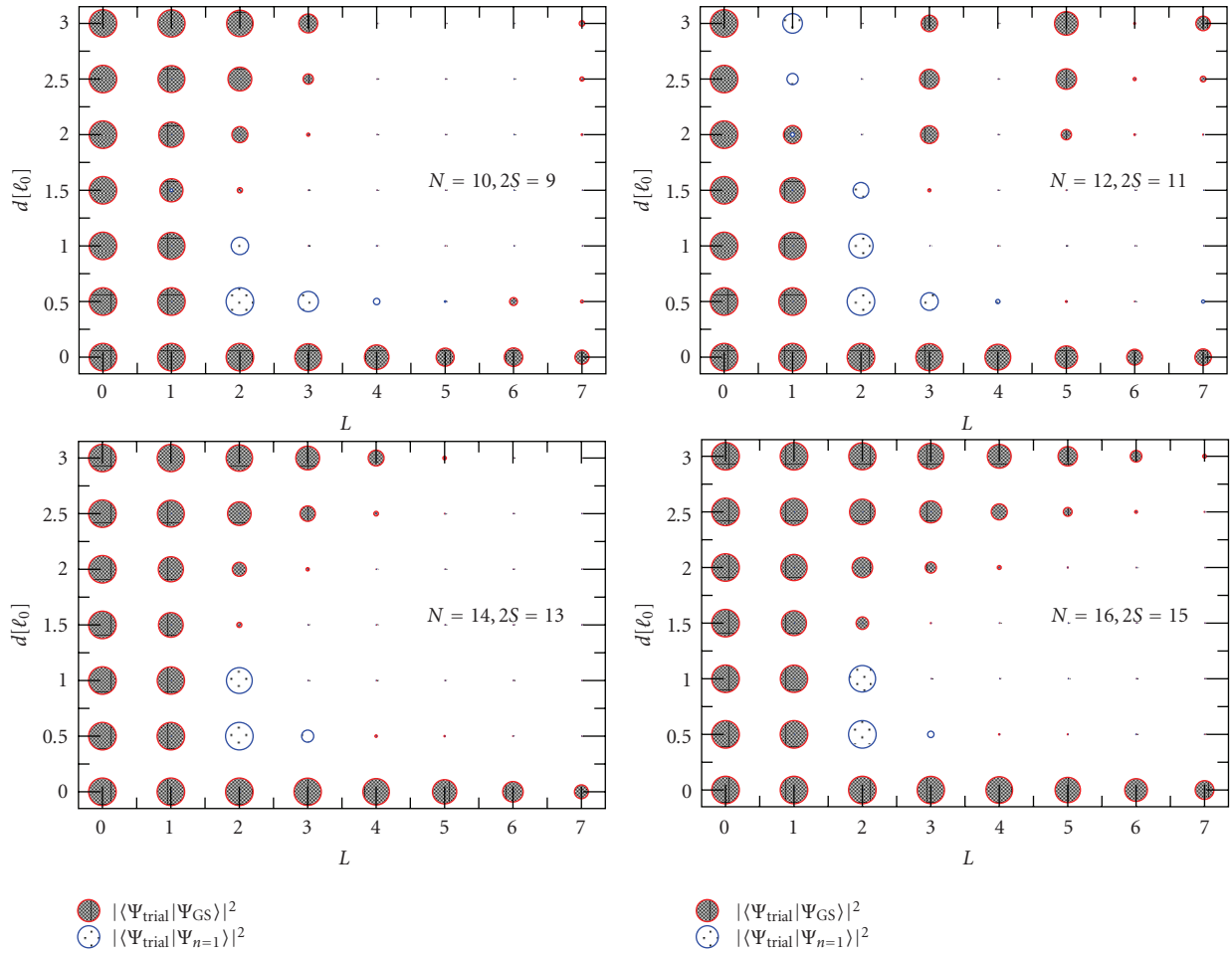

FIGURE 1: Overlaps of the trial states (3) with the exact eigenstates of the Coulomb Hamiltonian for a selection of system sizes $N = 10$, 12, 14, and 16 on the sphere. The magnitude of the overlap of the trial state with the exact ground state is indicated by the size of red dark shaded circles. Blue lightly shaded circles additionally indicate the overlap of the same trial states with the first excited state of the exact spectrum. Overlaps at $L = 0$ are equal to one by definition and give the overall scale. The trial states are very accurate at $d = 0$, giving a good description of the lowest energy mode in each sector of angular momentum (the Goldstone mode) up to large L. At finite layer separation d, the Goldstone mode is always present at small L but does not reach to similarly high values of angular momentum. The description is again more successful at very large d.

(3) is very successful, describing excited states up to high angular momentum accurately. This is shown in more detail in Figure 2(a), which displays the magnitude of the overlap as a function of wavevector k. Surprisingly, for $d = 0$, the overlap is very consistent with system size at given k, even though the Hilbert space dimension increases strongly with N. A very good description with overlaps above 0.8 is given up to a wavevector of $k \sim 2\ell_0^{-1}$. Turning back to Figure 1, we now focus on the overlaps at finite values of layer separation. At $d = 0.5\ell_0$, our trial states obtain significant overlaps only with the first excited state at $L = 1$. This is not due to a disappearance of the linearly dispersing mode, however. Rather, a level crossing appears with distinct excitations occurring at energies less than those of the Goldstone mode, as can be seen from the significant overlaps with the first excited-excited state in the sector of $L = 2$. At $N = 12$, the crossing of the $L = 2$ (3) eigenstates with the Goldstone mode occurs near $d/\ell_0 = 0.35$ (0.45). For layer separations below the first level crossing, the overlaps of the trial states with the exact eigenstates drop only slightly. Once again considering $N = 12$, the overlap of the first four eigenstates remains of the order of 0.9 for $d = 0.3\ell_0$, and for $L = 5$ it drops from 0.81 to 0.58. At $d > 1.5\ell_0$ this overlap with the first excited state again disappears, signalling the presence of additional low-lying excitations of a nature different from the linearly dispersing Goldstone mode.

Finally, at the largest value of $d = 3\ell_0$, the ansatz for the boosted trial wavefunctions becomes more accurate than at intermediate d, signalling the possible emergence of a distinct mode of low-lying excitations. Based on the overlap with the trial states, we can point out that there are strong finite-size effects in the physics at large d. As with $d = 0$, Figure 2(b) displays the numerical values of the overlaps at $d = 3$. These data single out the system with $N = 12$ particles as particularly poorly described by these trial states. Here, the physics at large d is clearly dominated by the shell filling

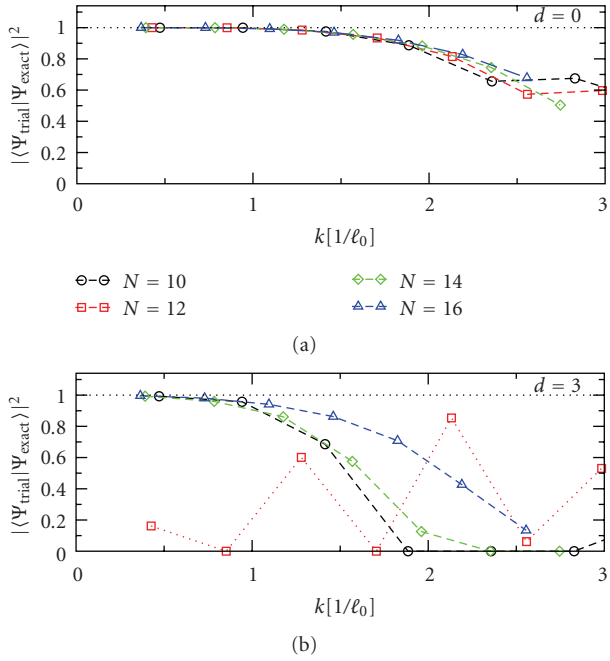

FIGURE 2: Overlaps of the trial states for the Goldstone mode at $d = 0$ (a) and $d = 3$ (b) with the exact state, as in Figure 1, plotted here as a function of wavevector $k \sim L/\sqrt{N_\phi/2}$. Despite the size of the Hilbert spaces increasing significantly between the smallest and largest system shown, the overlap remains roughly constant or maybe slightly increases with N. The region of high overlap extends roughly up to $k \approx 2\ell_0^{-1}$. The failure of this approach for $d = 3$ and $N = 12$ is discussed in detail in the text.

effects of composite fermions. As $N_\uparrow = N_\downarrow = 6$ electrons per layer precisely fill the lowest two shells of composite fermion orbitals in one quantum of effective flux, this system size is aliased with the situation where each layer forms its own incompressible $\nu = 2/5$ state with angular momentum zero in each layer—making it impossible to form higher angular momenta states by boosting one layer with respect to the other.

Before proceeding further, note the rather unusual feature that, excepting $N = 12$, the trial states give higher overlaps for larger systems at $d = 3\ell_0$. This unusual behaviour is related to a different manifestation of the composite fermion shell filling effect. As we have shown in [19], the *ground state* at large layer separation is a state in which each layer individually obeys Hund's rule and maximizes the angular momentum per layer $L_\sigma = L_\uparrow = L_\downarrow$, while both layers are combined into a total $L = 0$ state. Without modifying the correlations inside each layer, the same states with L_σ per layer can be paired into *excited states* with subsequently larger angular momenta, up to a maximum $L_{\max} = 2L_\sigma$. For the system sizes with partially filled composite fermion shells in each layer, one obtains the values of $L_\sigma = 3/2$ for $N = 10$, $L_\sigma = 5/2$ for $N = 14$, and $L_\sigma = 3/2 + 5/2 = 4$ for $N = 16$ particles. We therefore expect a low-lying mode of excitations with angular momenta up to $L_{\max} = 3$, $L_{\max} = 5$, and $L_{\max} = 8$, respectively. Indeed, upon inspection of the spectra, such a mode can be identified.

As an example, Figure 3 displays the spectra for the system with $N = 16$ particles, including different values of the layer separation. Indeed for $d = 3\ell_0$, shown in the bottom right panel, there is clear evidence of a mode of excitations terminating at $L = 8$. Its dispersion is approximately linear at small L; however, it has a quadratic component as well. This should be compared to the Goldstone mode at $d = 0$ (top left panel), for which linear dispersion is clearly realized up to high values of angular momentum.

Once the termination of the low-energy branch at $L_{\max} = 8$ is identified at large d, it becomes apparent that this feature of a jump in the spectrum at $L_{\max}$ exists at all values of layer separation shown, with the exception of the SU(2) invariant case of vanishing d. Note that this termination is a feature of composite *fermion* physics, explained by successively filling the lowest shells of these composite particles, while obeying Hund's rule. The observation that composite fermion physics intervenes at very small layer separation had been made previously by the current authors. While the 111 state can be regarded as a condensate of composite *bosons*, it was shown that an accurate description of the ground state requires a mixed-fluid description of both composite bosons and composite fermions at any finite layer separation [16, 20]. The identified jump may constitute evidence for the mixed-fluid picture in the excitation spectrum, but more study of these excitation spectra will certainly be required.

A linearly dispersing mode at small k exists at all values of the layer separation. The states which were shown in Figure 1 to have large overlap with the trial states (3) are highlighted by blue circles in the spectra shown in Figure 3. These states very accurately come to lie on a single line, which is true especially for the 111 state at $d = 0$, but also for the intermediate layer separations such as $d = 1\ell_0$, where the first excited state at $L = 2$ lies in the continuation of the line through the points at $L = 0$ and $L = 1$ and is shown to be associated to the Goldstone mode by its overlap. Judging by the spectra, it is also very suggestive that multiple level crossings occur at larger values of L, for example, at $L = 2$ for $d = 1.5\ell_0$. Finally, between $d = 2\ell_0$ and $d = 3\ell_0$, a change occurs in the association of the low-lying mode with the Goldstone mode trial states. For $d = 2\ell_0$, only the states up to $L = 2$ have a good overlap, and the remaining states of the already well-formed band of low-lying states in the exact spectrum are of a different nature. The transition to low overlaps occurs at a point where this band has a visible kink and flattens out. Finally at $d = 3\ell_0$, this low-lying band has good overlaps up to much higher momenta, which, as we have discussed above, is a reflection of two approximately uncoupled composite fermion Fermi seas which each maximizes its own angular momentum according to Hund's rule.

Given the existence of a linearly dispersing mode over the whole range of layer separations, we now consider how its velocity changes with d. Comparing the results obtained for different system sizes, a relatively strong dependence of the velocity $v = \partial E/\partial k$ is evident. Applying charging corrections to take account of the shift in the charge density of the

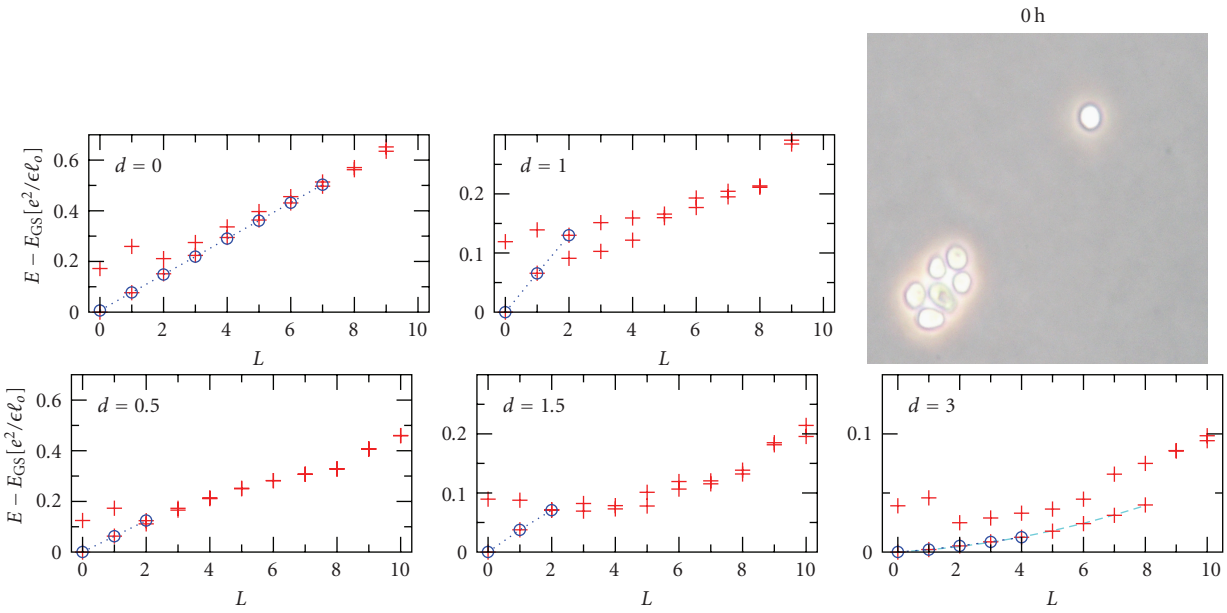

FIGURE 3: Spectra of the Coulomb Hamiltonian in the bilayer system on the sphere for $N = 16$ particles with $N_\phi = 15$ flux, for layer separations d ranging from $d = 0$ (top left) to $d = 3\ell_0$ (bottom right). Energies are indicated in units of $e^2/\epsilon\ell_0$ relative to the ground state energy E_{GS} at $L = 0$. Red crosses mark the lowest two eigenstates in each sector of given L. Blue circles indicate those states which were identified as part of the Goldstone branch by high overlaps (see Figure 1). At $d = 0$, the Goldstone mode is very well formed, while it is clearly visible at small and intermediate d how there are level crossings with additional low lying excitations. At $d = 3$, a mode of low-lying excitations is once again clearly separated from the rest of the spectrum, which terminates sharply at $L = 8$. Its dispersion is linear at small L, but it has a quadratic component responsible of the upturn at larger L. Note the change in the scale of the y-axis for the three columns of panels.

system [28] does not suffice to absorb these effects. Thus, in addition to measuring energies in units of the rescaled magnetic length $\ell_0' = \sqrt{\nu N_\phi/N}\ell_0$, we analyze the scaling of the mode velocity as a function of the inverse system size N^{-1}. These scalings are fitted well by linear extrapolation to the thermodynamic limit, as shown in the inset of Figure 4. The data for $N = 12$ and large layer separation are easily identified as outliers, due to the shell filling effects discussed above. Generally, the slope is decreasing with system size. However, at small finite layer separations the opposite scaling takes effect. The resulting estimates for the mode velocity in the thermodynamic limit shown in the main graph of Figure 4 therefore show a pronounced maximum near $d = \ell_0$, which has about twice the magnitude as the value found at $d = 0$. Beyond this point, the mode velocity decreases monotonically and drops to about 1/10th the value of the 111 state at layer separation $d = 3\ell_0$. In Figure 4, we have also explored how the velocity is affected when we depart from the case of completely balanced densities in both layers. When an additional particle is added to one of the layers, we continue to find a well-defined Goldstone mode across the full range of layer separations, and the velocity extrapolates to the same values for small d and in the limit of large d. However, in the region around $d \sim 1.5\ell_0$ where the vanishing of the condensate fraction indicates a phase transition, the velocity extrapolates to slightly higher values for the imbalanced case, that is, the lowest-lying excitations occur at higher energy. This may be indicative of the presence of pairing in this range of layer separations [19]. On the torus, a low-lying state has been found, which was interpreted as a pseudospin spiral state [17]. However, this mode does not occur in the spherical geometry. Further investigation will be needed to understand this difference.

A previous experiment [22] has probed the velocity of the neutral mode at layer separations near the transition into the incompressible phase at large d, obtaining a combined best fit of $v = 1.4 \times 10^4$ m/s for data at the three layer separations $d_1 = 1.61\ell_0$, $d_2 = 1.71\ell_0$, and $d_3 = 1.76\ell_0$. Based on linear extrapolation between our numerical data at $d = 1.5\ell_0$ and $d = 2\ell_0$, the corresponding estimates are $v(d_1) = 1.14 \times 10^4$ m/s, $v(d_2) = 1.21 \times 10^4$ m/s, and $v(d_3) = 1.33 \times 10^4$ m/s, all slightly smaller but within about 20% of the proposed fit to the experimentally obtained values. Had the data in [22] been fitted separately at each layer separation, the velocity at $d = 1.71\ell_0$ would have been estimated to be about 10% smaller than that at $d = 1.61\ell_0$, roughly reflecting the ratio of our predicted values. The data at $d = 1.76\ell_0$ appears to be rather noisier, probably due to the vicinity to the phase transition, and would be difficult to fit on its own. We suggest that a significant enhancement of the linear mode velocity should be seen deeper inside the interlayer coherent phase at smaller layer separation.

To summarize our results, we use the ansatz (3) to construct trial wavefunctions for a low-energy branch of excitations based on the exact ground state wavefunction. This ansatz is accurate at all interlayer spacings d when k is small, and it is accurate at all k when either d is small or d is large (so long as we do not have a filled shell

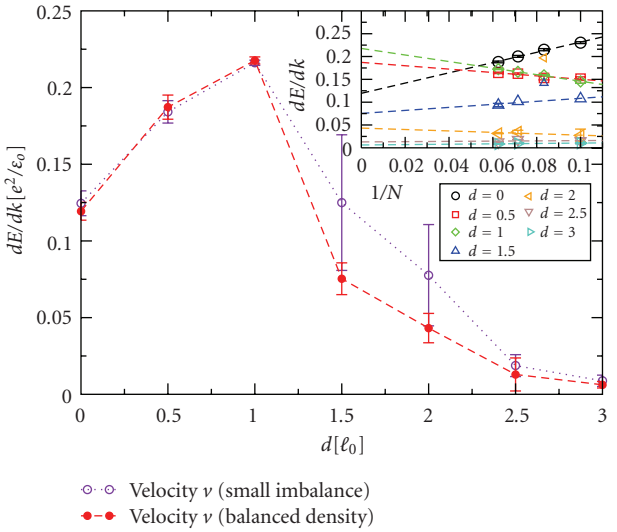

FIGURE 4: The velocity of the Goldstone mode depends strongly on the layer separation and peaks near $d \sim \ell_0$. The velocity has significant finite-size effects on the sphere, and therefore we extract an estimate of its value in the thermodynamic limit by extrapolating the finite-size values over the inverse system size (see inset). The main figure shows the resulting velocities for a density balanced bilayer, as well as for a slightly imbalanced system, as discussed in the main text.

configuration, whereupon only $k = 0$ is in this low energy branch). We find hints that certain aspects of the composite fermion physics persist to low d whereas certain aspects of the Goldstone mode physics persist to high d. Applying these results to the analysis of our numerical data, we show nonmonotonic behavior of the Goldstone mode velocity as a function of the layer separation d. It would be interesting to look for this nonmonotonicity of the Goldstone mode velocity experimentally.

Appendix

Angular Momentum of Two Coupled Subsystems

In this appendix, we will use the standard angular momentum notation $|l, m\rangle$ to indicate eigenstates of the L^2 and L_z operators.

We consider two subsystems $\uparrow$ and $\downarrow$ with corresponding angular momentum operators $\mathbf{L}_\uparrow$ and $\mathbf{L}_\downarrow$. These two subsystems combine to form the total system with angular momentum operator

$$\mathbf{L} = \mathbf{L}_\uparrow + \mathbf{L}_\downarrow. \tag{A.1}$$

Our objective is to show that given an eigenstate of the total system with $|l = 0, m = 0\rangle$ application of $(L_{+\uparrow})^J$ to this system will produce an eigenstate of the total system with $|l = J, m = J\rangle$. To achieve this, it is sufficient to show that

$$L_{+\uparrow}|J, J\rangle \sim |J + 1, J + 1\rangle. \tag{A.2}$$

Obviously, applying $L_{+\uparrow}$ to any state increments its overall L_z eigenvalue by one (or kills the state), so all that remains is to show that applying $L_{+\uparrow}$ to $|J, J\rangle$ results in an eigenstate $L = J + 1$ of L^2, that is, results in an eigenvalue of L^2 being given by $(J + 1)(J + 2)$.

Using (A.1), it is just a matter of some algebra to show that

$$\begin{aligned}[L_{+\uparrow}, L^2] &= 2L_{z\uparrow}L_{+\downarrow} - 2L_{+\uparrow}L_{z\downarrow} \\ &= 2(L_+ - L_{+\uparrow})(L_z + 1) - 2L_{z\downarrow}L_+.\end{aligned} \tag{A.3}$$

We then apply both sides of this equation to the state $|J, J\rangle$. Noting that L_+ kills $|J, J\rangle$, we obtain

$$\begin{aligned}L^2[L_{+\uparrow}|J, J\rangle] &= [L_{+\uparrow}(J(J + 1)) + 2L_{+\uparrow}(J + 1)]|J, J\rangle \\ &= (J + 1)(J + 2)[L_{+\uparrow}|J, J\rangle],\end{aligned} \tag{A.4}$$

which completes the proof.

From the particular form of the eigenstate, it further follows that it has a parity of $(-1)^J$ under reversal of the z-component of (pseudo-)spin. Noting that

$$L_{+,\text{total}}\,|\,L_{\text{total}} = L_{z,\text{total}} = J\rangle = 0, \tag{A.5}$$

and since $L_{\text{total}} = L_{+,\uparrow} + L_{+,\downarrow}$, we have $L_{+,\uparrow} = -L_{+,\downarrow}$ when applied to any state of the form $|L_{\text{total}} = L_{z,\text{total}} = J\rangle$ for any J. The trial state (3) can thus equivalently be obtained by applying $L^J_{+,\downarrow}$, since the state $|J, J\rangle$ is unique.

Acknowledgment

G. Möller acknowledges support from Trinity Hall Cambridge, as well as from the Institute of Complex Adaptive Matter (ICAM). SHS thanks the Aspen Center for Physics for its hospitality.

References

[1] S. Das Sarma and A. Pinczuk, Eds., *Perspectives in Quantum Hall effects*, Wiley, New York, NY, USA, 1997, see chapter 2 by J. Eisenstein and chapter 5 by S. M. Girvin and A. H. MacDonald.

[2] J. P. Eisenstein and A. H. MacDonald, "Bose-Einstein condensation of excitons in bilayer electron systems," *Nature*, vol. 432, no. 7018, pp. 691–694, 2004.

[3] K. Moon, H. Mori, K. Yang et al., "Spontaneous interlayer coherence in double-layer quantum Hall systems: charged vortices and Kosterlitz-Thouless phase transitions," *Physical Review B*, vol. 51, no. 8, pp. 5138–5170, 1995.

[4] B. I. Halperin, "Theory of the quantized Hall conductance," *Helvetica Physica Acta*, vol. 56, p. 75, 1983.

[5] S. Q. Murphy, J. P. Eisenstein, G. S. Boebinger, L. N. Pfeiffer, and K. W. West, "Many-body integer quantum Hall effect: evidence for new phase transitions," *Physical Review Letters*, vol. 72, no. 5, pp. 728–731, 1994.

[6] I. B. Spielman, J. P. Eisenstein, L. N. Pfeiffer, and K. W. West, "Resonantly enhanced tunneling in a double layer quantum hall ferromagnet," *Physical Review Letters*, vol. 84, no. 25, pp. 5808–5811, 2000.

[7] E. Tutuc, M. Shayegan, and D. A. Huse, "Counterflow measurements in strongly correlated GaAs hole bilayers: evidence for electron-hole pairing," *Physical Review Letters*, vol. 93, no. 3, Article ID 036802, 2004.

[8] R. D. Wiersma, J. G. S. Lok, S. Kraus et al., "Activated transport in the separate layers that form the $\nu_T = 1$ Exciton condensate," *Physical Review Letters*, vol. 93, no. 26, Article ID 266805, 2004.

[9] M. Kellogg, J. P. Eisenstein, L. N. Pfeiffer, and K. W. West, "Vanishing hall resistance at high magnetic field in a double-layer two-dimensional electron system," *Physical Review Letters*, vol. 93, no. 3, Article ID 036801, 2004.

[10] N. Kumada, K. Muraki, K. Hashimoto, and Y. Hirayama, "Spin degree of freedom in the $\nu = 1$ bilayer electron system investigated by nuclear spin relaxation," *Physical Review Letters*, vol. 94, no. 9, Article ID 096802, 2005.

[11] A. R. Champagne, J. P. Eisenstein, L. N. Pfeiffer, and K. W. West, "Evidence for a finite-temperature phase transition in a bilayer quantum hall system," *Physical Review Letters*, vol. 100, no. 9, Article ID 096801, 2008.

[12] K. Yang, K. Moon, L. Belkhir et al., "Spontaneous interlayer coherence in double-layer quantum Hall systems: symmetry-breaking interactions, in-plane fields, and phase solitons," *Physical Review B*, vol. 54, no. 16, pp. 11644–11658, 1996.

[13] Y. N. Joglekar and A. H. MacDonald, "Microscopic functional integral theory of quantum fluctuations in double-layer quantum Hall ferromagnets," *Physical Review B*, vol. 64, no. 15, Article ID 155315, 10 pages, 2001.

[14] Y. B. Kim, C. Nayak, E. Demler, N. Read, and S. Das Sarma, "Bilayer paired quantum Hall states and Coulomb drag," *Physical Review B*, vol. 63, no. 20, Article ID 205315, 9 pages, 2001.

[15] J. Schliemann, S. M. Girvin, and A. H. MacDonald, "Strong correlation to weak correlation phase transition in bilayer quantum Hall systems," *Physical Review Letters*, vol. 86, no. 9, pp. 1849–1852, 2001.

[16] S. H. Simon, E. H. Rezayi, and M. V. Milovanovic, "Coexistence of composite bosons and composite fermions in $\nu = 1/2 + 1/2$ quantum hall bilayers," *Physical Review Letters*, vol. 91, no. 4, Article ID 046803, 4 pages, 2003.

[17] K. Park, "Spontaneous pseudospin spiral order in bilayer quantum Hall systems," *Physical Review B*, vol. 69, no. 4, Article ID 045319, 6 pages, 2004.

[18] N. Shibata and D. Yoshioka, "Ground state of $\nu = 1$ bilayer quantum hall systems," *Journal of the Physical Society of Japan*, vol. 75, no. 4, Article ID 043712, 4 pages, 2006.

[19] G. Möller, S. H. Simon, and E. H. Rezayi, "Paired composite fermion phase of quantum hall bilayers at $\nu = 1/2 + 1/2$," *Physical Review Letters*, vol. 101, no. 17, Article ID 176803, 2008.

[20] G. Möller, S. H. Simon, and E. H. Rezayi, "Trial wave functions for $\nu = 1/2 + 1/2$ quantum Hall bilayers," *Physical Review B*, vol. 79, no. 12, Article ID 125106, 2009.

[21] M. Rasolt, F. Perrot, and A. H. MacDonald, "New gapless modes in the fractional quantum Hall effect of multicomponent fermions," *Physical Review Letters*, vol. 55, no. 4, pp. 433–436, 1985.

[22] I. B. Spielman, J. P. Eisenstein, L. N. Pfeiffer, and K. W. West, "Observation of a linearly dispersing collective mode in a quantum Hall ferromagnet," *Physical Review Letters*, vol. 87, no. 3, Article ID 036803, 4 pages, 2001.

[23] M. Kellogg, I. B. Spielman, J. P. Eisenstein, L. N. Pfeiffer, and K. W. West, "Observation of quantized Hall drag in a strongly correlated bilayer electron system," *Physical Review Letters*, vol. 88, no. 12, Article ID 126804, 4 pages, 2002.

[24] M. Kellogg, J. P. Eisenstein, L. N. Pfeiffer, and K. W. West, "Bilayer quantum Hall systems at $\nu_T = 1$: coulomb drag and the transition from weak to strong interlayer coupling," *Physical Review Letters*, vol. 90, no. 24, Article ID 246801, 4 pages, 2003.

[25] E. Tutuc and M. Shayegan, "Interaction and disorder in bilayer counterflow transport at filling-factor one," *Physical Review B*, vol. 72, no. 8, Article ID 081307, 4 pages, 2005.

[26] F. D. M. Haldane, "Fractional quantization of the hall effect: a hierarchy of incompressible quantum fluid states," *Physical Review Letters*, vol. 51, no. 7, pp. 605–608, 1983.

[27] A. Wójs, G. Möller, S. H. Simon, and N. R. Cooper, "Skyrmions in the moore-read state at $\nu = 5/2$," *Physical Review Letters*, vol. 104, no. 8, Article ID 086801, 4 pages, 2010.

[28] N. D'Ambrumenil and R. Morf, "Hierarchical classification of fractional quantum Hall states," *Physical Review B*, vol. 40, no. 9, pp. 6108–6119, 1989.

Hindawi Publishing Corporation
Advances in Condensed Matter Physics
Volume 2011, Article ID 258731, 8 pages
doi:10.1155/2011/258731

Research Article

From Coherent States in Adjacent Graphene Layers toward Low-Power Logic Circuits

Leonard F. Register, Dipanjan Basu, and Dharmendar Reddy

Department of Electrical and Computer Engineering, Microelectronics Research Center, The University of Texas at Austin, 10100 Burnet Road, Building 160, Austin, TX, 78758, USA

Correspondence should be addressed to Leonard F. Register, register@mer.utexas.edu

Received 31 May 2010; Accepted 19 August 2010

Academic Editor: Emanuel Tutuc

Colleagues and we recently proposed a new type of transistor, a Bilayer PseudoSpin Field Effect Transistor (BiSFET), based on many-body coherent states in coupled electron and hole layers in graphene. Here we review the basic BiSFET device concept and ongoing efforts to determine how such a device, which would be far from a drop-in replacement for MOSFETs in CMOS logic, could be used for low-power logic operation, and to model the effects of engineerable device parameters on the formation and gating of interlayer coherent state.

1. Introduction

The greatest roadblock to continued logic scaling is power consumption. Circuit heating can limit device density and clock frequencies beyond intrinsic device limits. Mobile device performance is limited by battery use. And it has been estimated that 7% of power consumption in the United States is already integrated circuit related [1]. Complementary metal-oxide semiconductor (CMOS) logic employing electron/n-channel and hole/p-channel metal-oxide field effect transistors (MOSFETs) has been the standard for many years. However, basic physics rather than technological limits now portend an "end of the roadmap"—referring in part to the International Technology Roadmap for Semiconductors (ITRSs) [2]—for CMOS scaling in the not too distant future. Specifically, thermionic emission of charge carriers over the gated channel barrier between the source and drain combined with the need for rapid switching appears to limit minimum supply voltages to 0.5 to 0.7 V at room temperature, and associated switching energies to a few aJ [2]. Of course, with this limit defined by thermionic emission, lower voltage and power operation would be possible at colder temperatures. However, for most conventional applications, logic or otherwise, a proposal for below room-temperature operation is a nonstarter. This need for continued scaling beyond the end of the roadmap for CMOS is motivating various efforts to produce transistors based on alternative switching mechanisms.

Of relevance to the subject of this special issue, colleagues and we recently proposed a new type of transistor, a Bilayer PseudoSpin Field Effect Transistor (BiSFET), based on many-body coherent states in coupled electron/n and hole/p type graphene layers [3]. Normally one does not associate coherent many-body states with room temperature. However, as a consequence of a synergy of graphene properties—a single atomic layer thick with nearly perfect electron-hole symmetry in the band structure, a low density of states and zero band gap—it has recently been predicted that this condensate might occur above room temperature in otherwise weakly coupled and oppositely charged graphene double/bilayer systems [4]. Under appropriate conditions, the predicted temperature for coherence could extend to slightly above $0.1E_F/k_B$ where E_F is the magnitude of the Fermi energy relative to the Dirac point [4], which translates to $n \approx p \approx 5\times10^{12}/\text{cm}^2$ in graphene for many-body-induced coherence above 300 K [3]. Single layer graphene sheets have been gated up to densities in excess of $10^{13}/\text{cm}^2$ [5]. The BiSFET represents one attempt to explore the applicability of

this novel predicted behavior for graphene bilayers to achieve device functionality.

In the following we review the basic BiSFET device concept (Section 2) [3], how such a device, which would be far from a drop-in replacement for MOSFETs in CMOS logic, could be used for low power logic operation (Section 3) [3, 6, 7], and ongoing work to examine the effects of engineerable device parameters on formation and "gating" of interlayer coherence (Section 4) [8].

2. The BiSFET Device Concept

A schematic of a BiSFET intended to represent only the essential device elements is shown Figure 1(a). A *p*-type and an *n*-type layer of graphene are separated by a dielectric tunnel barrier (or perhaps are just misaligned in order to limit the bare charge carrier transport/tunneling between layers, but the effects of such misalignment on the interlayer coherence has not yet been well explored). The region for coherence could be defined, for example, by increased carrier concentrations consistent with the introductory remarks, or by variation of the separation between the two layers or variation in the dielectric material as will be discussed. As illustrated, each graphene layer has a metallic contact and is electrostatically coupled to a gate electrode through a gate dielectric. Much like for a Josephson junction, the current flow between the layers is expected to be limited by the peak/critical interlayer current beyond which the coherence would collapse. Below the critical current and associated critical interlayer voltage, the layers would be essentially shorted together via the many-body-enhanced interlayer current flow, with current flow limited by the leads; beyond this voltage, current would drop toward the single particle tunneling limit. The required carrier densities could perhaps be induced under zero gate bias by use of differing work functions for the gates, or ferroelectric oxides as dielectrics, and/or back-gating. Applied gate voltage signals are intended only to balance or slightly unbalance the charge concentrations between layers to increase or degrade the interlayer coherence, and, thus, increase or decrease the interlayer critical current. Note that in many cases a switchable input signal to only one gate is required, leaving a good deal of flexibility in what constitutes the other "gate."

Preliminary estimates for the critical current and associated voltage are provided in [3]. Perhaps the most important results are two qualitative predictions: first, the critical current and associated voltage should depend on engineerable device parameters, allowing them to be designed subject to technological constraints; second, the critical voltage can be small compared to $k_BT/q \approx 26\,\text{mV}$ at room temperature allowing potentially very low voltage operation. Qualitatively expected *I*-*V* characteristics are illustrated in Figure 1(b).

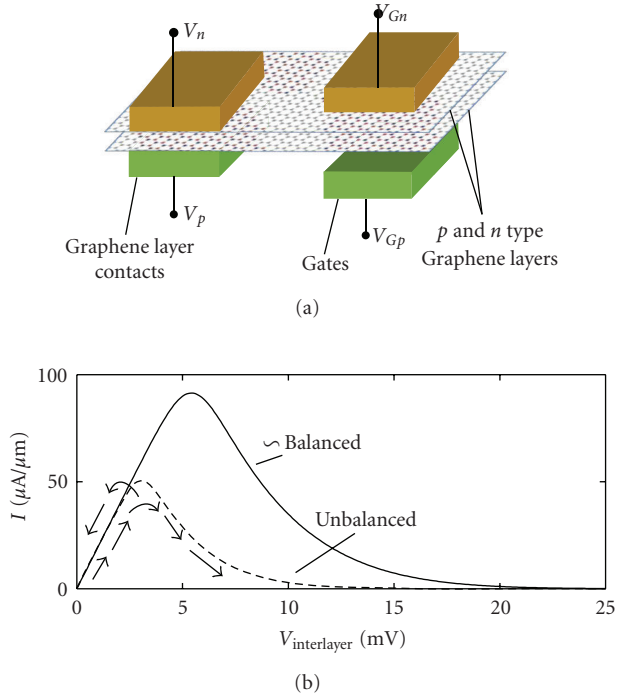

Figure 1: (a) Schematic illustration of BiSFET (with dielectrics not shown for clarity). (b) Qualitative estimation of interlayer current versus interlayer voltage for balanced and unbalanced charged distributions, consistent with the BiSFET model used in Section 2 as required for specificity. Arrows in (b) illustrate inverter operation as discussed in Section 3.

3. BiSFET Logic

Without an experimental realization of a BiSFET or even experimental evidence for formation of the condensate in adjacent layers of graphene at the time of writing, it might seem that exploring logic based on BiSFETs is a case of "putting the cart before the horse." However, such circuit level work helps measure the potential payoff of continuing device work, and informs that work through identification of critical device physics and technological challenges.

We also note that the *I*-*V* characteristics of Figure 1(b) are similar in some respect to those of resonant tunneling diodes, which have long been considered for logic applications. Indeed, the clocked biasing of the logic gates as discussed here has much in common with proposals for gated resonant tunneling diodes (RTDs), for example, [9, 10]. However, there are fundamental differences between how BiSFETs and gated RTDs operate, which are relevant to circuit design as well. For example, critical for low voltage circuit design, peak conductivity for a BiSFET would be intrinsically centered about a 0 V interlayer potential, with, again, critical voltages being small compared to k_BT/q. In an RTD, peak conductivity is associated with resonant band alignment, which may or may not occur under zero bias across the diode as defined not only by design but by device-to-device variances during fabrication, and is broadened by the thermal carrier distributions on either side of the junction in conventional RTD designs.

For the purposes of SPICE-based circuit simulation, we model the BiSFET as shown in Figure 2. To provide the required specificity for SPICE-based circuit simulation, the qualitative *I*-*V* behavior illustrated in Figure 1(b) has been

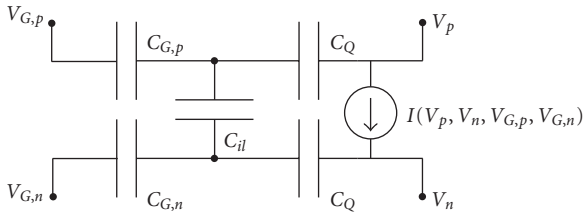

FIGURE 2: Circuit model of BiSFET used for SPICE simulation. $V_p - V_n$ is the interlayer voltage, and $V_{G,p}$ and $V_{G,n}$ are the gate voltages. $C_{G,p}$, $C_{G,n}$, and C_{il} are parallel plate capacitances between the p-type graphene layer and its gate, between the n-type graphene layer and its gate, and between the n and p graphene layers, respectively. C_Q are the quantum capacitances associated with the density of states of the individual graphene layers, and I is the interlayer current of all four applied voltages.

approximated via the smoothed current versus interlayer voltage relation,

$$I = G_o\left(V_p - V_n\right)\left[1 + \left(\frac{(V_p - V_n)/V_{\max}}{\exp\left(1 - \left|V_p - V_n\right|/V_{\max}\right)}\right)^4\right]^{-1/4}, \tag{1}$$

with gate dependent $V_{\max}$,

$$V_{\max} = V_{\max,o}\exp\left[-\frac{10\left|\Delta p - \Delta n\right|}{n+p}\right], \tag{2}$$

where G_o represents the ballistic Landauer-Büttiker limit of conductance, and Δn and Δp are the variations in charge densities with all four terminal voltages consistent with the model of Figure 2. There remains much work to be done on the device side to better quantify this behavior. However, we note that the actual form of the decay in the negative differential resistance (NDR) regime of (1), $I \approx G_o V_{\max}\exp(1 - |V_p - V_n|/V_{\max})$, is not critical to logic gates operation or power consumption [6]. Also, for specificity, for all the simulations presented below, the following model parameter values have been used in accordance with the calculations in [3]. All gate lengths have been chosen to be $L = 10$ nm. Unless otherwise specified, the gate/channel widths for BiSFETs shown in the circuits here are $W = 20$ nm for a W/L ratio of 2; larger specified values of W/L below indicate wider gates. Again for specificity, effective oxide thicknesses (EOTs) of 1 nm are assumed for gate and interlayer dielectrics corresponding to $C_g = C_{il} = 3.5 \times 10^{-6}$ F/cm^2, but this choice does not imply the use of the same oxides. To the contrary, the gate dialectics should be more insulating, while the interlayer dielectric should allow some single/bare electron tunneling which is necessary to allow the many-body-enhanced interlayer current on which the BiSFET relies [3, 8]. The nominal carrier densities in graphene layers were taken to be $p_o \approx n_o \approx 5 \times 10^{12}$ cm^{-2} which should theoretically allow room-temperature operation as discussed in Section 2. These densities could be provided by, for example, opposing gate work-functions of approximately ± 1 eV, respectively, or by one ± 1 eV gate work function and an opposing fixed back-gate bias.

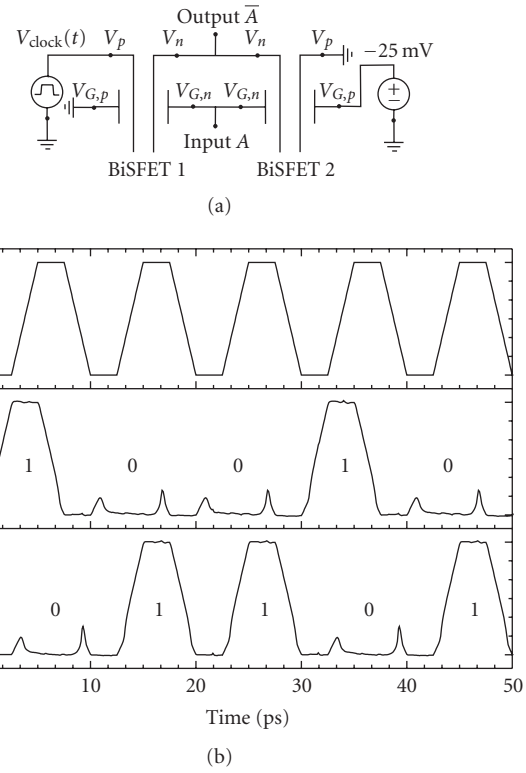

FIGURE 3: (a) BiSFET-based inverter layout and (b) clock signal, illustrated input voltage signal string (from a preceding inverter), and inverted output signal obtained using the SPICE circuit simulator.

Because of the substantial qualitative differences between BiSFET behavior and that of MOSFETs—that is, current decay rather than saturation with increased interlayer voltage, and perhaps weak dependence on gate voltage by comparison—entirely different ways of implementing Boolean logic are required using BiSFETs. The simplest of logic elements, an inverter, can be realized in a complementary layout as shown in Figure 3(a) where we have used a symbolic representation for the BiSFET. The unswitched "back-gate" voltages represent changes in work-functions, modulation doping, or actual back-gate voltages that produce an equivalent charge imbalance. Although this circuit appears similar to a CMOS inverter, the operation is notably different, with a clocked power supply $V_{\text{clock}}(t)$ [3, 6], as in, for example, [9]. $V_{\text{clock}}(t)$ is used because changing the input signal/voltage with a fixed power supply has no effect on the output signal. Instead, $V_{\text{clock}}(t)$ must be raised after the input signal is set for proper logic functionality. As illustrated via the arrows in Figure 1(b), as the clock voltage increases, it is split essentially equally between the two devices until the current reaches the peak allowed for the device with the smaller peak/critical current. Beyond that point the current can only decrease, forcing the voltage drop across the device with the larger critical current back toward zero while that for the device with the smaller critical current increases into the NDR region. With a 0 mV input signal and -25 mV on V_{Gp2}, BiSFET 2 will have a charge imbalance and the associated lower critical current, causing the output

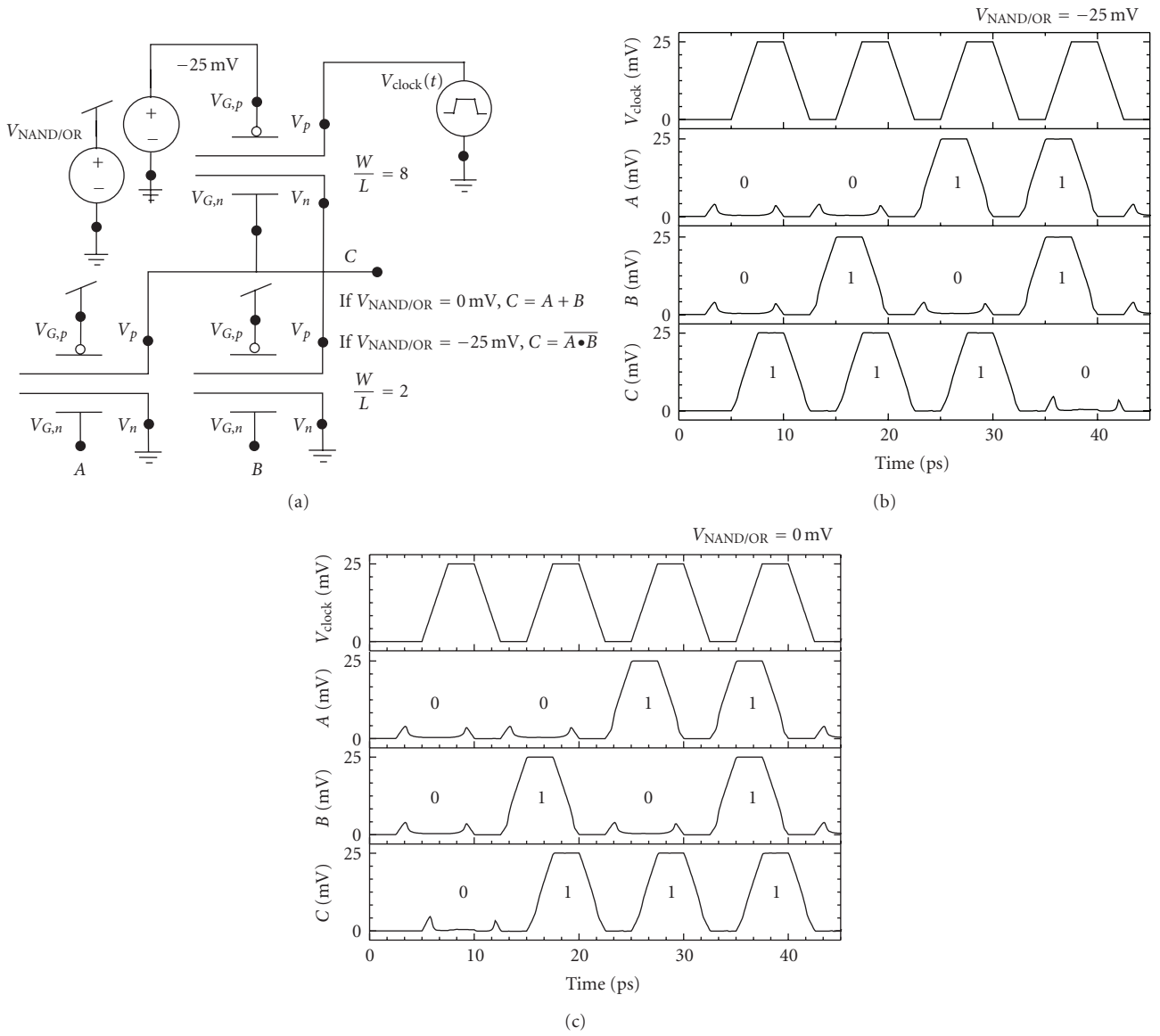

Figure 4: (a) A programmable NAND/OR Gate and SPICE simulation results of (b) NAND and (c) OR gate operation at 100 GHz.

signal to closely follow $V_{\text{clock}}(t)$, that is, to go high. With the input voltage high, +25 mV, however, the charge in BiSFET 2 is balanced and that in BiSFET 1 is unbalanced, $V_{\text{clock}}(t)$ is dropped predominantly across BiSFET 1, and the output signal remains low. Similarly, removing the input signal will have no effect on the output while the clock signal remains high; each gate also serves much like a latch.

Figure 3(b) shows the SPICE-simulated response for such an inverter. The clock signal is pulsed with a frequency of 100 GHz and peak clock voltage of 25 mV. A four-inverter output load was considered. The clock signal is delayed relative to the input signal by the 2.5 ps rise time, allowing the latter to be set before the inverter is clocked. Both input and output signals were subject to a fan-in and fan-out of four inverters, respectively. The average energy consumed per clock cycle per BiSFET was ∼0.01 aJ = 10 zJ. For comparison, the switching energy for current MOSFETs is ∼100 aJ, and 2020 "end of the roadmap" CMOS will have a switching energy on the scale of 5 aJ [2]. The drastic energy reductions are largely a function of the reduced operating voltage for this many-body-coherence-mediated switching mechanism that may be possible, where energies scale as the square of voltage, of course. However, these estimates are rough and do not consider the parasitic power losses of delivering the clock signal to each BiSFET. And, each BiSFET is switched on each clock cycle, for an effective activity factor of unity for an active clock.

Other logic gates such as NAND, NOR, OR, and XOR (exclusive OR) gates, and memory elements have also been implemented and verified by SPICE simulations [6, 7], as per the example of the potentially programmable NAND/OR gate of Figure 4. The average energy consumed per switching

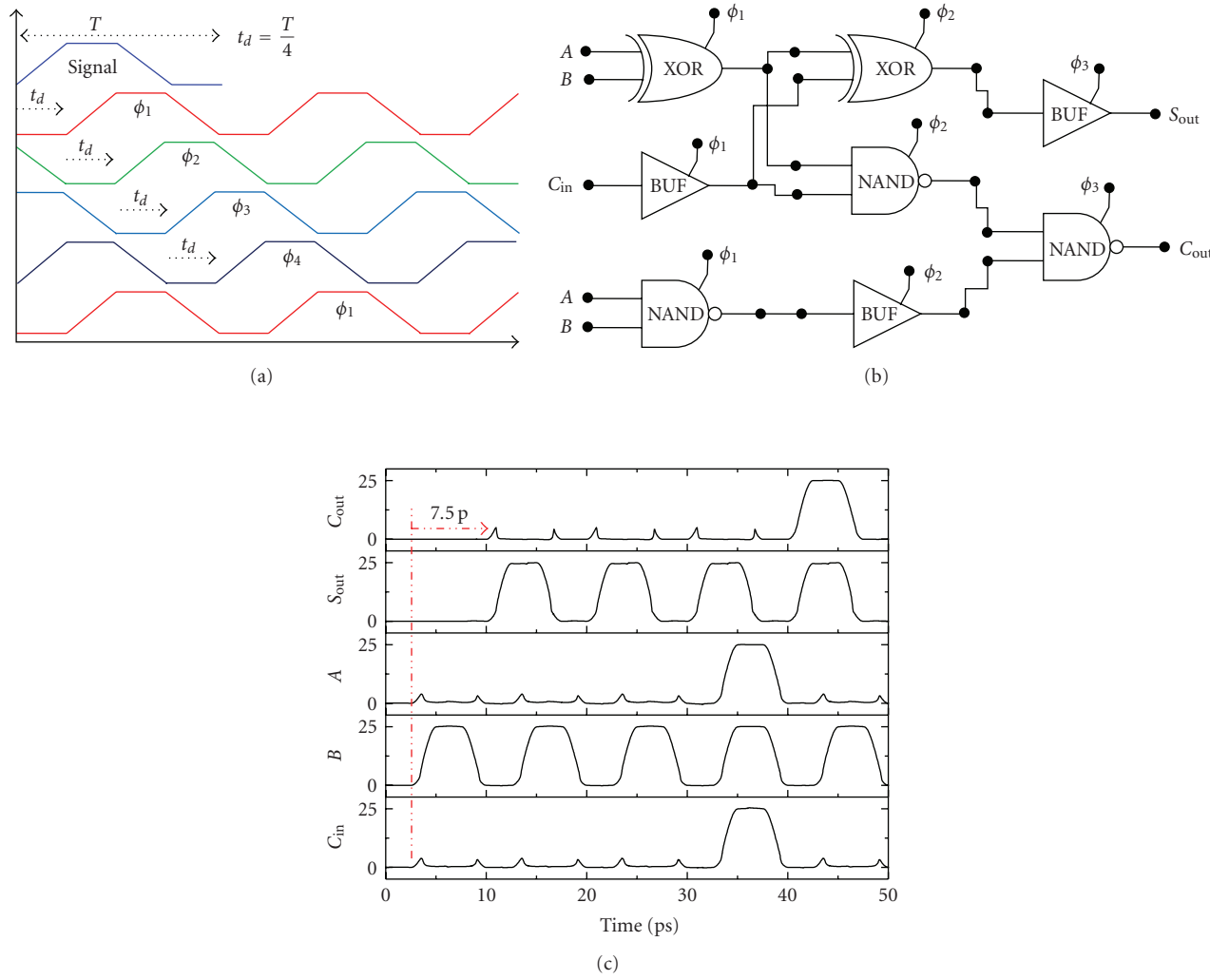

FIGURE 5: (a) Illustration of a four-phase clocking scheme, (b) a 1-bit full adder, and (c) inputs and sum (S) and carry (C) outputs with the delay between input and output shown.

operation per gate (not per BiSFET) was ~30 zJ for both the NAND and OR gates, respectively. We have also considered multistage circuits using a four-phase clock signal, as in [10], such as the adder of Figure 5 [7]. Note that although each gate in series requires a quarter-period delay in processing the signal, the inputs can be released once the output for each gate is set, and new inputs can be processed each clock cycle no matter how many subsequent gates there are in series.

4. Achieving and Gating Interlayer Coherence

To take a direct look at the many-body-interaction-induced interlayer coherence, we use a π-band tight-bond model of the graphene layers, treat the many-body interaction via a Fock approximation as within the original work predicting possible room-temperature coherence [4], and neglect any bare/single particle coupling here although it is ultimately required to support the critical current. The interlayer coherence is therefore driven entirely by the exchange interactions between the top (T) and bottom (B) layers,

$$V_F(\mathbf{R}_T, \mathbf{R}_B) = \frac{-e^2}{4\pi\varepsilon_0\varepsilon_r\sqrt{(\Delta R)^2 + d^2}} \times \sum_{\alpha,\mathbf{k},s} n_{\alpha,\mathbf{k},s}\phi_{\alpha,\mathbf{k},s}(\mathbf{R}_T)\phi^*_{\alpha,\mathbf{k},s}(\mathbf{R}_B). \quad (3)$$

Here, $\mathbf{R}_T$ and $\mathbf{R}_B$ are the 2D in-plane vectors for the atoms in the top and bottom graphene layers, respectively. $\Delta R = |\mathbf{R}_T - \mathbf{R}_B|$ is the magnitude of the in-plane component of the separation between the atoms, and d is the separation between the two layers, and the $\phi_{\alpha,\mathbf{k},s}(\mathbf{R})$ are the self-consistently calculated single particle Bloch functions subject to the Fock interaction, where α labels the band, $\mathbf{k}$ the wavevector, and s the spin state.

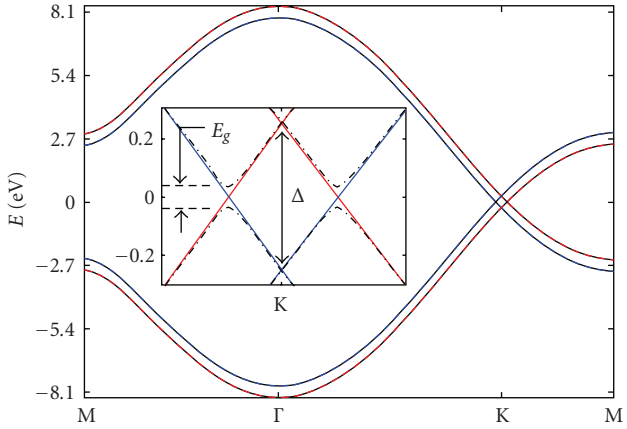

FIGURE 6: Energy bands of two graphene layers separated by 1.0 nm of SiO_2 (ε_r = 3.9), having layer potentials of $-\Delta/2$ (top layer—blue) and $+\Delta/2$ (bottom layer—red) in the uncoupled state (solid lines) along the high-symmetry directions in the Brillouin zone (shown above). Δ = 0.5 eV. Phase coherence between layers creates a correlated, lower energy state (black dash-dotted lines). The inset magnifies the low energy-spectrum, revealing a band gap E_g of 74 meV at 0 K for balanced top and bottom layer charge distributions with E_F located within the band gap.

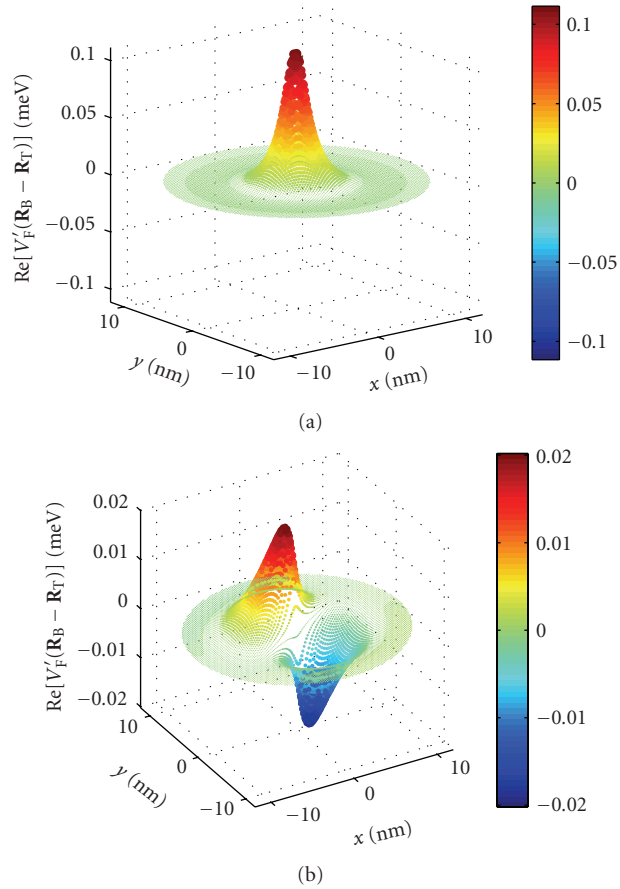

FIGURE 7: (a) Real part of $V'_F(\mathbf{R}_T,\mathbf{R}_B)$ for A_T-A_B coupling obtained by dividing $V_F(\mathbf{R}_T,\mathbf{R}_B)$ by $\exp[i\mathbf{k}_D \cdot (\mathbf{R}_T - \mathbf{R}_B)]$, as a function of $\mathbf{R}_T - \mathbf{R}_B$ for Δ = 0.5 eV, d = 1 nm, ε_r = 3.9, and balanced charge distributions at 0 K. The imaginary part essentially vanishes. $V'_F(\mathbf{R}_T,\mathbf{R}_B)$ for B_T-B_B is essentially identical except for a 180° degree phase shift. (b) Real part of $V'_F(\mathbf{R}_T, \mathbf{R}_B)$ for A_T-B_B coupling obtained under the same conditions. The imaginary part is rotated by 90°. $V'_F(\mathbf{R}_T,\mathbf{R}_B)$ for B_T-A_B coupling is essentially the complex conjugate of $V'_F(\mathbf{R}_T, \mathbf{R}_B)$ for A_T-B_B coupling.

Of course, self-consistent solutions can be obtained simply by setting the interlayer exchange interactions to zero. This solution corresponds to an uncorrelated/incoherent state with electrons isolated in one layer or the other. However, a self-consistent solution that yields a nonzero value of the interlayer exchange potential and eigenfunctions that overlap both layers is what we are after. Coherence results in a gap in the energy spectrum of the two-layer system near the points at which the conduction band of the top layer and the valence band of the lower would otherwise cross. For balanced charge distributions in the two layers (overall charge neutrality) the Fermi level falls within the center of the gap, energy is gained due to gap formation, and the coherent state becomes energetically favorable. This band splitting for such a correlated state (0 K temperature, balanced charge distributions of 6×10^{12} cm^{-2} corresponding to an interlayer potential splitting Δ of 0.5 eV, interlayer spacing of 1 nm, and dielectric permittivity ε_r = 3.9 of SiO_2) is illustrated in Figure 6, where the energy bands are plotted along the high-symmetry directions.

Figure 7 shows corresponding 0 K solutions for the self-consistent nonlocal Fock potential of (3). Note that the result depends greatly on which of the two atoms in the primitive unit cell of each layer are considered. Physically, the alignment (not the coupling) was Bernal-like for this particular simulation, but the result is essentially the same for a hexagonal-like alignment because the separation between the graphene layers is much greater than the nearest neighbor atomic separation within layers. Also note that, beyond being nonlocal within the plane of the layers, the coupling is neither Bernal-like nor hexagonal-like, but rather takes on an antihexagonal nature, at least in the absence of bare coupling. As further detailed in [8], along with initial efforts to consider the consequences for the critical interlayer current, this antihexagonal pattern of coupling is optimal for coupling the chiral valence band and conduction band electron states of the individual graphene layers to each other, states which have opposite relative phases between the two atomic sublattices for any given wavevector $\mathbf{k}$.

The need is for room-temperature coherence, however. As temperature increases, states below the condensate band gap begin to empty, and states above the condensate band gap begin to fill whose contributions to the condensate is of same magnitude but opposite sign to their counterparts below, breaking down the condensate, as again detailed in [8]. Figure 8(a) illustrates the resulting temperature dependence of the condensate for three different dielectric permittivities, exhibiting a universal behavior when normalized to the 0 K band gap. Thus, along with other considerations [4], obtaining a room-temperature condensate translates to finding a 0 K band gap greater than at least approximately $4k_BT$

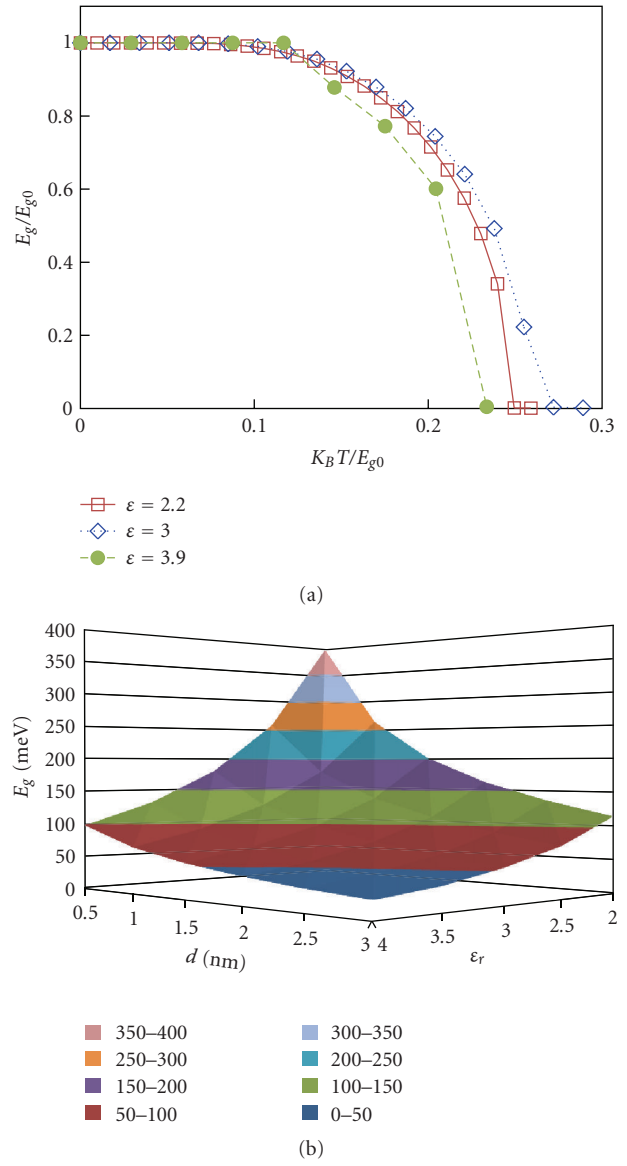

Figure 8: (a) Temperature dependence of the band gap for three different dielectric constants normalized to the 0 K band gap in each case, with $\Delta = 0.5$ eV, $d = 1$ nm, and balanced charge distributions. (b) 0 K band gap as a function of interlayer separation d and dielectric relative permittivity ε_r.

$\approx$ 100 meV. The 0 K band gap for various combinations of layer separation and displacement are shown in Figure 8(b). Among other things, it becomes clear that low-permittivity dielectrics are preferable, in contrast to the needs of CMOS devices (or to dielectrics encountered in III–V quantum well systems).

Finally, Figure 9 provides an example of degradation of the condensate with charge imbalance. In this case at least, the initial sensitivity is actually less than that of (2) used in SPICE simulations. This should not be that qualitatively critical, however, as the circuits are bistable and essentially any difference in critical currents should be sufficient to control the switching. On the other hand, with a bit more

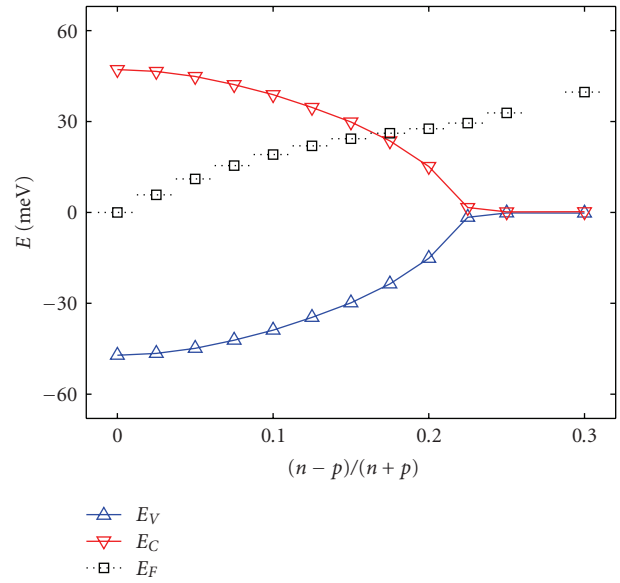

Figure 9: Energy band edges for the coherent state and Fermi level as a function of carrier imbalance between top layer electron density and bottom layer hole density, for graphene bilayers separated by 1 nm at 300 K with $\varepsilon_r = 3.0$ and $\Delta = 0.5$ eV.

charge imbalance, the coherence appears to completely collapse, for reasons detailed in [8], and more conventional logic may become possible.

5. Conclusion

We have reviewed ongoing efforts on the theory side to translate possible room-temperature many-body-induced interlayer coherence in graphene bilayers into a "beyond CMOS" switch, a Bilayer PseudoSpin Field Effect Transistor or BiSFET. The BiSFET is, however, currently only a concept based on novel predicted physics in a novel material system. And we recognize the limitations of theory, and the technological challenges to realization of BiSFETs even if theory holds. There are certainly no guarantees that such a device based on room-temperature many-body-mediated coherence between graphene layers can ever be realized. However, we believe that the potential benefits of ultra-low power logic well justify the efforts, theoretical as here as well as experimental, to more fully explore the possibility.

Acknowledgments

This work was supported through the NRI SWAN Center by the Semiconductor Research Corporation and the Texas Emerging Technology Fund, and by the U.S. Army Research Office.

References

[1] C. Hu, D. Chou, P. Patel, and A. Bowonder, "Green transistor—a V_{DD} scaling path for future low power ICs," in *International Symposium on VLSI Technology, Systems and Applications (VLSI-TSA '08)*, pp. 14–15, April 2008.

[2] International Technology Roadmap for Semiconductors, http://www.itrs.net/.
[3] S. K. Banerjee, L. F. Register, E. Tutuc, D. Reddy, and A. H. MacDonald, "Bilayer pseudospin field-effect transistor (BiSFET): a proposed new logic device," *IEEE Electron Device Letters*, vol. 30, no. 2, pp. 158–160, 2009.
[4] H. Min, R. Bistritzer, J.-J. Su, and A. H. MacDonald, "Room-temperature superfluidity in graphene bilayers," *Physical Review B*, vol. 78, no. 12, Article ID 121401, 2008.
[5] P. Avouris, Z. Chen, and V. Perebeinos, "Carbon-based electronics," *Nature Nanotechnology*, vol. 2, no. 10, pp. 605–615, 2007.
[6] D. Reddy, L. F. Register, E. Tutuc, and S. K. Banerjee, "Bilayer pseudospin field-effect transistor: applications to Boolean logic," *IEEE Transactions on Electron Devices*, vol. 57, no. 4, pp. 755–764, 2010.
[7] D. Reddy, L. F. Register, E. Tutuc, G. D. Carpenter, A. H. MacDonald, and S. K. Banerjee, "Bilayer pseudospin field effect transistor for beyond CMOS logic," INC6 Grenoble, France, May 2010.
[8] D. Basu, L. F. Register, D. Reddy, A. H. MacDonald, and S. K. Banerjee, "Tight-binding study of electron-hole pair condensation in graphene bilayers: gate control and system-parameter dependence," *Physical Review B*, vol. 82, Article ID 075409, 9 pages, 2010.
[9] T. Akeyoshi, K. Maezawa, and T. Mizutani, "Weighted sum threshold logic operation of MOBILE (monostable-bistable transition logic element) using resonant-tunneling transistors," *IEEE Electron Device Letters*, vol. 14, no. 10, pp. 475–477, 1993.
[10] C. Pacha, P. Gloesekötter, K. Goser, U. Auer, W. Prost, and F.-J. Tegude, "Resonant tunneling transistors for threshold logic circuit applications," in *Proceedings of the 9th IEEE Great Lakes Symposium on VLSI*, pp. 344–345, IEEE Computer Society Press, Ann Arbor, Mich, USA, 1999.